



ELO 30

This is to certify that the

dissertation entitled

SMECTITE CLAYS, MUSCOVITE MICA, AND HYDROTALCITE USED AS FILLERS AND REINFORCEMENTS IN THE FORMULATION OF EPOXY-BASED COMPOSITES

presented by

MUH S. WANG

has been accepted towards fulfillment of the requirements for

Ph.D. degree in CHEMISTRY

THOMAS J. PINNAVAIA

Date August 26, 1993

MSU is an Affirmative Action/Equal Opportunity Institution

0-12771

LIBRARY Michigan State University

PLACE IN RETURN BOX to remove this checkout from your record.

TO AVOID FINES return on or before date due.

DATE DUE	DATE DUE
受视 1 9 1906	
JIN 1 1 EU	
JUN 1 9 1999	
090503	

MSU Is An Affirmative Action/Equal Opportunity Institution

'n

SMECTITE CLAYS, MUSCOVITE MICA, AND HYDROTALCITE USED AS FILLERS AND REINFORCEMENTS IN THE FORMULATION OF EPOXY-BASED COMPOSITES

By

Muh S. Wang

A DISSERTATION

Submitted to
Michigan State University
in partial fulfillment of the requirements
for the degree of

DOCTOR OF PHILOSOPHY

Department of Chemistry

1993

ABSTRACT

SMECTITE CLAYS, MUSCOVITE MICA, AND HYDROTALCITE USED AS FILLERS AND REINFORCEMENTS IN THE FORMULATION OF EPOXY-BASED COMPOSITES

By

Muh S. Wang

Three representative smectite clays (montmorillonites) and a muscovite mica have been investigated as potential fillers for epoxy resin EPON-828 cured by meta-phenylenediamine (MPDA). The tensile strength of the clay-epoxy composite was found to depend mainly on clay pretreatment or surface treatment. Composite strengths increased in the order of surface treatments, freeze-drying < cationic surfactant alkylammonium chloride < anionic dispersant Na-polyacrylate. Furthermore, the composite strength decreased whereas the composite modulus increased with increasing the mineral concentration up to 35 wt%. Several characterization methods including Fourier transform infrared spectroscopy (FTIR), X-ray powder diffraction (XRD), and X-ray photoelectron spectroscopy (XPS) were used to establish property-strength relationships. Scanning electron microscopy (SEM) showed that the composite strength was well-correlated with the clay dispersion in the epoxy matrix. Besides, surface treatment played an very important role in determining clay filling limits and processing problems as well. Among the minerals investigated, Volclav HPM-20 exhibited the highest filling limit (~40 wt%) and composite strength, whereas Alsibronz Mica-4 exhibited the best processability and composite modulus.

A new class of clay-epoxy nanocomposite materials has been prepared by the spontaneous self-polymerization of the epoxy resin and the concomitant delamination of 9.6-Å-thin smectite clay layers at elevated temperatures. The epoxy polymerization-clay delamination temperature (PDT) was dependent on the heating rate and cation-exchanged montmorillonite (CEM). The replacement of interlayer ions Na⁺ and Ca²⁺ in the pristine clay by H⁺, NH₄⁺, and acidic onium ions H₃N(CH₂)_n. $_{1}COOH_{1}^{+}$, $[H_{3}N(CH_{2})_{n}NH_{2}]^{+}$, $[H_{3}N(CH_{2})_{n}NH_{3}]^{2+}$, $[H_{3}N(CH_{2})_{n-1}CH_{3}]^{+}$ (n = 6 and 12) facilitated the polymerization-delamination process over the temperature range 198-287 °C. In general, the PDT increased with decreasing cation acidity and decreasing basal spacing of the CEM. Evidence for the nanocomposite formation was provided in part by the dramatic liquid-to-powder transformation of the clay-epoxy mixture. The delamination of montmorillonite was further confirmed by XRD and transmission electron microscopy (TEM). No clay reflections appeared in the XRD patterns, and the TEM micrographs revealed interlayer spacings up to ~2.000 Å for a clay-epoxy nanocomposite containing 5 wt% [H₃N(CH₂)₁₁COOH]⁺-montmorillonite. Differential scanning calorimetry (DSC) studies of this clay-epoxy system showed that the PDT remained constant, whereas the heat of reaction decreased as the clay concentration increased from 1 to 20 wt%. The heat of reaction, activation energy, and activation free energy of the acidic organoclay-catalyzed epoxy polymerization were 53.7, 25.9, and 34.6 kcal/mol, respectively.

Another new class of clay-epoxy nanocomposite materials has been prepared by the spontaneous self-polymerization of the same epoxy resin and the concomitant delamination of 4.8-Å-thin hydrotalcite layers at elevated temperatures. The PDT was dependent on the heating rate, clay

concentration, and anion-exchanged hydrotalcite (AEH). The replacement of interlayer ions CO_3^{2-} in the pristine hydrotalcite by basic organic anions $H_2N(CH_2)_{11}COO^-$, $HOOC(CH_2)_nCOO^-$, and $[OOC(CH_2)_nCOO]^{2-}$ (n=4 and 10) facilitated the polymerization-delamination process over the temperature range 322-373 °C. The PDT increased with decreasing basal spacing of the AEH. Evidence for the delamination of the AEHs and CEMs was similar. No clay reflections appeared in the XRD patterns, and the TEM micrographs revealed interlayer spacings up to ~200 Å for a clay-epoxy nanocomposite containing 5 wt% $H_2N(CH_2)_{11}COO^-$ -hydrotalcite. DSC studies of this clay-epoxy system showed that the PDT and the heat of reaction decreased as the clay concentration increased from 1 to 20 wt%. The heat of reaction, activation energy, and activation free energy of the basic organoclay-catalyzed epoxy polymerization were 53.8, 25.7 and 42.5 kcal/mol, respectively.

ACKNOWLEDGMENTS

I would like to thank Dr. Thomas J. Pinnavaia for his guidance and financial support throughout the course of this work. I would also like to thank the committee faculty Dr. Harry A. Eick, Dr. Eugene LeGoff, and Dr. Larry T. Drzal for their time and help. Special thanks go to Dr. Larry T. Drzal and Mr. Mike J. Rich in the Composite Center and Dr. Karen L. Klomparens in the Electron Optics Center for their research facilities and helpful discussions

I would like to extend my thanks to my friends, in and out of the laboratory, for their friendships. Finally but most importantly, I am grateful to my family in Taiwan for their unconditional support over the years.

TABLE OF CONTENTS

			Page
LIST	OF TABL	ES	viii
LIST	OF FIGU	RES	x
LIST	OF ABBR	EVIATIONS	xvi
CHA	PTER I.	A COMPARATIVE STUDY OF TENSILE PROPERTIES OF SMECTITE CLAY- AND MUSCOVITE MICA-EPOXY COMPOSITES	
A.	Introduct	ion	1
В.	Experime	ntal	4
C.	Results a	nd Discussion	10
D.	Conclusion	ons	33
E.	List of R	eferences	35
CHAI	PTER II.	CLAY-POLYMER NANOCOMPOSITES FORMED FROM ACIDIC MONTMORILLONITES AND EPOXY RESIN	
A.	Introduct	ion	38
B.	Experime	ntal	39
C.	Results a	nd Discussion	42
D.	Conclusion	ons	70
E.	List of R	eferences	73

CHAPTER III. CLAY-POLYMER NANOCOMPOSITES FORMED FROM BASIC HYDROTALCITES AND EPOXY RESIN

A.	Introduction	75
B.	Experimental	78
C.	Results and Discussion	81
D.	Conclusions	104
E.	List of References	106

LIST OF TABLES

Table	,	Page
I.1.	Smectite clays and muscovite mica investigated as fillers	
	for epoxy resin EPON-828	6
I.2.	Tensile strengths and Young's moduli of 2 wt% clay- and	
	mica-epoxy composites	11
I.3.	Relative tensile strengths and Young's moduli of 7 wt%	
	clay- and mica-epoxy composites	13
I.4.	Approximate filling Limits of the smectite clays and	
	muscovite mica for epoxy resin EPON-828	21
I.5.	Intensity ratios of FTIR bands and curing degrees of 7	
	wt% clay- and mica-epoxy composites	25
I.6.	Physicochemical properties of the smectite clays and	
	muscovite mica	30
I.7.	Surface elemental concentrations of the smectite clays and	
	muscovite mica measured by XPS	31
I.8.	Relative concentrations of surface elements excluding	·
	carbon of the smectite clays and muscovite mica measured	
	by XPS	32

II.1.	DSC and XRD data for epoxy polymerizations catalyzed	
	by 5 wt% protonated aminocarboxylic acid- and primary	
	diamine montmorillonites	53
II.2.	Estimated epoxy cure percents due to protonated	
	aminocarboxylic acids and primary diamines	57
II.3.	Pre-exponential factors for epoxy polymerizations	
	catalyzed by 5 wt% protonated aminocarboxylic acid-	
	montmorillonites	67
II.4.	DSC and XRD Data for epoxy polymerizations catalyzed	
	by 5 wt% proton-, ammonium ion-, and alkylammonium-	
	montmorillonites	69
III.1.	DSC and XRD Data for epoxy polymerizations catalyzed	
	by 5 wt% aminocarboxylate- and dicarboxylate-	
	hydrotalcites	91
III.2.	Estimated epoxy cure percents due to aminocarboxylate-	
	and dicarboxylate-hydrotalcites	94
III.3.	Pre-exponential factors for epoxy polymerizations	
	catalyzed by 5 wt% 12-aminolaurate-hydrotalcite	102
III.4.	DSC, XRD, and TEM data for epoxy polymerizations	
	catalyzed by 5 wt% protonated 12-aminolauric acid-	•
	montmorillonite and 12-aminolaurate-hydrotalcite	103

LIST OF FIGURES

Figure		Page
I.1.	Structures of smectite clays (e.g., montmorillonite $(Na_mCa_n)(Al_{4-x-y}Mg_xFe_y)Si_8O_{20}(OH)_4$ where $0.4 < m + 1$	
	2 n = x + y < 1.2) and muscovite mica	
	K ₂ Al ₄ (Si ₆ Al ₂)O ₂₀ (OH) ₄	3
I.2.	General structure of diglycidyl ether of bisphenol A	
	(DGEBA) (e.g., epoxy resin EPON-828: 88% of $n = 0$,	
	10% of $n = 1$, and 2% of $n = 2$) and the structure of the	
	curing agent meta-phenylenediamine (MPDA)	5
I.3.	Scanning electron microscopy (SEM) micrographs of	
	fractured surfaces of epoxy composites containing 7 wt%	
	(a) Volclay HPM-20, (b) Claytone-PS, (c) freeze-dried	
	montmorillonite 1-2 μm, and (d) Alisibronz Mica-4	15
I.4.	Relative tensile modulus as a function of the mineral	
	concentration for epoxy composites containing (•)	
	Volclay HPM-20 and (o) Alisibronz Mica-4	16
I.5.	SEM micrographs of fractured surfaces of epoxy	
	composites containing (a) 2, (b) 7, (c) 25, and (d) 35	
	wt% Volclay HPM-20	18

I.6.	Relative tensile strength as a function of the mineral	
	concentration for epoxy composites containing (•)	
	Volclay HPM-20 and (o) Alisibronz Mica-4	19
I.7.	Transmission Fourier transform infrared (FTIR) spectrum	
	of epoxy resin EPON-828; the analytical and reference	
	bands are 916 cm ⁻¹ (epoxy ring, stretching) and 1184	
	cm ⁻¹ (Ph-H, in-plane deformation) bands, respectively	23
I.8.	X-ray powder diffraction (XRD) patterns of	
	semicrystalline Volclay HPM-20, highly crystalline	
	Alisibronz Mica-4, and amorphous cured epoxy resin	
	EPON-828	27
I.9.	Increases in basal (d ₀₀₁) spacings for the dehydrated	
	smectite clays and muscovite mica (bottom patterns)	
	embedded in cured epoxy resin EPON-828 (top patterns):	
	Claytone-PS, freeze-dried montmorillonite 1-2 µm,	
	Volclay HPM-2, and Alisibronz Mica-4	28
II.1.	XRD powder patterns of (a) [H ₃ N(CH ₂) ₁₁ COOH] ⁺ -	
	montmorillonite (AAC12-Mont.) (25 °C), (b) AAC12-	
	Mont. (229 °C, 1 min) and (c) a clay-epoxy	
	nanocomposite containing 5 wt% AAC12-Mont	44
II.2.	Transmission electron microscopy (TEM) micrographs of	
	a clay-epoxy nanocomposite containing 5 wt%	
	[H ₃ N(CH ₂) ₁₁ COOH] ⁺ -montmorillonite: (a) x10,000 and	
	(b) x58,000	45

II.3.	Differential scanning calorimetry (DSC) thermogram of	
	the epoxy polymerization catalyzed by 5 wt%	
	[H ₃ N(CH ₂) ₁₁ COOH] ⁺ -montmorillonite, a heating rate of	
	20 °C/min being used	46
II.4.	DSC thermogram of the uncatalyzed self-polymerization	
	of epoxy resin EPON-828, a heating rate of 20 °C/min	
	being used	48
II.5.	DSC thermogram of $[H_3N(CH_2)_{11}COOH]^+$	
	montmorillonite, a heating rate of 20 °C/min used	49
II.6.	Thermogravimetric analysis (TGA) curve of	
	[H ₃ N(CH ₂) ₁₁ COOH] ⁺ -montmorillonite, a heating rate of	
	20 °C/min used	50
II.7.	Spatial arrangements of interlayer cations in	
	montmorillonites: (a) $[H_3N(CH_2)_{11}COOH]^+$, (b)	
	$[H_3N(CH_2)_{12}NH_3]^{2+}$, and (c) $[H_3N(CH_2)_{12}NH_2]^+$	55
II.8.	Onset temperature of the epoxy polymerization-clay	
	delamination as a function of the clay concentration for	
	(•) $[H_3N(CH_2)_{11}COOH]^+$ - and (•) $[H_3N(CH_2)_5COOH]^+$ -	
	montmorillonites	58
II.9.	DSC thermograms of epoxy polymerizations catalyzed by	
	0.2 wt% (a) $[H_3N(CH_2)_{11}COOH]^+$ and (b)	
	[H ₃ N(CH ₂) ₅ COOH] ⁺ -montmorillonites, a heating rate of	
	20 °C/min being used	59
II. 10.	Heat of reaction as a function of the clay concentration	
	for (•) $[H_3N(CH_2)_{11}COOH]^+$ and (0)	
	[H ₂ N(CH ₂) ₅ COOH] ⁺ -montmorillonites	61

DSC thermograms of the epoxy polymerization catalyzed	
by 5 wt% [H ₃ N(CH ₂) ₁₁ COOH] ⁺ -montmorillonite at	
various heating rates: 10, 15, 20, and 25 °C/min	63
Linear relationship between the natural logarithm of the	
heating rate φ and the reciprocal of the peak maximum	
temperature T _p for epoxy polymerizations catalyzed by 5	
wt% (•) $[H_3N(CH_2)_{11}COOH]^+$ and (0)	
[H ₃ N(CH ₂) ₅ COOH] ⁺ -montmorillonites	64
DSC thermograms of epoxy polymerizations catalyzed by	
5 wt% (a) $[H_3N(CH_2)_{11}CH_3]^+$ and (b)	
[H ₃ N(CH ₂) ₅ CH ₃] ⁺ -montmorillonites., a heating rate of	
20 °C/min being used	71
General structure of anionic clays or layered double	
hydroxides (LDHs); e.g., hydrotalcite	
$Mg_6Al_2(OH)_{16}(CO_3)\cdot 4H_2O$, where $M^{2+}=Mg^{2+}$; $M^{3+}=$	
Al^{3+} ; and $A^{n-} = CO_3^{2-}$	76
XRD patterns of (a) hydrotalcite (HT), (b) month-old	
	82
	Q 2
	by 5 wt% [H ₃ N(CH ₂) ₁₁ COOH] ⁺ -montmorillonite at various heating rates: 10, 15, 20, and 25 °C/min

III.4.	TEM micrograph of a clay-epoxy nanocomposite	
	containing 5 wt% H ₂ N(CH ₂) ₁₁ COO-hydrotalcite:	
	x72,000	85
III.5.	DSC thermogram of the epoxy polymerization catalyzed	
	by 5 wt% H ₂ N(CH ₂) ₁₁ COO-hydrotalcite, a heating rate	
	of 20 °C/min being used.	86
III.6.	DSC thermogram of H ₂ N(CH ₂) ₁₁ COO-hydrotalcite, a	
	heating rate of 20 °C/min being used	87
III.7.	TGA curve of H ₂ N(CH ₂) ₁₁ COO-hydrotalcite, a heating	
	rate of 20 °C/min used	88
III.8.	XRD patterns of (a) "H ₂ N(CH ₂) ₅ COO"-hydrotalcite or	
	meixnerite $Mg_6Al_2(OH)_{16}(OH)_2 \cdot 4H_2O$ and (b)	
	hydrotalcite	93
III.9.	DSC thermograms of epoxy polymerizations catalyzed by	
	H ₂ N(CH ₂) ₁₁ COO-hydrotalcite at various clay	
	concentrations: 1, 5, 10, and 20 wt%	96
III. 10.	Onset temperature of the epoxy polymerization-clay	
	delamination as a function of the clay concentration for	
	H ₂ N(CH ₂) ₁₁ COO ⁻ -hydrotalcite	97
III.11.	Heat of reaction as a function of the clay concentration	
	for (•) $H_2N(CH_2)_{11}COO^-$ -hydrotalcite (0)	
	[H ₃ N(CH ₂) ₁₁ COOH] ⁺ -montmorillonite	98
III.12	DSC thermograms of the epoxy polymerization catalyzed	
	by 5 wt% H ₂ N(CH ₂) ₁₁ COO-hydrotalcite at various	
	heating rates: 10, 15, 20, and 25 °C/min	99

LIST OF ABBREVIATIONS

AAA Aminoacid anion

AAC Aminoacid cation

ABM-4 Alisibronz mica-4

CEC Cation-exchange capacity

CT-PS Claytone-PS

DGEBA Diglycidyl ether of bisphenol A

DRFTIR Diffuse-Reflectance Fourier transform infrared

spectroscopy

HPM-20 Volclay HPM-20

HT Hydrotalcite

MMT 1-2 Montmorillonite 1-2

Mont. Montmorillonite

MPCC Microfine Panther Creek catalyst

MPDA meta-Phenylenediamine

phr parts per 100 g of the resin

RTM Relative ultimate tensile modulus

RTS Relative ultimate tensile strength

UTS United Testing System

CHAPTER I

A COMPARATIVE STUDY OF TENSILE PROPERTIES OF SMECTITE CLAY- AND MUSCOVITE MICA-EPOXY COMPOSITES

A. INTRODUCTION

Layered aluminosilicates such as kaolin (1-4), talc (5-8), and mica (9-12) are commonly used as fillers for thermoplastics and occasionally, thermosets. The major advantages of layered aluminosilicates are natural abundance, very low cost, low abrasiveness to processing equipment, and increased composite dimensional stability. Another advantage of layered aluminosilicates is their platy shapes or two-dimensional (2-D) aspect ratios. However, clay minerals such as kaolin and talc usually have aspect ratios less than 20, which limits clay minerals as fillers instead of reinforcements in terms of mechanical strengths. Smectite clays (e.g., montmorillonite) exhibit an additional swelling property in aqueous electrolyte solutions and polar and moderately polar organic solvents (13, 14). Thus smectite clays are capable of a wide range of aspect ratios (10-10³). depending on the degree of clay delamination (or exfoliation). This unique property could act to increase the dispersion of smectite clays in a polymer matrix and improve mechanical properties of the clay-polymer composite. In the present study, three representative smectite clays (montmorillonites) and a muscovite mica have been investigated as potential

fillers for epoxy resin EPON-828 cured by meta-phenylenediamine (MPDA).

Montmorillonite and muscovite are 2:1 layered aluminosilicates in accord with the ratio of two tetrahedral silica SiO₂ sheets and an octahedral gibbsite Al(OH)₃ sheet comprising each of the layers, as shown in Figure I.1 (14). Montmorillonite (Na_mCa_n)(Al_{4-x-v}Mg_xFe_v)Si₈O₂₀(OH)₄ (where 0.4 < m + 2 n = x + y < 1.2) and muscovite $K_2Al_4(Si_6Al_2)O_{20}(OH)_4$ differ primarily in their chemical compositions and layer charges. The layer charge per unit cell of muscovite is -2, arising from the one-fourth substitution of Si⁴⁺ ions for Al³⁺ ions in tetrahedral sheets. The negative charge is balanced by interlayer K⁺ ions, and adjacent layers are bonded by strong ionic bonding. On the other hand, a layer charge per unit cell of montmorillonite ranges from -0.4 to -1.2, arising from the partial substitution of Al³⁺ ions for Mg²⁺ and Fe²⁺ ions in the octahedral sheet and to a lesser extent, that of Si⁴⁺ ions for Al³⁺ ions in tetrahedral sheets. The negative charge is balanced by various interlayer cations such as Na⁺ and Ca²⁺. These inorganic interlayer cations in montmorillonite can be easily replaced by various alkylammonium ions to form organophilic montmorillonites or organoclays.

Epoxy resins are commonly used as matrices for high-performance composites. A variety of base resins, curing agents, and catalysts are available to meet various properties and processing characteristics. Liquid resins have relatively low viscosity and long gelation time. Cured epoxy resins possess several desirable properties such as low cure shrinkage, high mechanical strength, thermal stability, excellent adhesion, and good chemical and electrical resistance. The major type of epoxy resins is diglycidyl ether of bisphenol A (DGEBA) and the general structure is

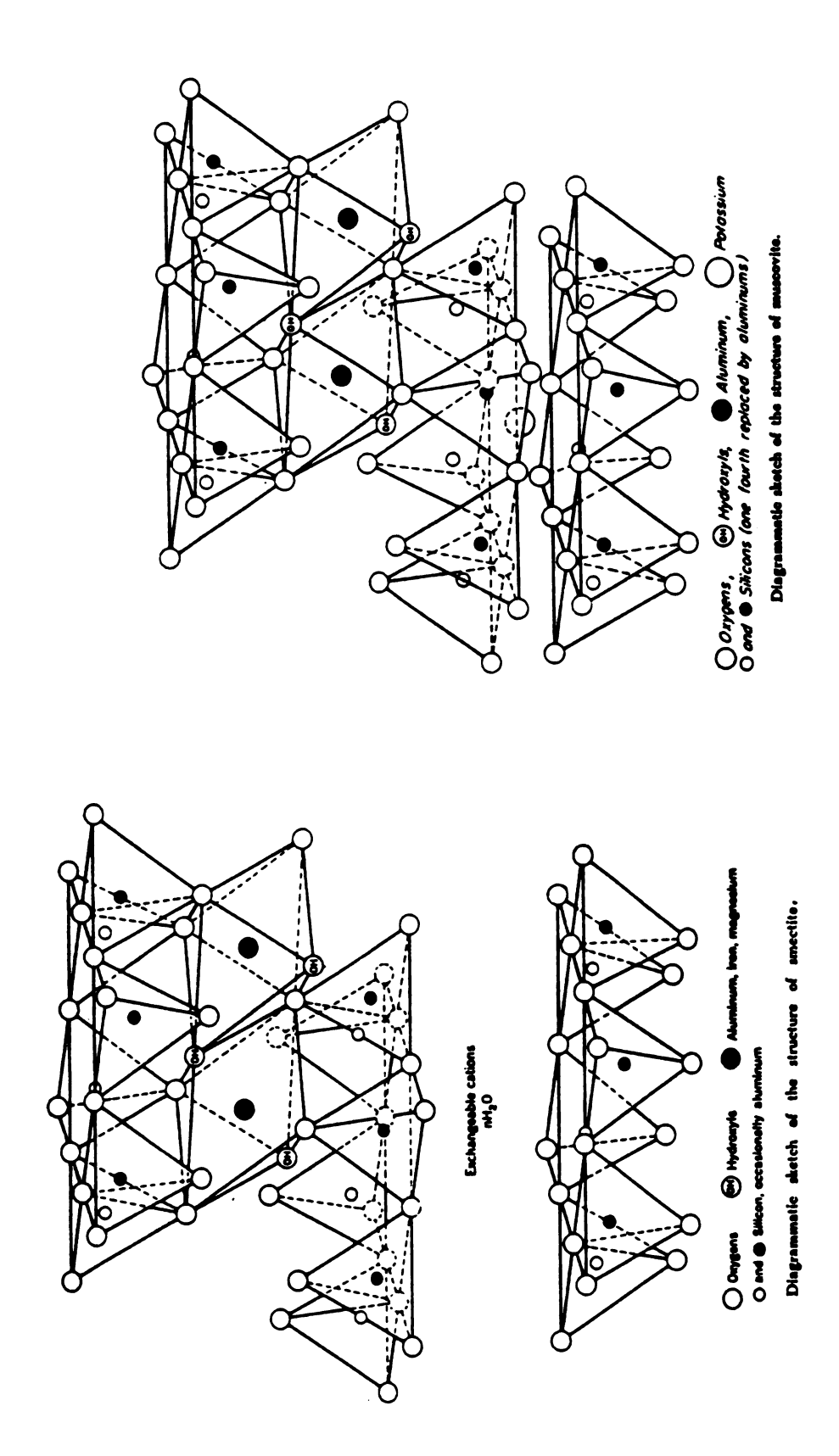


Figure 1.1. Structures of smeetite clays (e.g., montmorillonite (Na_mCa_n)(Al_{4-x-y}Mg_xFe_y)Si₈O₂₀(OH)₄, where 0.4 < m + 2 n = x + y < 1.2) and muscovite mica $K_2AI_4(Si_6AI_2)O_{20}(OH)_4$.

shown in Figure I.2 (15, 16). Low molecular-weight liquid resins have n values between 0 and 1. The selected epoxy resin for study, EPON-828 (Shell) has the following distribution of n values: n = 0 (88%); n = 1 (10%); and n = 2 (2%) (15, 16). The average n value and molecular weight of the epoxy resin are 0.14 and 378, respectively.

B. EXPERIMENTAL

Materials

Listed in Table I.1, Microfine Panther Creek Catalyst and Volclay HPM-20 (American Colloid) are Na⁺- and Ca²⁺-montmorillonites treated with ~ 0.1 wt% anionic dispersant Na-polyacrylate -(CH₂CH(COONa))-n, respectively. Claytone-40 and Claytone-AF are conventional and selfdispersing dimethyldioctadecylammonium-montmorillonites, respectively. Claytone-AF was prepared by using a higher amine-to-clay ratio of 100 (vs. 80) meq/100 g. Claytone-PS is methylbenzyldioctadecylammoniummontmorillonite. It was noted that Claytones (E.C.C. America) were dried without washing after cation-exchange reactions or cationic surfactant treatment. Freeze-dried Na⁺-montmorillonites with different particle size distributions (0.1-2 µm) were prepared by fractionating and then freezedrying source clay SWy-1, Wyoming Na⁺-montmorillonite (Clay Minerals Depository at the University of Missouri, Columbus, MO). Alsibronz Mica-4 (Franklin Mineral Products) is a water-ground muscovite. Epoxy resin EPON-828 (Shell) and meta-phenylenediamine (Aldrich) were used as received.

Figure I.2. General structure of diglycidyl ether of bisphenol A (DGEBA) (e.g., epoxy resin EPON-828: 88% of n = 0, 10% of n = 1, and 2% of n = 2) and the structure of the curing agent meta-phenylenediamine (MPDA).

Table I.1. Smectite Clays and Muscovite Mica Investigated as Fillers for Epoxy Resin EPON-828

Mineral	Abbreviation	Description
Microfine P.C. Catalyst	MPCC	Na-polyacrylate-treated Ca ²⁺ -montmorillonite
Volclay HPM-20	HPM-20	Na-polyacrylate-treated Na ⁺ -montmorillonite
Claytone-40	CT-40	$[(CH_3)_2N(C_{18}H_{37})_2]^+$ -mont. (80 meq)*
Claytone-AF	CT-AF	$[(CH_3)_2N(C_{18}H_{37})_2]^+$ -mont. (100 meq)*
Claytone-PS	CT-PS	$[(CH_3)(C_6H_5CH_2)N(C_{18}H_{37})_2]^+$ -mont.
Montmorillonite 1-2	MMT 1-2	Freeze-dried Na ⁺ -montmorillonite (1-2 µm)
Montmorillonite 0.5-1	MMT 0.5-1	Freeze-dried Na ⁺ -montmorillonite (0.5-1 µm)
Montmorillonite 0.1-0.5	MMT 0.1-0.5	Freeze-dried Na ⁺ -montmorillonite (0.1-0.5 µm)
Alisibronz Mica-4	ABM-4	Water-ground muscovite

^{*}The miliequivalent of the alkylammonium ion used for 100 g of montmorillonite.

Specimen Preparation

The smectite clays and muscovite mica were preheated at 150 °C overnight to remove most surface and interlayer water. Depending on the weight percent, the appropriate amount of the preheated mineral was portion by portion added to 15.0 g of epoxy resin EPON-828 in a 250 mL plastic beaker on a hot plate at 75 °C. The mineral-epoxy mixture was magnetically stirred at 75 °C for 1 h. The weight of MPDA was included in the total weight used to calculate mineral weight percents. Meanwhile, 2.175 g (or 14.5 parts per 100 g of the resin (phr)) of MPDA (mp, 62 °C) was melted in a 50 mL plastic beaker at 75 °C. The melted MPDA was then poured into the mineral-epoxy mixture and it was again stirred at 75 °C for 2 min. The whole mixture was then degassed in a VWR Scientific 1410 vacuum oven (~ 25 torr) at 75 °C for 25 min. As for HPM-20 and MPCC at 25 and 35 wt%, the processing temperature was gradually decreasing to ~ 60 °C to prevent premature cures during degassing. The degassed mixture was poured into a silicon rubber mold and cured at 75 °C for 2 h and 125 °C for another 2 h, a ramp rate of 3 °C/min being used. After the oven was gradually cooled down to room temperature (~ 1.5 h), the composite specimens $(1.50 \times 4.00 \times 25.40 \text{ mm}^3)$ were taken from the oven and polished until the deviation of thickness was ± 0.01 mm.

Characterization

Tensile testing was performed at ambient temperature by using a United Testing System (UTS). Neither strain gage nor extensometer was used and the strain rate was 0.51 mm/min (or 0.02 in/min). The relative ultimate tensile strengths (RTS) and Young's moduli (RTM) of clay- and

mica-epoxy composites were based on those of the cured epoxy resin tested in the same experimental conditions.

SEM micrographs of fractured surfaces of the composite specimens were obtained by a JEOL SEM T-330 scanning electron microscope, operating at an accelerating voltage of 15 kV and in the backscattered electron imaging (BEI) mode. The fractured composite specimens after tensile testing were used without any further treatment. The nonconductive composite specimens were coated with ~ 20 nm gold to prevent charging (or imaging artifacts). Gold-coating was performed by a Polaron sputter coater, using argon as the medium gas. The coater voltage and current were set at 2.5 kV and 25 mA. The target-to-specimen distance and exposure time were 50 mm and 1 min, respectively.

Diffuse-reflectance FTIR studies were carried out by using a Perkin-Elmer FTIR 1850 Fourier transform infrared spectrometer, using KBr powder as the reference (or background). Powdered composites were obtained by filing the tested, fractured specimens. To minimize the deviation of the linear intensity-concentration relationship, the powdered composites were ground down to 10-20 µm in particle sizes and then diluted to 5 wt% with KBr powder. Spectra subtraction was performed over the frequency range 450 cm⁻¹ to 4000 cm⁻¹.

X-ray powder diffraction (XRD) patterns were obtained by a Philips XRG-3000 X-ray diffractometer equipped with a Ni-filtered Cu- K_{α} radiation source (λ : 1.5406 and 1.5444 Å). The tube voltage and current were set at 30 kV and 20 mA, respectively. The preheated clays and mica were evenly dispersed on vacuum grease-coated glass slides, which were then tapped to obtain thin but uniform sample thickness. However, the tested, fractured specimens of the cured epoxy resin and composites were

placed on the sample holder (or rotating analysis disk) directly. The samples were then recorded by monitoring the diffraction angle 20 from 2° to 45°. The scanning speed and the step size were 2°/min and 0.025°, respectively.

XPS studies were carried out by using a PHI 5400 X-ray photoelectron spectrometer equipped with a Mg K_{α} standard source (PHI 04-548) and an Al K_{α} toroidal monochromatic source (PHI 10-410). The monochromatic Al source operating at 600 W (15 kV, 40 mA) was used for all the sample analyses. The preheated clays and mica were dispersed on analysis stubs by using double-sided tapes. The XPS spectra were obtained at a system base pressure of $\sim 10^{-9}$ mbar. The lens was set in the large area, small solid angle mode, and the size of the analysis area was set for a 3.3-mm-diameter circle. Data points were collected in the fixed analyzer transmission mode by using a position sensitive detector and a 1800 hemispherical analyzer. Pass energies were set at 178.95 eV for the elemental survey scans (0-1200 eV) and at 35 eV for the higher resolution narrow scans of the individual elemental regions. The C_{1s} binding energy of the carbon peak was set to 285.0 eV for calibration purposes.

Surface areas of the clays and mica were measured by a Quantachrome Quantasorb Jr. surface area analyzer, using N₂ and He as adsorbate and carrier gas, respectively. The samples were degassed at 125 °C for 12 h, and the surface areas of the samples were determined by using three-point BET plots.

Cation-exchange capacities of the clays and mica were determined by a Fisher Scientific Accumnet 750 selective ion analyzer and the method proposed by Busenberg and Clemency (17).

The pH values of 7 wt% clay- and mica-aqueous suspensions were measured by the same selective ion analyzer at room temperature, a pH electrode being used instead. The pH value of the slightly acidic deionized water used was adjusted to 7.0 with 0.1 N NaOH.

C. RESULTS AND DISCUSSION

Survey

A survey (Table I.2) indicates that the tensile strengths of 2 wt% clay-epoxy composites depend on the pre-treatment or more precisely, surface treatment of the smectite clays. Composite strengths increase in the order of surface treatment, freeze-drying < cationic surfactant alkylammonium chloride < anionic dispersant Na-polyacrylate. Obviously, interlayer cations Na⁺ and Ca²⁺ in Na-polyacrylate treated montmorillonites do not play an important role in determining composite strengths. This also holds true for various interlayer quaternary alkylammonium ions in alkylammonium-montmorillonites. Besides, the differences in particle sizes among freeze-dried Na⁺-montmorillonites (0.1-2 μ m) are too small to have any significant effects on the composite strengths. Therefore, Volclay HPM-20, Claytone-PS and freeze-dried Na⁺-montmorillonite 1-2 μ m have been chosen as representatives of the three types of smectite clays for further investigation. The reference is a water-ground muscovite mica, Alsibronz Mica-4.

Tensile Moduli

Recently, Ahmed and Jones (18) published a comprehensive review of reinforcement theories for particulate-polymer composites and concluded

Table I.2. Tensile Strengths and Young's Moduli of 2 wt% Clay- and Mica-Epoxy

Composites

Mineral	Tensile Strength (ksi)	RTS* (%)	Tensile Modulus (ksi)	RTM* (%)
MPCC	12.36 ± 0.09	96	211 ± 4	103
HPM-20	12.18 ± 0.20	95	212 ± 4	104
CT-40	11.08 ± 0.26	86	206 ± 1	101
CT-AF	10.82 ± 0.18	84	213 ± 7	104
CT-PS	10.67 ± 0.29	83	212 ± 5	104
MMT 1-2	9.95 ± 0.17	77	208 ± 6	102
MMT 0.5-1	9.94 ± 0.35	77	212 ± 4	104
MMT 0.1-0.5	9.58 ± 0.37	74	203 ± 3	100
ABM-4	10.81 ± 0.36	84	235 ± 8	115

^{*}Relative ultimate tensile strengths and Young's moduli are based on those (12.87 \pm 0.01 and 204 \pm 6 ksi) of the cured epoxy resin EPON-828 tested at 20 \pm 2 °C.

that a fresh theoretical approach together with systematic experimental studies was needed. The previously proposed models with assumptions and oversimplifications often require empirical parameters and/or constants for curve fitting and thus have limited applications. In general, mechanical properties of particulate-polymer composites depend on the filler, polymer matrix, and filler-matrix interface or interphase (19). As for the filler, the size, shape, size distribution, surface area, aspect ratio, orientation (or anisotropy), and aggregation are factors affecting composite mechanical properties. Moreover, the filler-matrix adhesion and particle-particle interactions of aggregates in the matrix cannot be experimentally quantified (18). This makes it more difficult to develop a theoretical model that can satisfactorily predict mechanical properties, especially mechanical strengths of particulate-polymer composites.

Summarized in Tables I.2 and I.3, the relative tensile moduli of the clay- and mica-epoxy composites show that the smectite clays and muscovite mica investigated enhance the tensile modulus of cured epoxy resin EPON-828. Moreover, the composite modulus increases with increasing the mineral concentration. These are because the epoxy matrix is replaced by higher modulus clay (111 GPa or 1.61 x 10⁴ ksi) and mica (172 GPa or 2.49 x 10⁴ ksi) (20). Clay particles and mica flakes restrict molecular motions and reduce the glassy-state free volume of the epoxy matrix. This makes the stress relaxation of the epoxy matrix more difficult and results in an increase in the modulus. The clay concentration being equal, the composite moduli remain constant regardless of the smectite clays filled. Mica is the better modulus reinforcement than clay because of the greater Young's modulus and aspect ratio of mica, according to Nielsen equations (20) for particulate-filled composites:

Table I.3. Relative Tensile Strengths and Young's Moduli of 7 wt% Clay- and Mica-Epoxy Composites

Mineral	Relative Tensile Strength* (%)	Relative Tensile Modulus* (%)
HPM-20	92 ± 2	108 ± 4
CT-PS	80 ± 4	107 ± 5
MMT 1-2	60 ± 4	106 ± 5
ABM-4	82 ± 3	134 ± 8

^{*}Based on the ultimate tensile strength and Young's modulus of the cured epoxy resin EPON-828 tested in the same experimental conditions.

$$\frac{E_c}{E_m} = \frac{1 + AB\varphi}{1 - BC\varphi}$$

$$A = k - 1;$$
 $B = \frac{\frac{E_f}{E_m} - 1}{\frac{E_f}{E_m} + A};$ $C = 1 + \frac{\varphi(1 - \varphi_m)}{\varphi_m^2}$

where E_c , E_m , and E_f are the moduli of the composite, matrix, and filler, respectively; k is the Einstein coefficient; φ is the volume fraction; and φ_m is the maximum packing volume fraction. The Einstein coefficient describes the shape (or aspect ratio) effect of the filler on viscosity and it can be determined by the rheological method. Other things being equal, the fiber and the sphere have the highest and the lowest k values, respectively.

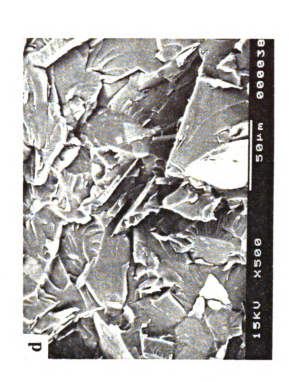
As shown in Figure I.3, the SEM micrographs of fractured surfaces of the composite specimens show that aspect ratios of embedded mica flakes are in the range of 20 to 50 and those of embedded clay particles are less than 5. Figure I.4 shows a comparison of HPM-20 and ABM-4 with respect to the relative composite modulus as a function of the mineral concentration up to 25 wt%. The linear relationship of the relative composite tensile modulus (E) and the mineral weight percent (ϕ) for HPM-20 and ABM-4 can be expressed by the following empirical equations:

$$%E_{HPM20} = 100 + 1.33\phi$$

$$%E_{ABM4} = 101 + 4.54\phi$$

Figure I.3. Scanning electron microscopy (SEM) micrographs of fractured surfaces of epoxy composites containing 7 wt% (a) Volclay HPM-2, (b) Claytone-PS, (c) freezedried montmorillonite 1-2 μ m, and (d) Alisibronz Mica-4.









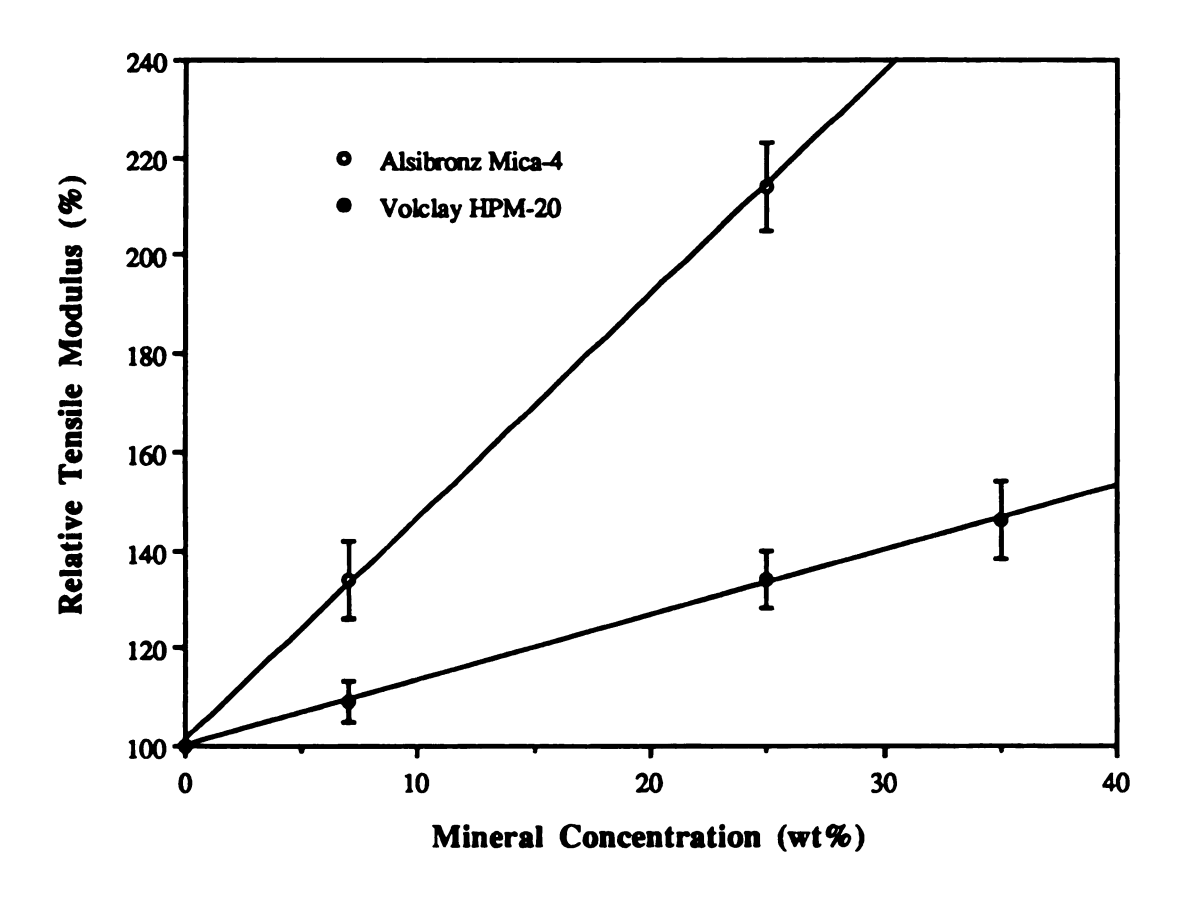


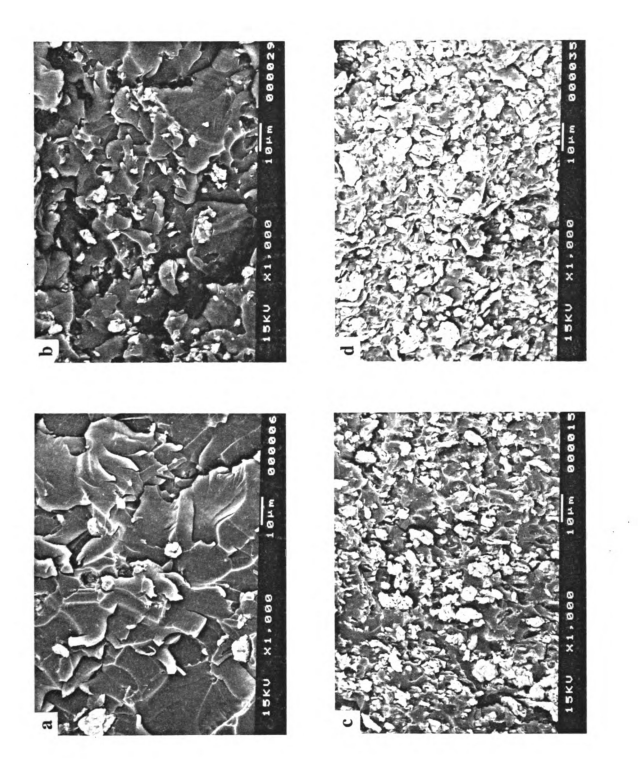
Figure I.4. Relative tensile modulus as a function of the mineral concentration for epoxy composites containing (•) Volclay HPM-20 and (o) Alisibronz Mica-4.

Tensile Strengths

The relative tensile strengths (Tables I.2 and I.3) of the clay- and mica-epoxy composites show that the smectite clays and muscovite mica investigated are not reinforcements but fillers for cured epoxy resin EPON-828. Furthermore, the composite strength decreases with increasing the mineral concentration. As shown in the SEM micrographs of fractured surfaces of the composite specimens in Figure I.3, clean surfaces of clay particles and mica flakes suggest that there is no strong adhesion between the mineral and the matrix. Consequently, the fracture occurs at the mineral-matrix interface and the load can not effectively pass along to the mineral. The clay concentration being equal, the composite strength varies whereas the composite modulus remains constant within experimental errors. This is because the tensile strength is determined by the weakest point of the specimen whereas the tensile modulus is a bulk property.

Table I.3 and Figure I.3 also show that the clay composite strength is well correlated with the clay dispersion in the epoxy matrix. Arising from poor dispersion, mineral aggregates would act as weak points for mechanical failure and reduce composite strengths. The degree of aggregation should increase with increasing the mineral concentration. Despite their small sizes (1-2 μm), freeze-dried Na⁺-montmorillonite particles flocculate and form aggregates up to 50 μm. As a result, MMT 1-2 exhibits the lowest composite strength among the representative smectite clays and muscovite mica. On the contrary, HPM-20 exhibits the best dispersion and the highest composite strength. In Figure I.5 the SEM micrographs show that even at 25 and 35 wt% most of HPM-20 particles and aggregates are less than 10 μm and still relatively well dispersed in the epoxy matrix. Figures I.6 shows a comparison of HPM-20 and ABM-4

Figure L5. SEM micrographs of fractured surfaces of epoxy composites containing (a) 2, (b) 7, (c) 25, and (d) 35 wt% Volclay HPM-20.



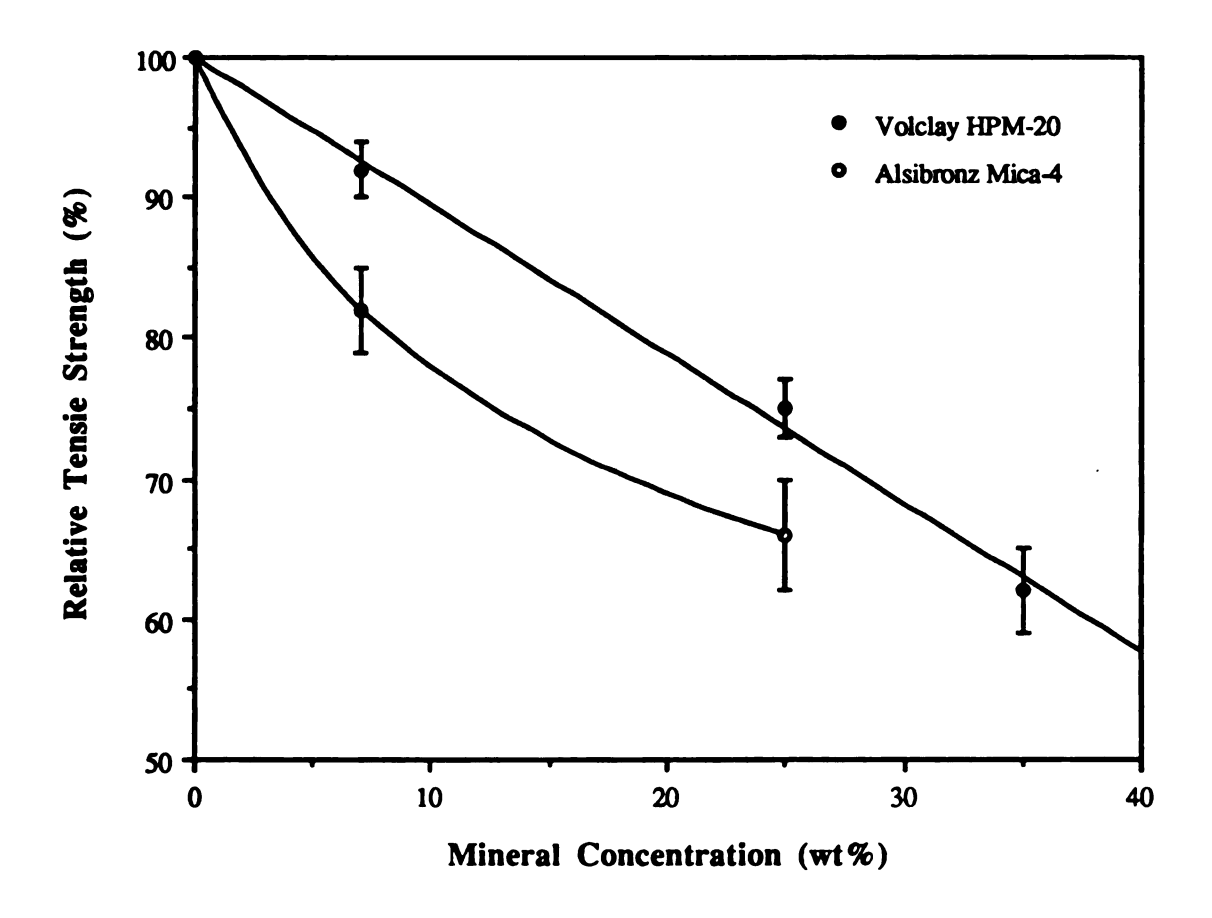


Figure I.6. Relative tensile strength as a function of the mineral concentration for epoxy composites containing (•) Volclay HPM-20 and (o) Alisibronz Mica-4.

with respect to the relative composite strength as a function of the mineral concentration up to 25 wt%. The relative composite strength of ABM-4 appears to level off at high mica concentrations presumably because mica has relatively high aspect ratios. It should be noted that ABM-4 and MMT 1-2 are not surface-treated with any adhesion-enhancing agents such as surfactants, dispersing agents, and coupling agents.

Processing Problems

During specimen preparation it was easier to process the muscovite smectite clays. Na-polyacrylate treated mica than any of the montmorillonites (MPCC and HPM-20) accelerated the epoxy-amine cure reduced the gelation time (or working life). Long-chain alkylammonium-montmorillonites (CTs) produced tenaciously entrapped air in clay-epoxy mixtures. These processing problems are due to the anionic dispersant Na-polyacrylate and cationic surfactant alkylammonium chloride on clay surfaces, respectively. The degassing problem of Claytones might be somewhat alleviated if they were washed with deionized water or alcohol after cation-exchange reactions or cationic surfactant treatment. Freezedried Na⁺-montmorillonites (MMTs) caused demixing problems and low filling limits. This, once again, reflects effects of clay pre-treatment or surface treatment. Freeze-drying changes clay morphologies and results in fluffy clays. However, an increase in the clay surface area enhances the adhesion between hydrophilic clay particles instead of the clay and the epoxy matrix. The approximate filling limits of the representative smectite clays and muscovite mica in our experimental conditions are listed in Table I.4. The data shows that pre-treatment affects not only processability but also the filling limit. Owing to the degassing problem of CT-PS and the

Table I.4. Approximate Filling Limits of the Smectite Clays and Muscovite Mica for Epoxy Resin EPON-828

Mineral	Filling Limit (wt%)	
HPM-20	40	
CT-PS	30	
MMT 1-2	10	
ABM-4	30	

Note: The weight of MPDA is included in the total weight.

low filling limit (~ 10 wt%) of MMT 1-2, only HPM-20 and ABM-4 at higher concentrations (25 and 35 wt%) have been investigated.

Curing Degrees

The mechanical properties of polymers and composites depend strongly on their curing degrees (or extent of polymerization). Diffuse-Reflectance Fourier transform infrared spectroscopy (DRFTIR or DRIFTS) provides a fast way to study curing degrees of the cured epoxy resin and mineral-epoxy composites by using tested, fractured specimens in this study. However, transmission FTIR spectroscopy is the only way to obtain the FTIR spectrum of the pure liquid epoxy resin, as shown in Figure I.7. The infrared characteristic bands of epoxy groups absorbing at 916 and 863 cm⁻¹ diminish gradually as the amine-epoxy reaction proceeds at elevated temperatures. The curing process can be expressed by the following simplified equations:

$$R^{1}NH_{2}$$
 + CH_{2} -CHR \longrightarrow $R^{1}HN$ -CH₂-CHR (I.1)

OH
$$R^1$$
HN-CH₂-CHR + CH₂-CHR \longrightarrow R^1 N(CH₂-CHR)₂ (1.2)

Byrne et al. (21) and Chalesworth (22, 23) independently concluded that the reaction rates (Equations I.1 and I.2) were indistinguishable. Swarin and Wims (24) used differential scanning calorimetry (DSC) to study the amine-epoxy reaction and obtained a single exotherm peak. That is, the two reactions take place virtually at the same time and only the overall reaction is detected. The 916 cm⁻¹ band is the better analytical band because it is

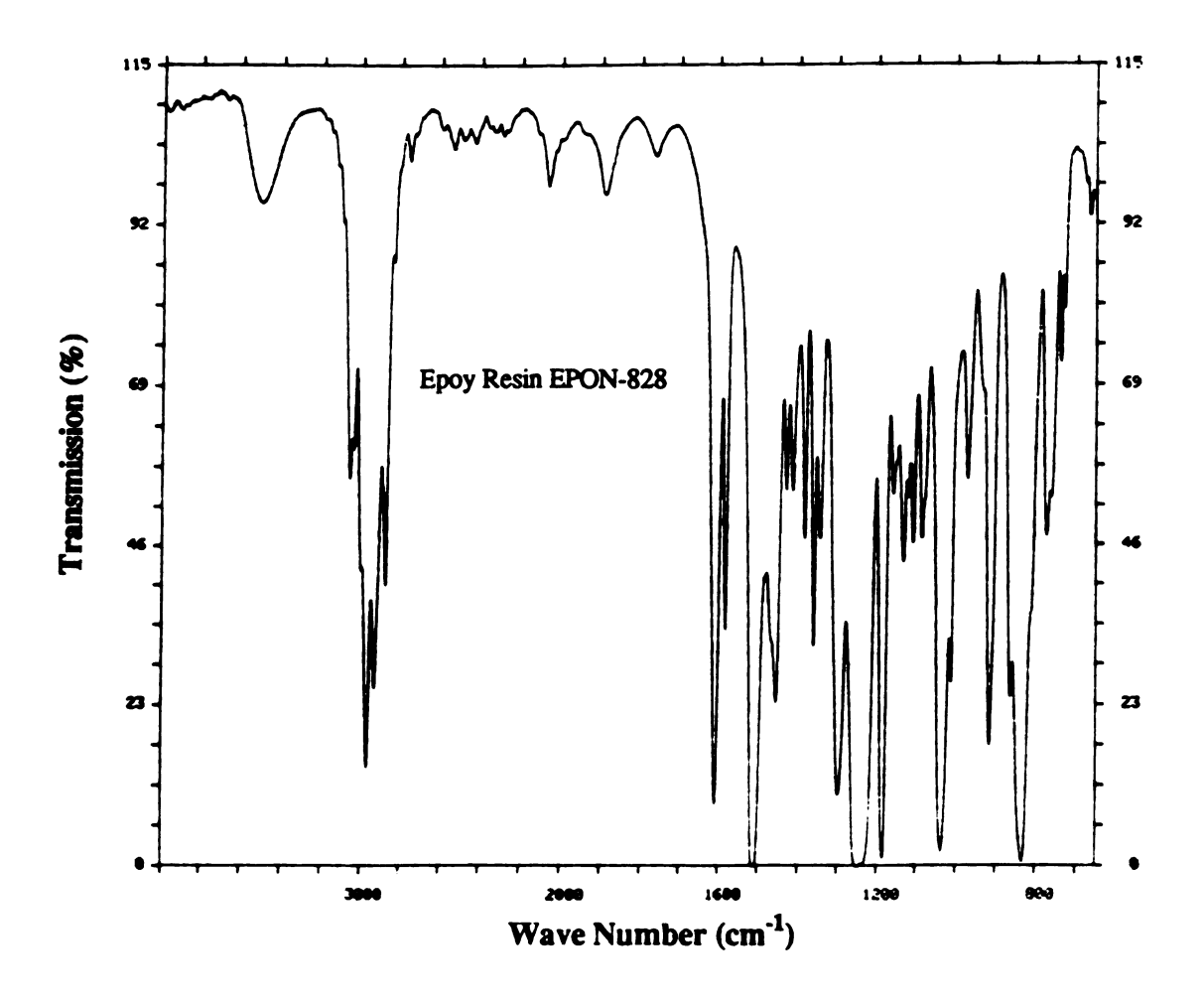


Figure I.7. Transmission Fourier transform infrared (FTIR) spectrum of epoxy resin EPON-828; the analytical and reference bands are 916 cm⁻¹ (epoxy ring, stretching) and 1184 cm⁻¹ (Ph-H, in-plane deformation) bands, respectively.

much less overlapped with another band. The band intensity ratio is defined as the integrated intensity ratio of the 916 cm⁻¹ band (epoxy ring, stretching) to the 1184 cm⁻¹ band (aromatic hydrogen, in-plane deformation). Since no aromatic rings participate in the reaction, the intensity of the 1184 cm⁻¹ reference band should remain constant as the polymerization proceeds.

Listed in Table I.5, the band intensity ratios show that the smectite clays and muscovite mica have little effects on the cure extent of the epoxy resin after a long cure cycle at elevated temperatures (2 h at 75 °C and another 2 h at 125 °C). The curing degree of EPON-828 cured by 14.5 wt% MPDA under the same cure cycle was determined as 93% by Schiering et al. (25), using the cured epoxy thin-film and the 1034 cm⁻¹ reference band (aromatic hydrogen, out-of-plane deformation). Based on that value, the curing degrees of 7 wt% clay- and mica-epoxy composites are ~ 94% regardless of the smectite clays and muscovite mica.

It was noted that HPM-20 (e.g., at 7 and 35 wt%) alone could not cure the epoxy resin even at 125 °C for several days, although it accelerated the epoxy-amine reaction. It is possible that the reaction temperature is not high enough for the polyacrylate-epoxy reaction. However, it is more likely that the concentration of 0.1 wt% Napolyacrylate on the clay surface is too small to cure the epoxy resin completely.

Intercalation

X-ray powder diffraction (XRD) patterns serve as excellent fingerprints for crystalline samples. More importantly, XRD patterns can often be recognized even when they are superimposed upon one another.

Table I.5. Intensity Ratios of FTIR Bands and Curing Degrees of 7 wt% Clay- and Mica-Epoxy Composites

Mineral	Intensity Ratio ^a (x 10 ⁻²)	Curing Degree ^b (%)
NONE	7.58	93.0
HPM-20	6.65	93.9
CT-PS	5.89	94.7
MMT 1-2	6.57	94.0
ABM-4	6.86	93.7

^a916 cm⁻¹ (epoxy ring, stretching)/1184 cm⁻¹ (Ph-H, in-plane deformation).

b2 h cure at 75 °C and another 2 h cure at 125 °C.

XRD has proved useful and convenient by using the tested, fractured specimens directly in this study. Namely, basal spacings of pristine clays and micas embedded in the epoxy matrix can be measured directly and no powdered composites are required. As shown in Figure I.8, the XRD patterns of ABM-4, EPON-828, and HPM-20 indicate that the muscovite mica is crystalline whereas the cured epoxy resin is amorphous and that the smectite clay is semicrystalline or polycrystalline. The relatively low crystallinity of smectite clays arises from their structural defects and small crystal sizes (14).

As shown in Figure I.9 (bottom patterns), the reduced basal spacings (9.8-14.1 Å) of dehydrated HPM-20, MMT 1-2, and CT-PS are due to the loss of most interlayer water after the smectite clays were preheated at 150 °C overnight. On the contrary, preheat treatment does not reduce the basal spacing of ABM-4 simply because no interlayer water exists in the pristine muscovite mica in the first place. Figure I.9 (top patterns) also shows that there are small increases in basal spacings (0.2-1.4 Å) for the smectite clays and no changes for the muscovite mica when they are embedded in the epoxy matrix. The result suggests that some epoxy monomers may be intercalated and to a lesser extent, cured by MPDA on the clay interlayer surfaces, although it clearly indicates that nothing happens in the mica galleries.

According to Nakamae and co-workers' work (26-29) on stress transmission in particulate-epoxy composites, an increase in basal spacing or crystal strain may be attributed to stress transferred from the epoxy matrix to clay particles. The crystal strain of mica flakes may be too small to be detected by our X-ray diffractometer. However, the concept of crystal strain has yet to be proved valid for the composite tensile strength, which

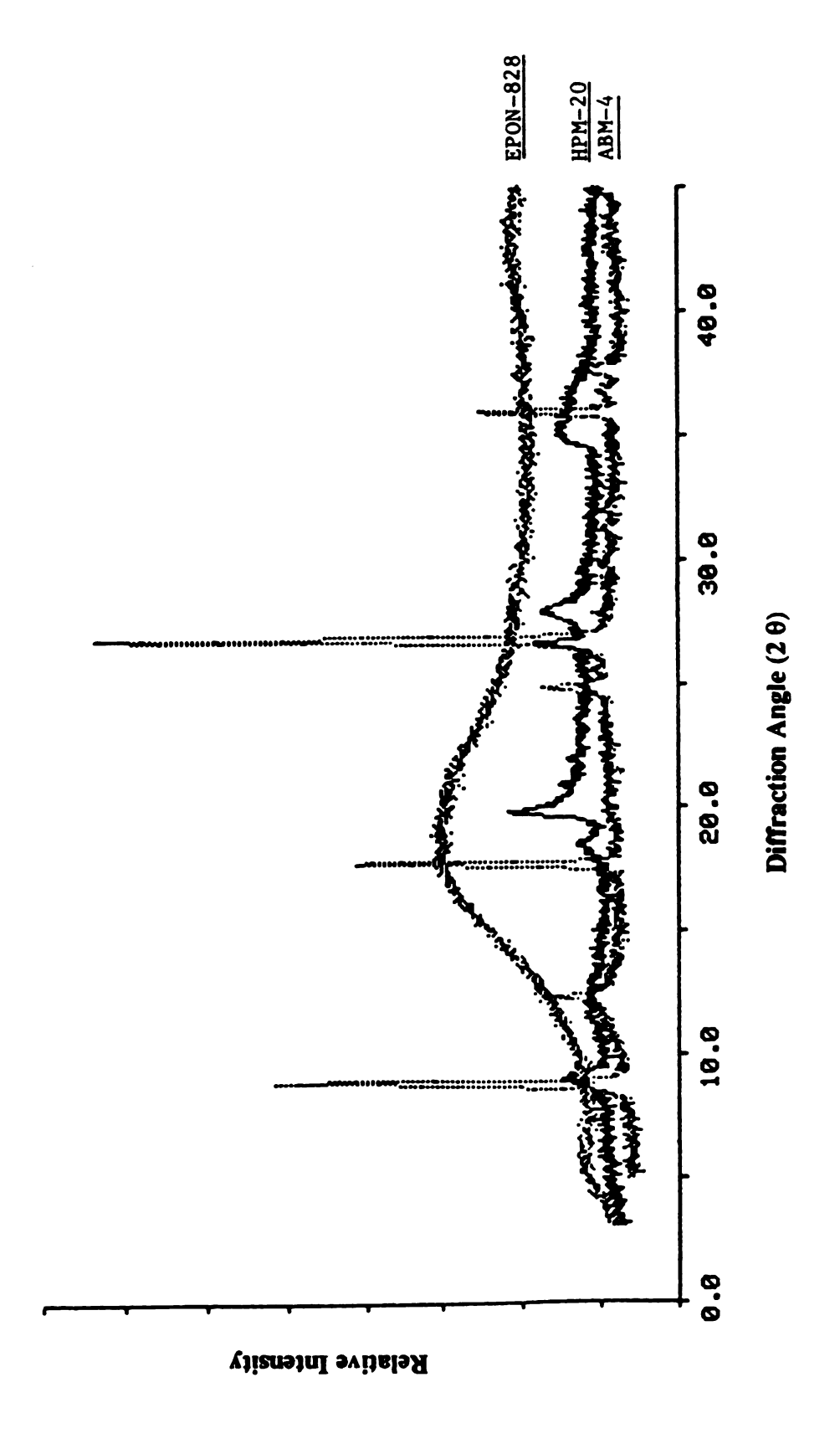
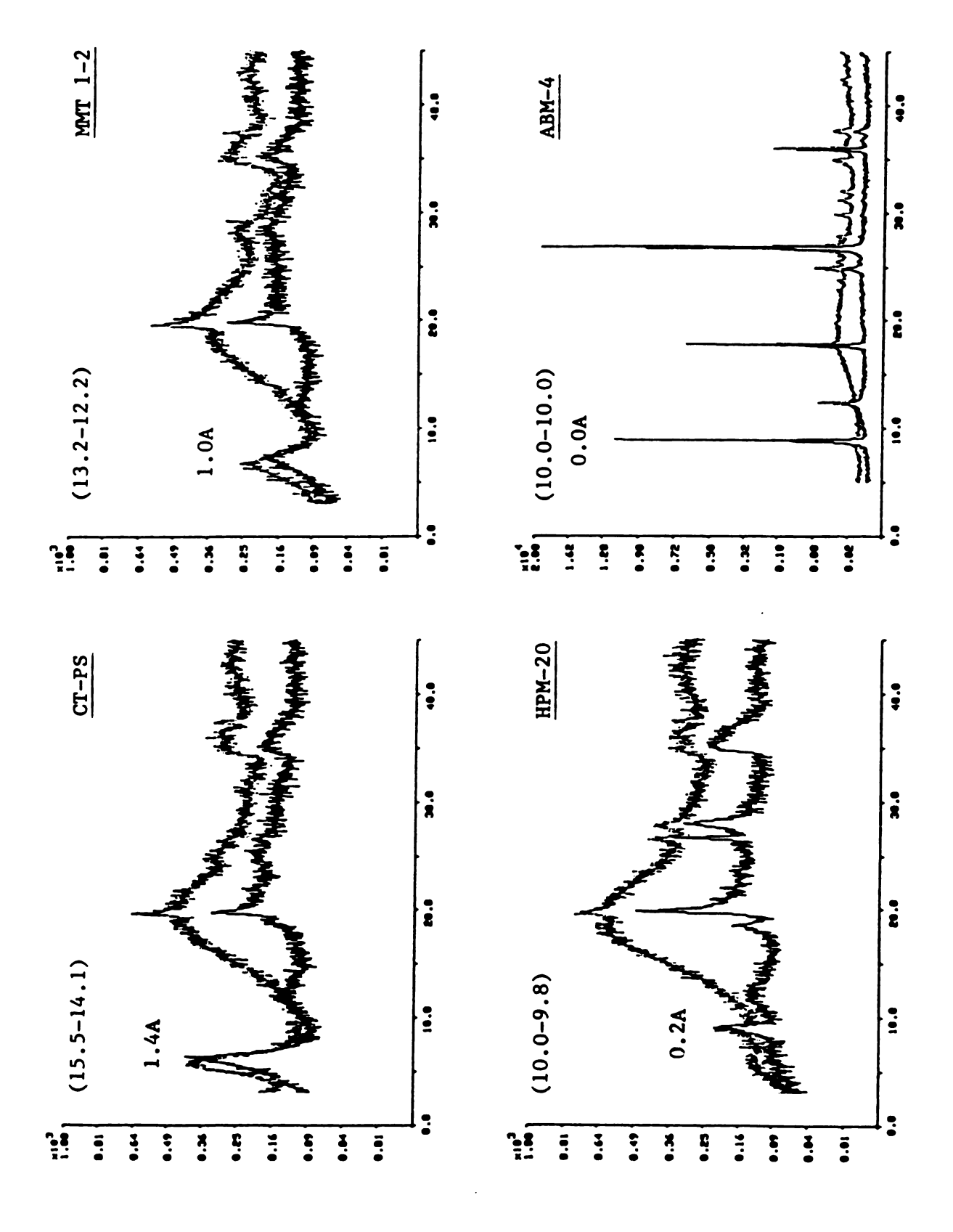


Figure I.8. X-ray powder diffraction (XRD) patterns of semicrystalline Volclay HPM-20, highly crystalline Alisibronz Mica-4, and amorphous cured epoxy resin EPON-828.

Figure I.9. Increases in basal (d_{001}) spacings for the dehydrated smectite clays and muscovite mica (bottom patterns) embedded in cured epoxy resin EPON-828 (top patterns): Claytone-PS, freeze-dried Montmorillonite 1-2 μ m, Volclay HPM-2, and Alisibronz Mica-4.



is more sensitive to stress transmission than the composite tensile modulus. Nevertheless, it is certain that most or all epoxy monomers and oligomers are cured by MPDA outside the clay particles.

Surface Composition

Mineral particles with high surface free energies are hydrophilic and tend to flocculate in a polymer matrix. Moreover, surface free energy is a function of the surface area and surface elemental/chemical composition. Table I.6 lists physicochemical properties such as surface area, cation-exchange capacity (CEC) and basicity/acidity of the smectite clays and muscovite mica. However, none of the clay properties measured accounts solely for the clay dispersion in the epoxy matrix or the composite tensile strength.

X-ray photoelectron spectroscopy (XPS) has been used to determine relative concentrations and chemical states of surface elements of clay minerals (30-32) and zeolites (33-35). XPS sampling depths range from 10 to 30 Å for most inorganic samples, (36) and basal spacings are 10 to 14 Å for the dehydrated smectite clays and muscovite mica. Thus, the XPS data obtained are based on the two to three outermost clay and mica surface layers. Table I.7 indicates that MMT 1-2, HPM-20, and ABM-4 contain 17.6-13.2% contaminant carbon. It is reasonable to assume that CT-PS contains the average concentration of contaminant carbon 14.9%. The extremely high concentration of intrinsic carbon (45.7%) and the presence of nitrogen are due to $[(CH_3)(C_6H_5CH_2)N(C_{18}H_{37})_2]^+$ ions on the clay surface and in the two outermost clay galleries.

The relative concentrations of surface elements excluding carbon are listed in Table I.8. Named by the major interlayer ion, Na⁺-

Table I.6. Physicochemical Properties of the Smectite Clays and Muscovite Mica

Mineral	Surface Area (m²/g)	C.E.C.# (meq/100 g)	pH Value ^b
MMT 1-2	53.92 ± 1.16	82.48 ± 0.50	9.34 ± 0.01
HPM-20	30.25 ± 0.89	61.67 ± 0.50	9.21 ± 0.01
CT-PS	6.40 ± 0.29	0.51 ± 0.14	7.78 ± 0.02
ABM-4	2.91 ± 0.03	0.88 ± 0.15	6.32 ± 0.05

^aC.E.C.: Cation exchange capacity.

^bBased on 7 wt% mineral aqueous suspensions at 25 °C.

Table L7. Surface Elemental Concentrations of the Smectite Clays and Muscovite

Mica Measured by XPS

	Relative Concentration (%)			
Element	MMT 1-2	HPM-20	CT-PS	ABM-4
C (1s)	17.64 ± 2.36	13.93 ± 2.41	60.59 ± 0.22	13.17 ± 1.44
Mg (1s)	2.15 ± 0.15	1.64 ± 0.15	0.62 ± 0.10	0.55 ± 0.06
Fe (2p)	0.50 ± 0.21	0.61 ± 0.30	0.35 ± 0.18	0.35 ± 0.16
Na (1s)	1.60 ± 0.10	1.55 ± 0.08	0.26 ± 0.11	0.66 ± 0.16
Ca (2p)	0.66 ± 0.07	0.54 ± 0.07	ND	ND
N (1s)	ND	ND	0.83 ± 0.11	ND
K (2p)	ND	ND	ND	5.32 ± 0.28
Al (2p)	11.90 ± 0.25	12.16 ± 1.52	6.32 ± 0.58	18.94 ± 0.44
Si (2p)	28.82 ± 0.48	29.81 ± 0.68	14.32 ± 0.26	23.18 ± 0.56
O (1s)	36.73 ± 1.68	39.77 ± 0.93	16.73 ± 0.95	37.66 ± 0.86

ND: Non-detectable.

Table I.8. Relative Concentrations of Surface Elements Excluding Carbon of the Smectite Clays and Muscovite Mica Measured by XPS

	Relative Concentration (%)			
Element	MMT 1-2	HPM-20	CT-PS	ABM-4
Mg (1s)	2.58 ± 0.20	1.87 ± 0.11	1.59 ± 0.22	0.64 ± 0.06
Fe (2p)	0.69 ± 0.35	0.71 ± 0.34	0.98 ± 0.46	0.40 ± 0.19
Na (1s)	1.91 ± 0.20	1.81 ± 0.06	0.74 ± 0.13	0.77 ± 0.20
Ca (2p)	0.76 ± 0.01	0.64 ± 0.08	ND	ND
N (1s)	ND	ND	$2.15 \pm .24$	ND
K (2p)	ND	ND	ND	6.12 ± 0.23
Al (2p)	14.44 ± 0.52	13.97 ± 1.26	16.24 ± 1.49	21.81 ± 0.15
Si (2p)	35.16 ± 0.28	34.91 ± 1.00	36.05 ± 0.53	26.69 ± 0.55
O (1s)	44.45 ± 0.69	46.10 ± 0.65	42.26 ± 2.08	43.37 ± 0.77

ND: Non-detectable.

montmorillonites, MMT 1-2 and HPM-20 contain not only Na⁺ but Ca²⁺ interlayer ions. No Ca²⁺ but some Na⁺ ions remain in CT-PS after the cation-exchange reaction or cationic surfactant treatment. The presence of K⁺ ion and the relatively low Si⁴⁺/Al³⁺ ratio (1.22 vs. 2.22-2.50) verify that ABM-4 is a muscovite mica. As mentioned earlier, a negative layer charge of montmorillonite arises primarily from the partial substitution of Al³⁺ ions for Mg²⁺ in the octahedral sheet and the negative charge is balanced by various interlayer cations. The relatively high Mg²⁺ concentration and CEC value of MMT 1-2 might be somewhat related to the aggregation or poor dispersion of the clay particles in the epoxy matrix. However, the differences in Mg²⁺ concentrations (0.7-1.0%) among the smectite clays are very small, and the CEC value increases with increasing the surface area as well (14). Thus, the poor dispersion of MMT 1-2 in the epoxy matrix is mainly due to the high surface area of MMT 1-2, resulting from freeze-drying.

D. CONCLUSIONS

All the smectite clays and muscovite mica investigated reduce the tensile strength but enhance the tensile moduli of epoxy resin EPON-828 cured by MPDA. Among them, Volclay HPM-20 exhibited the highest filling limit and composite strength, whereas Alsibronz Mica-4 exhibited the best processability and composite modulus.

For the clay-epoxy composites, surface treatment determines processing problems, filling limits, clay dispersions, and tensile strengths. Composite strengths increase in the order of surface treatment, freezedrying < cationic surfactant alkylammonium chloride < anionic dispersant

Na-polyacrylate. The clay concentration being equal, tensile composite strengths vary whereas tensile composite moduli remain constant within experimental errors.

LIST OF REFERENCES

- 1. S. N. Maiti and B. H. Lopez, J. Appl. Polym. Sci., 44, 353 (1992).
- P. Godard, J. L. Wertz, J. J. Biebuyck, and J. P. Mercier, *Polym. Eng. Sci.*, 29, 127 (1989).
- 3. C. G. Ek, Rheol. Acta, 27, 279 (1988).
- 4. G. M. Newaz, Polym. Compos., 7, 176 (1986).
- 5. S. N. Maiti and K. K. Sharma, J. Mater. Sci., 27, 313 (1992).
- 6. M. A. Ramos and J. P. V. Matheu, *Polym. Compos.*, 9, 105 (1988).
- 7. J. E. Stamhuis, Polym. Compos., 9, 72 (1988).
- 8. D. M. Bigg, Polym. Compos., 8, 115 (1987).
- 9. J. P. Trotignon, L. Demdoum, and J. Verdu, Composites, 23, 2563 (1992).
- 10. S. F. Xavier and J. M. Schultz, J. Mater. Sci., 25, 2428 (1990).
- 11. S. Inubushi, T. Ikeda, S. Tazuke, S. Satoh, Y. Terada, and Y. Kumagai J. Mater. Sci., 23, 1182 (1988).
- 12. S. Cacoutis, R. T. Woodhams, and P. G. K. Van de Poll, *Polym. Compos.*, 9, 51 (1988).
- 13. J. T. Pinnavaia, Science, 220, 365 (1983).
- 14. R. E. Grim, "Clay Mineralogy," 2nd ed., McGraw-Hill, New York (1968).
- 15. C. A. May, Ed., "Epoxy Resins," 2nd ed., Marcel Dekker, New York (1988).

- 16. H. Lee and K. Neville, "Handbook of Epoxy Resins," McGraw-Hill, New York (1967).
- 17. E. Busenberg and C. V. Clemency, Clays Clay Miner., 21, 213 (1973).
- 18. S. Ahmed and F. R. Jones, J. Mater. Sci., 25, 4933 (1990).
- 19. X. B. Chen and X. S. Wu, Polymer, 33, 3639 (1992).
- 20. L. E. Nielsen, J. Appl. Phys., 4, 4626 (1970).
- 21. C. A. Byrne, G. L. Hagnauer, N. S. Schneider, and R. W. Lenz, Polym. Compos., 1, 71(1980).
- 22. J. M. Charlesworth, J. Polym. Sci., polym. Phys. Ed., 17, 1557 (1979).
- 23. J. M. Charlesworth, J. Polym. Sci., polym. Phys. Ed., 17, 1571 (1979).
- 24. S. J. Swarin and A. M. Wims, Anal. Calorim., 4, 155 (1976)
- D. W. Schiering, J. E. Katon, L. T. Drzal, and V. B. Gupta, J. Appl. Polym. Sci., 34, 2367 (1987).
- 26. A.-R. Xu, T. Nishino, and K. Nakamae, *Polymer*, 33, 5167 (1992).
- 27. K. Nakamae, T. Nishino, and A.-R. Xu, Polymer, 33, 2720 (1992).
- 28. T. Nishino, and A.-R. Xu, T. Miyamoto, K. Matsumoto, and K. Nakamae, J. Appl. Polym. Sci., 45, 1239 (1992).
- K. Nakamae, T. Nishino, and A.-R. Xu, K. Matsumoto, and T. Miyamoto, J. Appl. Polym. Sci., 40, 2231 (1990).
- 30. N. Davison, W. R. McWhinnie, and A. Hooper, Clays Clay Miner., 39, 22 (1991).
- 31. M. L. Occelli, J. M. Stencel, and S. L. Suib, J. Mol. Catal., 64, 221 (1991).

- 32. M. Stoecker, K. J. Jens, T. Riis, and J. K. Grepstad, J. Chem. Soc., Faraday Trans. 1, 84, 1863 (1988).
- M. J. Remy, M. J. Genet, P. F. Lardinois, and P. P. Notte, J. Phys. Chem., 96, 2614 (1992).
- B. L. Meyers, T. H. Fleisch, G. J. Ray, J. T. Miller, and J. B. Hall,
 J. Catal., 110, 82 (1988).
- T. H. Fleisch, B. L. Meyers, G. J. Ray, J. B. Hall, and C. L. Marshall, J. Catal., 99, 117 (1986).
- 36. R. S. Swingle, II and R. S. Riggs, Anal. Chem., 5, 267 (1975).

CHAPTER II

CLAY-POLYMER NANOCOMPOSITES FORMED FROM ACIDIC MONTMORILLONITES AND EPOXY RESIN

A INTRODUCTION

Delaminated smectite clays (e.g., montmorillonite) have recently been shown to be useful materials for the design of polymer-based composite materials with novel mechanical and physical properties. One especially intriguing system, recently reported by Okada and co-workers (1, 2), is based on the exfoliation of [H₃N(CH₂)₁₁COOH]⁺-montmorillonite in a semicrystalline nylon-6 (or polyamide-6) matrix. The 9.6-Å-thin clay layers greatly improved the tensile strength (107 vs. 69 MPa), tensile modulus (2.1 vs. 1.1 Gpa), and heat distortion temperature (152 vs. 65 °C) relative to nylon-6. Kojima et al. (3) found that replacing protonated 12-aminolauric acid by protonated ε-caprolactam as the clay exchange cation imparted comparable composite tensile strength and modulus, but the higher heat distortion temperature (164 vs. 152 °C) to nylon-6.

Fujiwara and Sakamota (4) chose a very specific organoclay-polymer system to demonstrate the swelling of the clay layers in a thermoplastic polyamide matrix. [H₃N(CH₂)₅COOH]⁺-montmorillonite (9 g) was dispersed in ε-caprolactam (20 g) and the mixture was heated at 250 °C to form a clay/nylon-6 composite. The basal spacing of the organoclay in the

nylon matrix was found to be 20 Å. Related experiments have been carried out by using protonated 12-aminolauric acid $[H_3N(CH_2)_{11}COOH]^+$ as the exchange cation (5, 6). The interlayer spacing was in the range of 51-210 Å for organic montmorillonite content 5-30 wt%. For protonated ε -caprolactam as the exchange cation, the interlayer spacing was found to be ~ 250 Å (3).

It has also been reported in the patent literature (7) that swelled montmorillonite ($d_{001} = 50 \text{ Å}$) improved mechanical properties of an amine-cured epoxy resin. [$H_3N(CH_2)_{11}COOH$]⁺-montmorillonite slightly enhanced the impact resistance (1.08 vs. 0.91 J/m) and the heat distortion temperature (207 vs. 193 °C) of epoxy resin Epicoat-828 cured by p, p'-diaminodiphenylsulfone (DDS). However, it was necessary to use N, N-dimethylformamide as a swelling solvent to achieve clay delamination.

Since epoxides are reactive toward self-polymerization to polyethers, it was of interest to us to investigate the direct polymerization of an epoxy resin in the galleries of montmorillonite. The epoxy resin selected for the present study was the same epoxy resin EPON-828 as used before.

B. EXPERIMENTAL

Materials

Source clay SWy-1 (Wyoming Na⁺-montmorillonite) was obtained from the Clay Minerals Depository at the University of Missouri (Columbus, MO). Epoxy resin EPON-828 (Shell), aminocarboxylic acids $H_2N(CH_2)_{n-1}COOH$, primary diamines $H_2N(CH_2)_nNH_2$, and primary amines $CH_3(CH_2)_nNH_2$ (n = 6, and 12) (Aldrich) were used as received.

H₂N(CH₂)_{n-1}COOH, H₂N(CH₂)_nNH₂, or CH₃(CH₂)_nNH₂ (10 mmol) was dissolved in 1 L of a 0.01 N (0.02 N for [H₃N(CH₂)_nNH₃]Cl₂) HCl solution at 60 °C. Source clay SWy-1 (10 g) was thoroughly dispersed in the appropriate 0.01 N solution of interest at 60 °C for 3 h. The cation-exchanged montmorillonite was separated from the centrifugate and washed with deionized water. Centrifugation and washing were repeated until no white AgCl precipitate was observed when a drop of 0.1 N AgNO₃ was added to the centrifugate. The washed onium ion-exchanged montmorillonite was dispersed in 600 mL of deionized water and freezedried in a Labconco Freeze Dryer Model 18. The freeze-dried onium ion-montmorillonite was then sieved to < 325-mesh.

The onium ion-montmorillonite (0.79 g) was added to 15 g of epoxy resin EPON-828 and the 5/95 (w/w) clay/epoxy mixture was magnetically stirred in a 250-mL beaker at 75 °C for 30 min. The beaker was sealed with aluminum foil and the temperature was then raised at a rate of ~ 20 °C/min to the clay delamination-epoxy polymerization temperature. The liquid-to-powder transformation of the mixture and the concomitant formation of the clay-epoxy nanocomposite took place within a period of one minute. The transformation was accompanied by an increase in the bulk volume (up to sixfold) and a large amount of heat released.

Characterization

The clay-epoxy nanocomposite sample for powder XRD studies was firmly pressed onto a Rigaku sample holder. The diffraction pattern was then recorded by monitoring the diffraction angle 2θ from 2° to 45° on a Rigaku Rotaflex Ru-200BH X-ray diffractometer. The diffractometer was

equipped with a Ni-filtered Cu- K_{α} radiation source operated at 45 kV and 100 mA. The scanning speed and the step size used were 2°/min and 0.02°, respectively. Quartz was used as a calibration standard.

A small amount of clay-epoxy nanocomposite powder for TEM studies was added to a Spurr's mixture in a silicon rubber mold, which was then placed in an oven at 70 °C overnight. The cured epoxy block was trimmed and thin-sectioned with a diamond knife in a microtome. The resulting ultra-thin sections (~ 90 nm in thickness) were mounted on a plastic-film support on a copper grid and examined by a JEOL 100CX transmission electron microscope operated at an accelerating voltage of 100 kV.

The organoclay-epoxy resin mixture for DSC analysis (5 mg) was placed in an aluminum sample pan, which was then sealed hermetically. The sample and reference pans were placed in the cell of a Du Pont 910 differential scanning calorimeter. The DSC cell was then heated under nitrogen (50 mL/min) to 350 °C at a rate of 20 °C/min. Indium (mp, 156.6 °C and ΔH_m , 28.42 J/g) was used for DSC calibrations. In the case of the neat epoxy resin, the temperature was raised to 450 °C under the same experimental conditions. However, the sample size was reduced to 2.5 mg to prevent the build-up pressure from breaking loose the sealed sample pan.

[H₃N(CH₂)₁₁COOH]⁺-montmorillonite (20 mg) for TGA analysis was placed in a platinum sample container, which was then placed in the thermobalance of a Du Pont 990 thermogravimetric analyzer. The sample weight was tared and the sample was then heated under nitrogen (100 mL/min) to 650 °C at a rate of 20 °C/min.

An equivalent set of experiments using $[H_3N(CH_2)_{n-1}CH_3]^+$ (n = 6 and 12), NH_4^+ , and H^+ as exchange cations was carried out under the same experimental conditions.

C. RESULTS AND DISCUSSION

Primary amines and acid anhydrides (equivalent to carboxylic acids) are two types of most commonly used curing agents for epoxy resins because primary amino and carboxylic groups are highly reactive toward epoxy rings. Protonated aminocarboxylic acids and primary diamines $[H_3N(CH_2)_{n-1}COOH]^+$, $[H_3N(CH_2)_{n}NH_2]^+$, and $[H_3N(CH_2)_{n}NH_3]^{2+}$ (n = 6 and 12) have been used as delaminating agents or catalysts rather than curing agents in this work. It is essential to treat these organic acids and diamines with dilute aqueous HCl solution. Acid treatment converts aminocarboxylic acids and primary diamines into the corresponding water-soluble onium ions, which can easily replace interlayer cations such as Na⁺ and Ca²⁺ in montmorillonite. More importantly, protonation weakens the carbon-oxygen bond and facilitates the epoxy ring opening.

It is not the undissociated acid $H_2N(CH_2)_{n-1}COOH$ but the dipolar ion structure (I) that accounts for the chemical and physical properties of an aminocarboxylic acid. When an aminoacid dissolves in aqueous HCl solution, protonation converts the dipolar ion I into the cation II.

$$H_3N(CH_2)_{n-1}CO$$
 $+H^+$ $H_3N(CH_2)_{n-1}COH$ II

Evidence of Clay Delamination

The delamination of the onium ion-montmorillonites in the cured epoxy resin may be confirmed by X-ray powder diffractometry (XRD). For instance, as shown in Figure II.1c, no clay diffraction peaks are observed for a clay-epoxy nanocomposite containing 5 wt% $[H_3N(CH_2)_{11}COOH]^+$ -montmorillonite. Only a very diffuse scattering peak characteristic of the amorphous cured epoxy resin (or polyether) appears in the XRD pattern. The absence of a 17.0-Å peak for $[H_3N(CH_2)_{11}COOH]^+$ -montmorillonite (Figure II.1a) suggests that the clay tactoids have been exfoliated and the 9.6-Å-thin clay layers dispersed at the molecular level. However, it may also mean that the clay basal spacing is greater than 44.2 Å (e.g., $2\theta = 2^\circ$) or the clay layered structure collapses. The clay peaks with reduced intensities (Figure II.1b) show the clay layered structure partially collapses after pristine $[H_3N(CH_2)_{11}COOH]^+$ -montmorillonite is heated at 229 °C under nitrogen for 1 min, as explained later.

Transmission electron microscopy (TEM) provides unambiguous evidence for the delamination of $[H_3N(CH_2)_{11}COOH]^+$ -montmorillonite in the cured epoxy resin. As shown in Figure II.2, the TEM micrographs of a 5 wt% clay-polyether nanocomposite reveal that the micron-sized clay tactoids indeed have been exfoliated by the polymer. The interlayer spacing ranges up to $\sim 0.2~\mu m$ or 2,000 Å. Additional complementary results such as the reaction temperature and the heat of reaction are obtained from differential scanning calorimetry (DSC). Figure II.3 shows the DSC curve of a 5/95 (w/w) mixture of $[H_3N(CH_2)_{11}COOH]^+$ -montmorillonite and epoxy resin EPON-828. The thermogram indicates that the spontaneous clay exfoliation-epoxy polymerization takes place at an onset temperature of

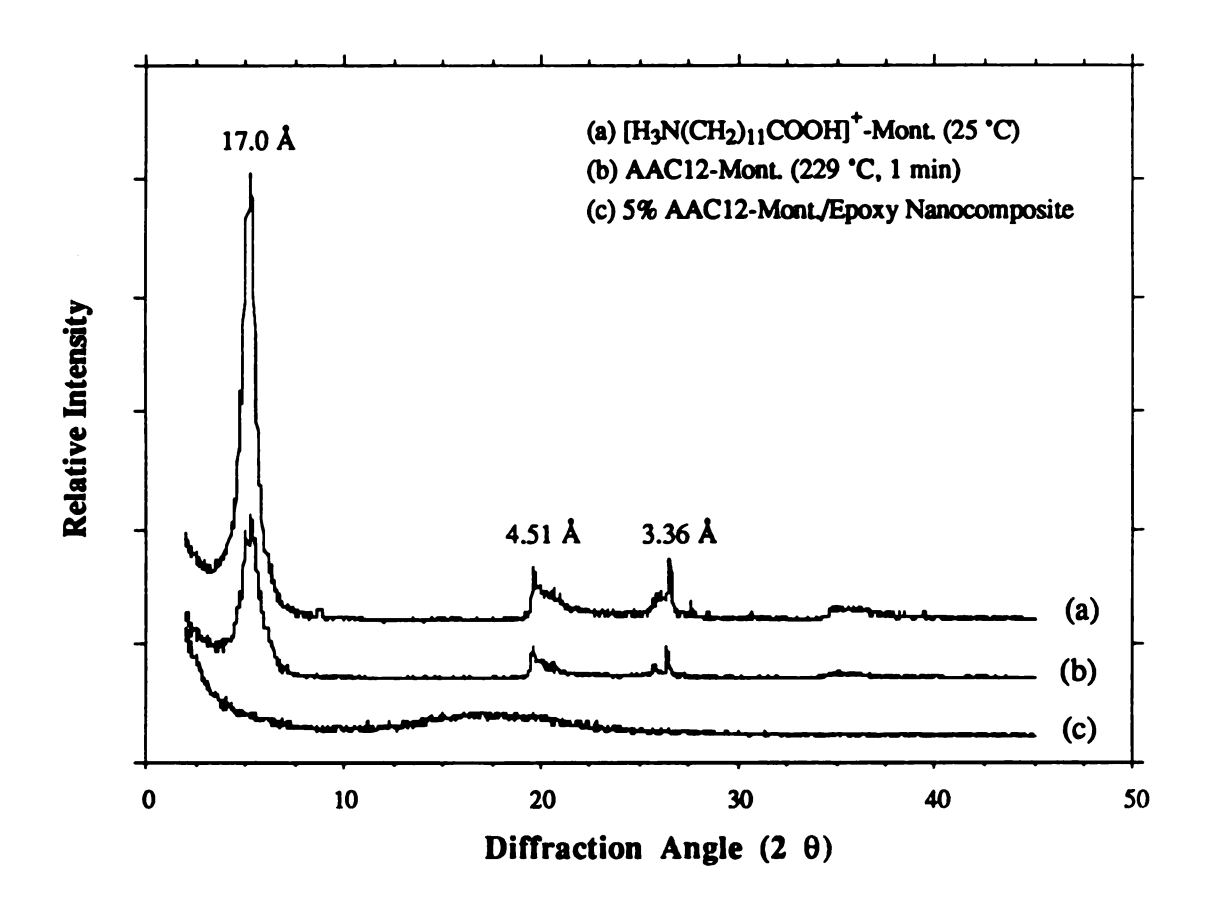


Figure II.1. X-ray powder diffraction (XRD) patterns of (a) $[H_3N(CH_2)_{11}COOH]^+$ -montmorillonite (AAC12-Mont.) (25 °C), (b) AAC12-Mont. (229 °C, 1 min) and (c) a clay-epoxy nanocomposite containing 5 wt% AAC12-Mont.

Figure II.2. Transmission electron microscopy (TEM) micrographs of a clay-epoxy nanocomposite containing 5 wt% $[H_3N(CH_2)_{11}COOH]^+$ -montmorillonite: (a) x10,000 and (b) x58,000.





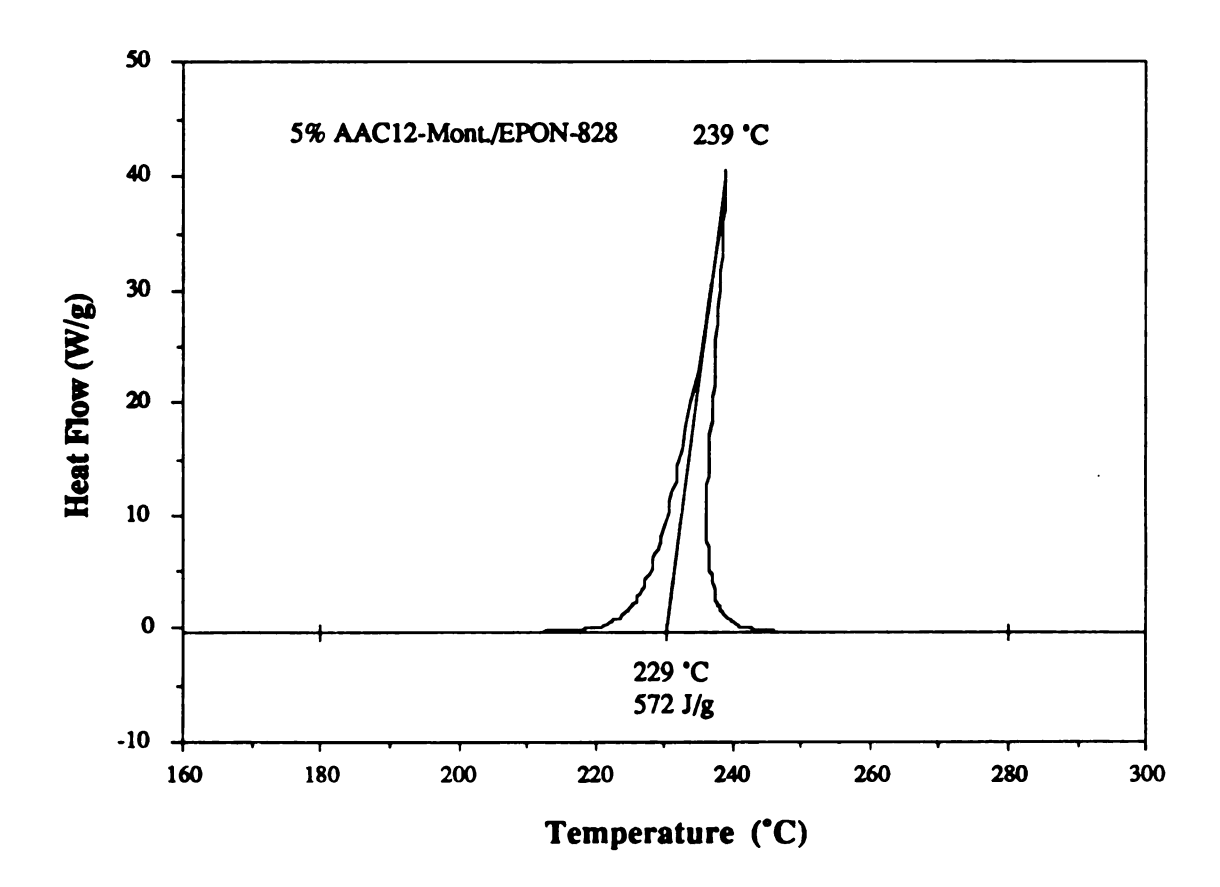


Figure II.3. Differential scanning calorimetry (DSC) thermogram of the epoxy polymerization catalyzed by 5 wt% [H₃N(CH₂)₁₁COOH]⁺-montmorillonite, a heating rate of 20 °C/min being used.

229 °C. Based on the integrated peak area and the heating rate, the heat of reaction is 572 J/g.

For comparison, the DSC thermograms of the neat epoxy resin and $[H_3N(CH_2)_{11}COOH]^+$ -montmorillonite are shown in Figures II.4 and II.5, respectively. It should be noted that the scale of the heat flow in Figure II.5 is much smaller than that in either Figure II.3 or II.4. Without an effective catalyst (acid or base), the homo- or self-polymerization of the epoxy resin involves the initiation reaction (Equation II.1) and etherification (Equation II.2) to form polyether at elevated temperatures. R'OH is any impurity solvent (e.g., water) or epoxy monomer possessing one or two hydroxyl groups (EPON-828: 10% of n = 1 and 2% of n = 2).

R'OH +
$$CH_2$$
-CHR $\xrightarrow{\Delta}$ R'O-CH₂-CHR (II.1)

OH
$$R'O-CH_2-CHR + n CH_2-CHR$$
 $\xrightarrow{\Delta}$ $R'O(CH_2-CHRO)_nCH_2-CHR$ (II.2)

As shown in Figures II.5 and II.6, DSC and TGA curves indicate that $[H_3N(CH_2)_{11}COOH]^+$ -montmorillonite loses surface and interparticle pore water between 40 and 200 °C. Interlayer water is liberated in the region of 200-300 °C. The loss of hydroxyl groups in the clay framework (or dehydroxylation) occurs between 300 and 650 °C. It is noted that 12-aminolauric acid (mp, 186 °C) loses the crystal water and totally decomposes over temperature ranges 200-400 °C and 400-500 °C, respectively. The heat absorption and the weight loss shown by the DSC and TGA curves, respectively, substantiate the XRD pattern (Figure II.1b) that the partial loss of interlayer water results in the reduced peak intensity

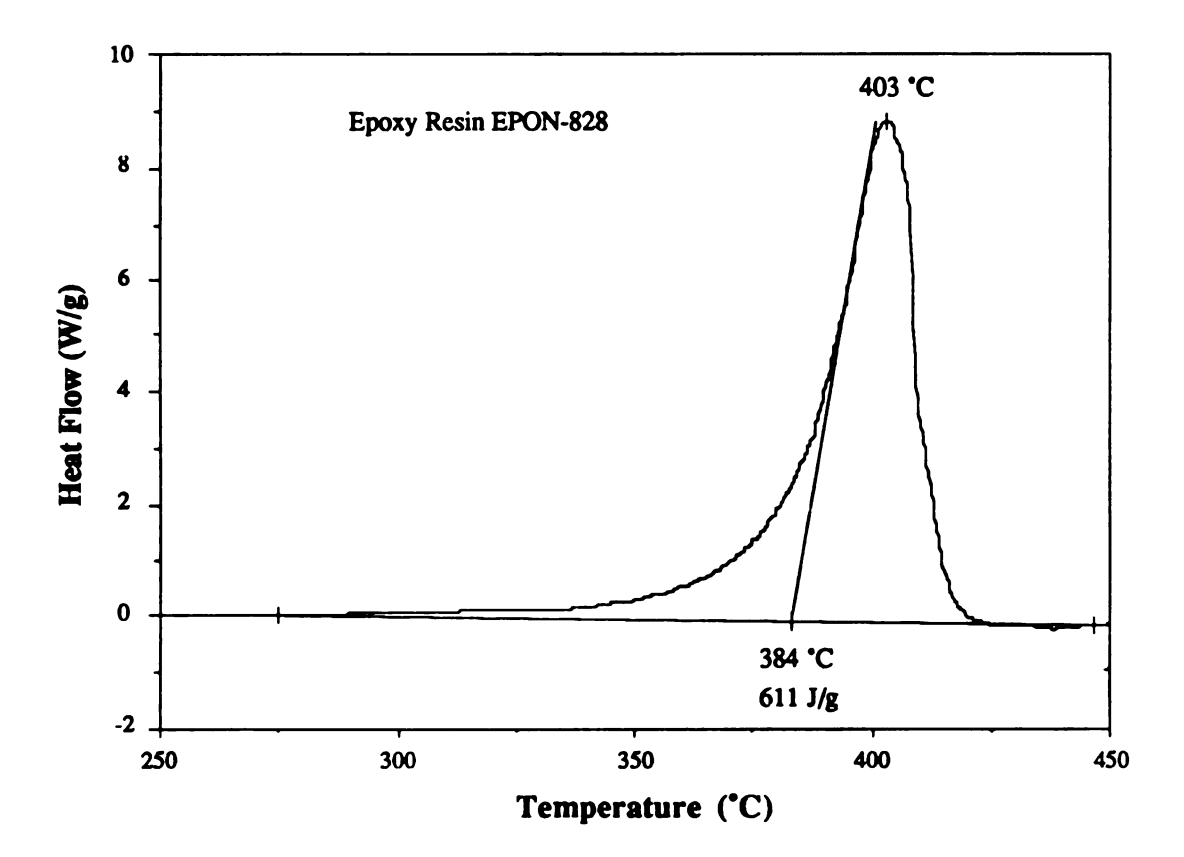


Figure II.4. DSC thermogram of the uncatalyzed self-polymerization of epoxy resin EPON-828, a heating rate of 20 °C/min being used.

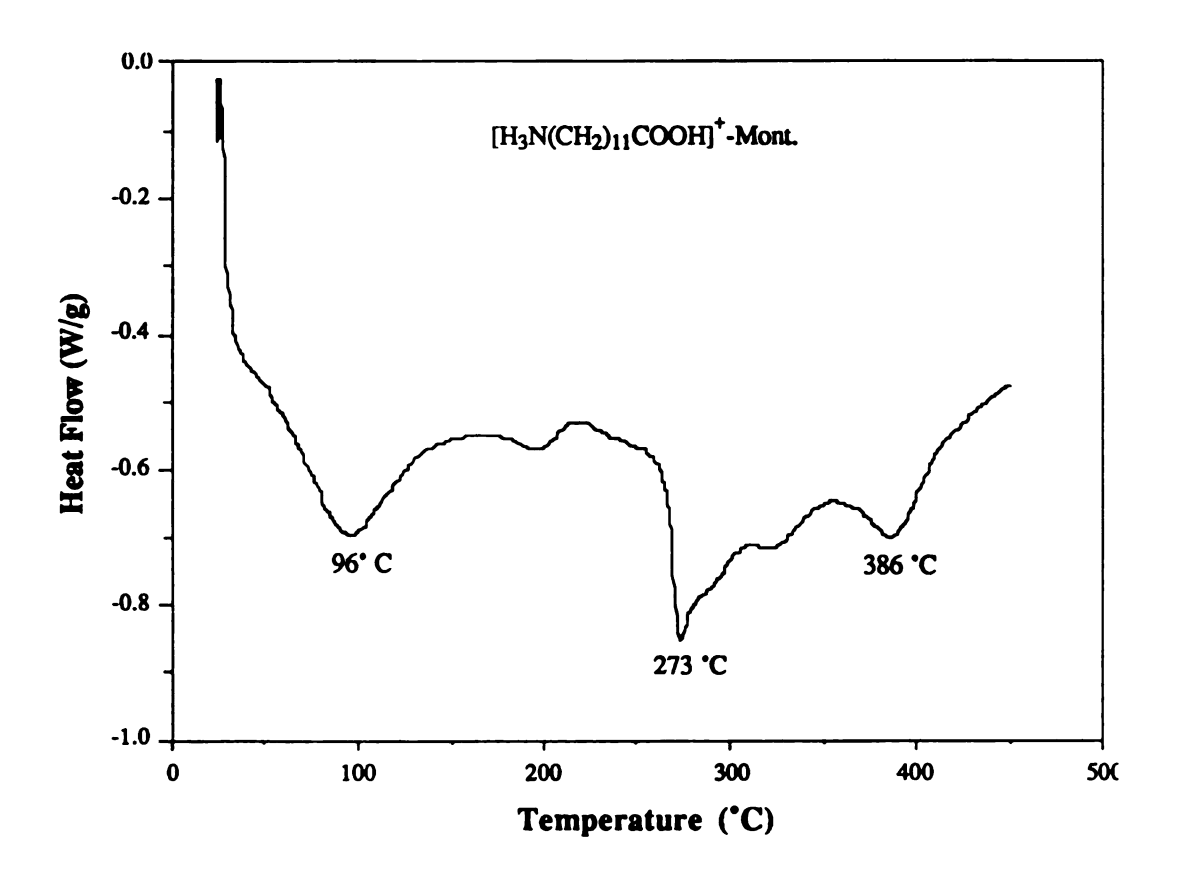


Figure II.5. DSC thermogram of $[H_3N(CH_2)_{11}COOH]^+$ -montmorillonite, a heating rate of 20 °C/min used.

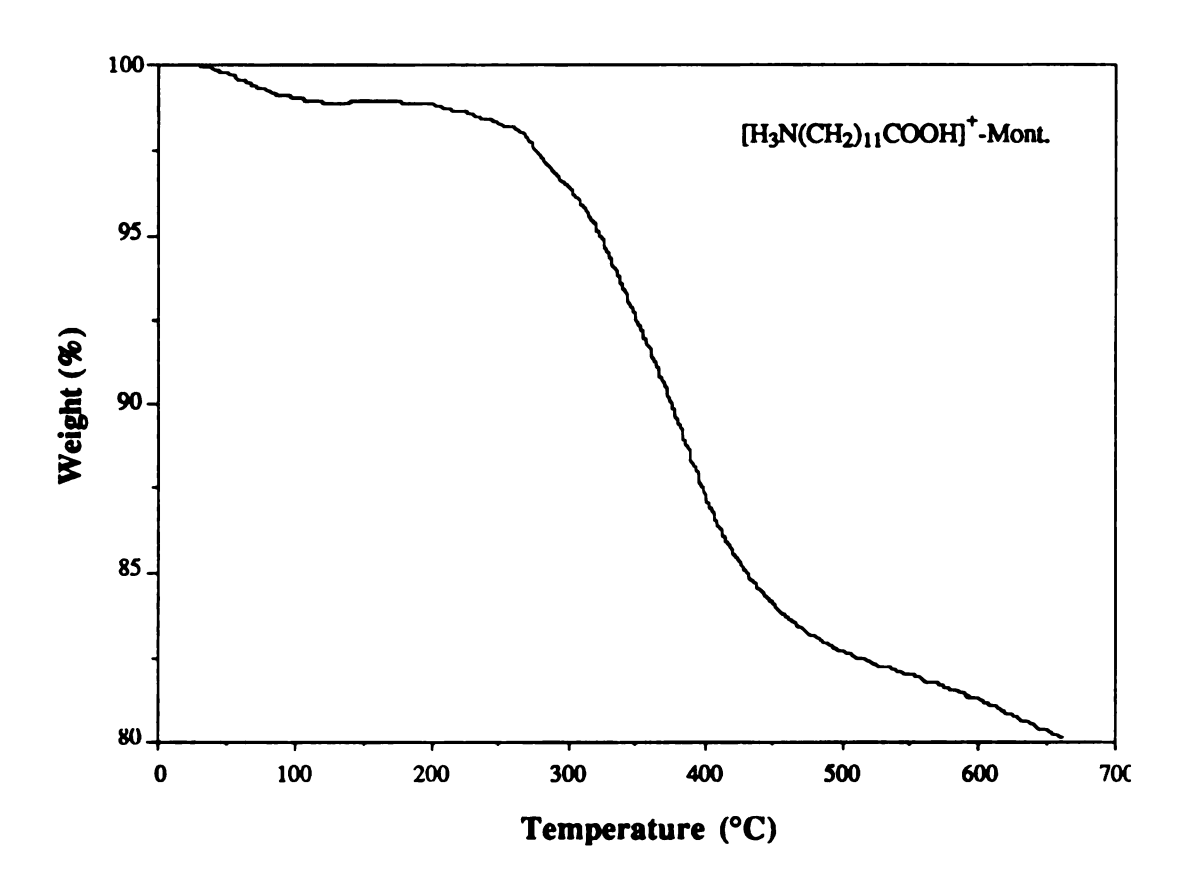


Figure II.6. Thermogravimetric analysis (TGA) curve of $[H_3N(CH_2)_{11}COOH]^+$ -montmorillonite, a heating rate of 20 °C/min used.

for $[H_3N(CH_2)_{11}COOH]^+$ -montmorillonite heated at 229 °C for 1 min. More importantly, the heat of reaction for $[H_3N(CH_2)_{11}COOH]^+$ -montmorillonite (especially 5 wt%) is much smaller than that for either the uncatalyzed epoxy polymerization or the epoxy polymerization catalyzed by 5 wt% $[H_3N(CH_2)_{11}COOH]^+$ -montmorillonite

Reaction Mechanism

According to the evidence presented above, the delamination of the onium ion-montmorillonites in the epoxy resin or epoxy polymerizations catalyzed by the onium ion-montmorillonites at elevated temperatures can be rationalized by the following general equations:

Protonation:

$$O$$
 CH_2 - CHR + H^+A
 CH_2 - CHR + A
(II.3)

Initiation:

$$R^{1}NH_{2} + CH_{2}-CHR \longrightarrow R^{1}HN-CH_{2}-CHR + H^{+}$$
 (II.5)

OH OH OH OH
$$R^1$$
HN-CH₂-CHR + CH₂-CHR \longrightarrow R^1 N(CH₂-CHR)₂ + H^+ (II.6)

Propagation:

$$R^{2}OH + n CH_{2}-CHR$$
 $\xrightarrow{H^{+}}$ $R^{2}O(CH_{2}-CHRO)_{n-1}CH_{2}-CHR + H^{+}$ (II.7)

where H⁺A is any protonated aminocarboxylic acid or primary diamine; R¹NH₂ is any molecule containing one or two amino groups; and R²OH is any monomer or oligomer possessing one or more hydroxyl groups. At the delamination-polymerization temperature, epoxy monomers first react with protonated aminocarboxylic acids and primary diamines intercalated on the edges of clay particles. The protonation of epoxy rings (Equation II.3) takes place first, followed by the cleavage of epoxy rings (Equations II.4-6). The reactions rapidly propagate toward clay interlayer space and the propagation causes the expansion of the clay gallery region. In the meantime, various acid-catalyzed etherifications (Equation II.7) occur to form polyether in the expended region and this results in the complete delamination of clay layers. The cured epoxy resin or polyether in the clay galleries becomes phase-segregated from the uncured resin. This gives rise to the liquid-to-powder transformation characteristic and a substantial (ca. 5-6 fold) increase in the bulk volume upon the formation of clay-epoxy nanocomposites. The rapid and complete clay delamination-epoxy polymerization is accompanied by a large heat of reaction.

Reaction Temperature

Listed in Table II.1, the onset temperatures of the epoxy polymerization-montmorillonite delamination reactions increase in the order $[H_3N(CH_2)_{n-1}COOH]^+ < [H_3N(CH_2)_nNH_3]^{2+} < [H_3N(CH_2)_nNH_2]^+$ (n = 6 and 12). That is, the polymerization-delamination temperature increases

Table II.1. DSC and XRD Data for Epoxy Polymerizations Catalyzed by 5 wt %

Protonated Aminocarboxylic acid- and Primary Diamine-Montmorillonites^a

Interlayer Cation	PolymDel. Temp. ^b (°C)	Heat of Reaction (J/g)	Heat of Polym. ^c (kcal/mol)	Basal Spacing (Å)
$[H_3N(CH_2)_{11}COOH]^+$	229 ± 1	572 ± 16	54.4 ± 1.5	17.05 ± 0.14
[H ₃ N(CH ₂) ₅ COOH] ⁺	248 ± 1	565 ± 6	53.7 ± 0.5	13.33 ± 0.01
$[H_3N(CH_2)_{12}NH_3]^{2+}$	271 ± 1	566 ± 8	53.8 ± 0.8	13.39 ± 0.08
$[H_3N(CH_2)_6NH_3]^{2+}$	273 ± 2	568 ± 7	54.0 ± 0.7	13.12 ± 0.05
$[H_3N(CH_2)_{12}NH_2]^+$	281 ± 2	563 ± 7	53.5 ± 0.7	13.48 ± 0.03
[H ₃ N(CH ₂) ₆ NH ₂] ⁺	287 ± 2	557 ± 3	53.0 ± 0.3	13.19 ± 0.07

^aDSC data were obtained by using a heating rate of 20 °C/min.

^bThe onset epoxy polymerization-clay delamination temperature.

^cThe heat of polymerization for the epoxy equivalent is halved.

with decreasing acidity of the interlayer cation. Protonation weakens the carbon-oxygen bond and facilitates epoxy ring opening. For a homologous series of the onium ions, the polymerization-delamination temperature is correlated with the basal (d_{001}) spacing of the onium ion-montmorillonite. A larger basal spacing gives the epoxy monomers easier access to the interlayer onium ions and this leads to a lower polymerization-delamination temperature. In general, the basal spacing of an organoclay depends primarily on the alkyl chain length (or carbon number) and the spatial arrangement of the onium ion intercalated on the gallery surfaces (8).

It is noted that all the onium ion-montmorillonites used in this study. except [H₃N(CH₂)₁₂COOH]⁺-montmorillonite (17.0 Å), have similar basal spacings (13.1-13.5 Å). The small basal spacings indicate that the shortand long-chain protonated aminocarboxylic acids and primary diamines lie flat and form monolayers in the clay galleries. As shown in Figure II.7, the spatial arrangement of divalent $[H_3N(CH_2)_{12}NH_3]^{2+}$ in montmorillonite is due to strong ionic bonding between ammonium groups and negativelyunusually charged lavers. The small basal spacing [H₃N(CH₂)₁₂NH₂]⁺-montmorillonite might arise from the sharing of a proton between two adjacent amino groups.

Heat of Reaction

Table II.1 shows that the heat of the polymerization-delamination reaction (557-572 J/g) remains constant within experimental errors regardless of the exchange cations used. Since the heat of reaction arises primarily from the polymerization of the epoxy resin, it should remain unchanged provided the epoxy concentration (wt%) is constant. The average heat of reaction is 565 J/g for 5/95 (w/w) organoclay/epoxy resin,

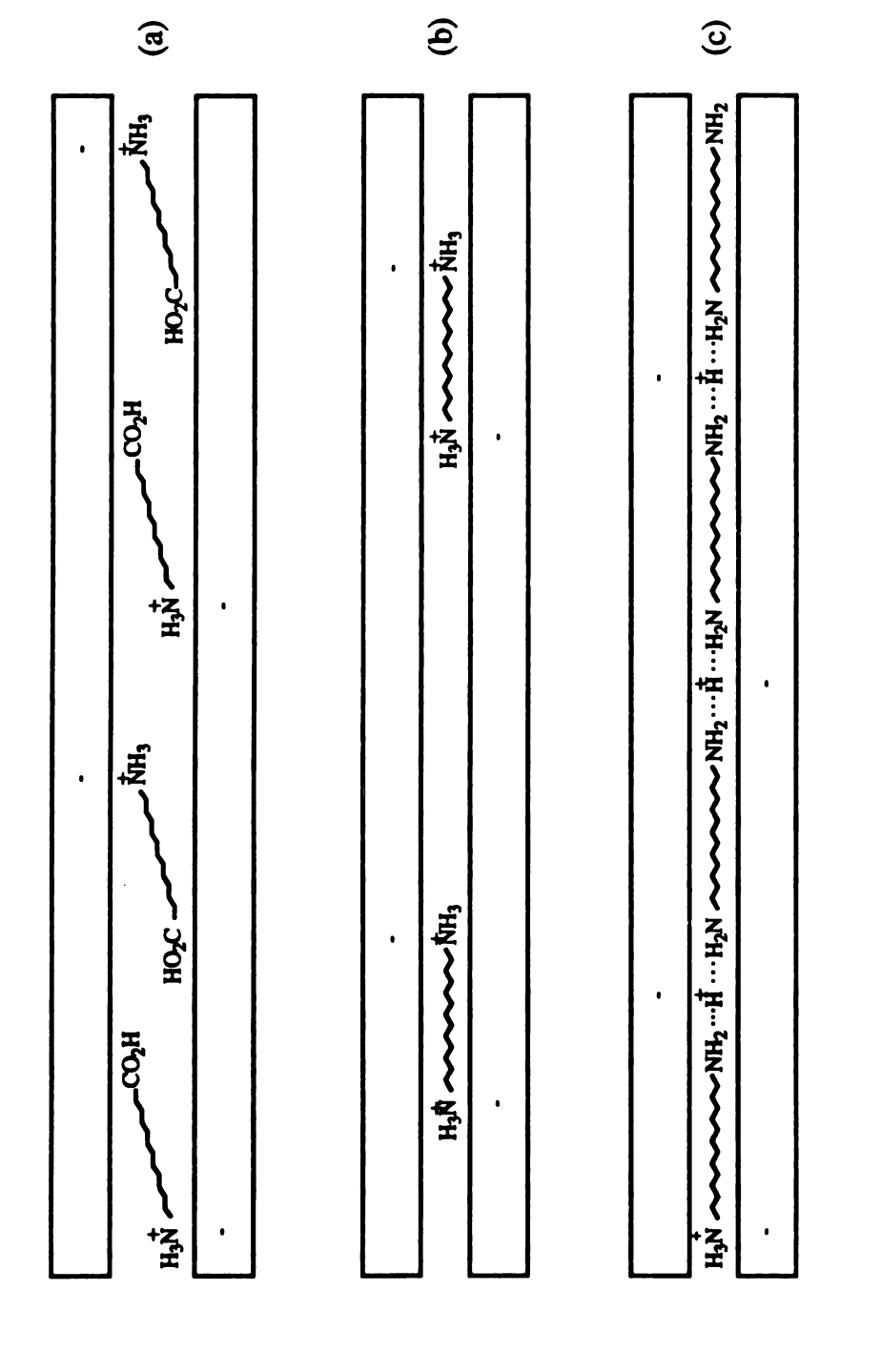


Figure II.7. Spatial arrangements of interlayer cations in montmorillonites: (a) [H₃N(CH₂)₁₁COOH]⁺, (b) $[H_3N(CH_2)_{12}NH_3]^{2+}$, and (c) $[H_3N(CH_2)_{12}NH_2]^+$.

or 595 J/g for the neat epoxy resin. This value is equivalent to a value of 53.7 kcal/mole or 26.9 kcal/mole for the epoxy equivalent, which is a typical value for the epoxy resin cured by primary amines (9, 10). However, Table II.2 shows that the amount of the onium ions used (1.80-3.57 mmol) to form the nanocomposites is sufficient to cure only 1.4-2.9 % of the epoxy resin. Therefore, the major reaction is the acid-catalyzed epoxy etherification.

Effects of Clay Concentration

[H₃N(CH₂)₁₁COOH]⁺- and [H₃N(CH₂)₅COOH]⁺-montmorillonites have been chosen for further investigation because they have relatively low reaction temperatures. Figure II.8 shows that the polymerizationdelamination temperature rapidly decreases and levels off as the clay concentration reaches 1 wt% for [H₃N(CH₂)₁₁COOH]⁺-montmorillonite or 5 wt% for [H₃N(CH₂)₅COOH]⁺-montmorillonite. That is, only a very small organoclay concentration is sufficient to effectively catalyze the epoxy polymerization and dramatically reduces the epoxy polymerization temperature. For instance, the uncatalyzed epoxy self-polymerization temperature is 384 °C, compared to 241 and 264 °C for epoxy polymerizations catalyzed by 0.2 wt% [H₃N(CH₂)₁₁COOH]⁺- and H₃N(CH₂)₅COOH]⁺-montmorillonites, respectively. However, in Figure II.9 the broad DSC curves indicate that such epoxy polymerizations are relatively sluggish. Moreover, the relatively small values of the heat of reaction (560 and 545 J/g) indicate that a clay concentration of 0.2 wt% is too small to achieve the complete epoxy polymerization. Based on the extrapolated heat of reaction obtained below, the curing degrees are 93.8 and 91.1% for epoxy polymerizations catalyzed by 0.2 wt%

Table II.2. Estimated Epoxy Cure Percents Due to Protonated Aminocarboxylic

Acids and Primary Diamines

Interlayer Cation	Formula Weight	Equiv. Weight ^a	# mmol ^b	Cure Equiv.	%Epoxy Cure ^b
[H ₃ N(CH ₂) ₁₁ COOH] ⁺	216	115	3.32	3	1.98
[H ₃ N(CH ₂) ₅ COOH] ⁺	132	108	3.52	3	2.10
$[H_3N(CH_2)_{12}NH_3]^{2+}$	202	106	1.80	4	1.43
$[H_3N(CH_2)_6NH_3]^{2+}$	118	103	1.85	4	1.48
$[H_3N(CH_2)_{12}NH_2]^+$	201	114	3.35	4	2.67
[H ₃ N(CH ₂) ₆ NH ₂] ⁺	117	107	3.57	4	2.83

^aThe resulting weight of 100 g of montmorillonite SWy-1 (cation exchange capacity, 76.4 meq/100g) after the cation-exchange reaction.

^bBased on 100g of 5/95 (w/w) organoclay/epoxy resin (251 mmol or 503 meq).

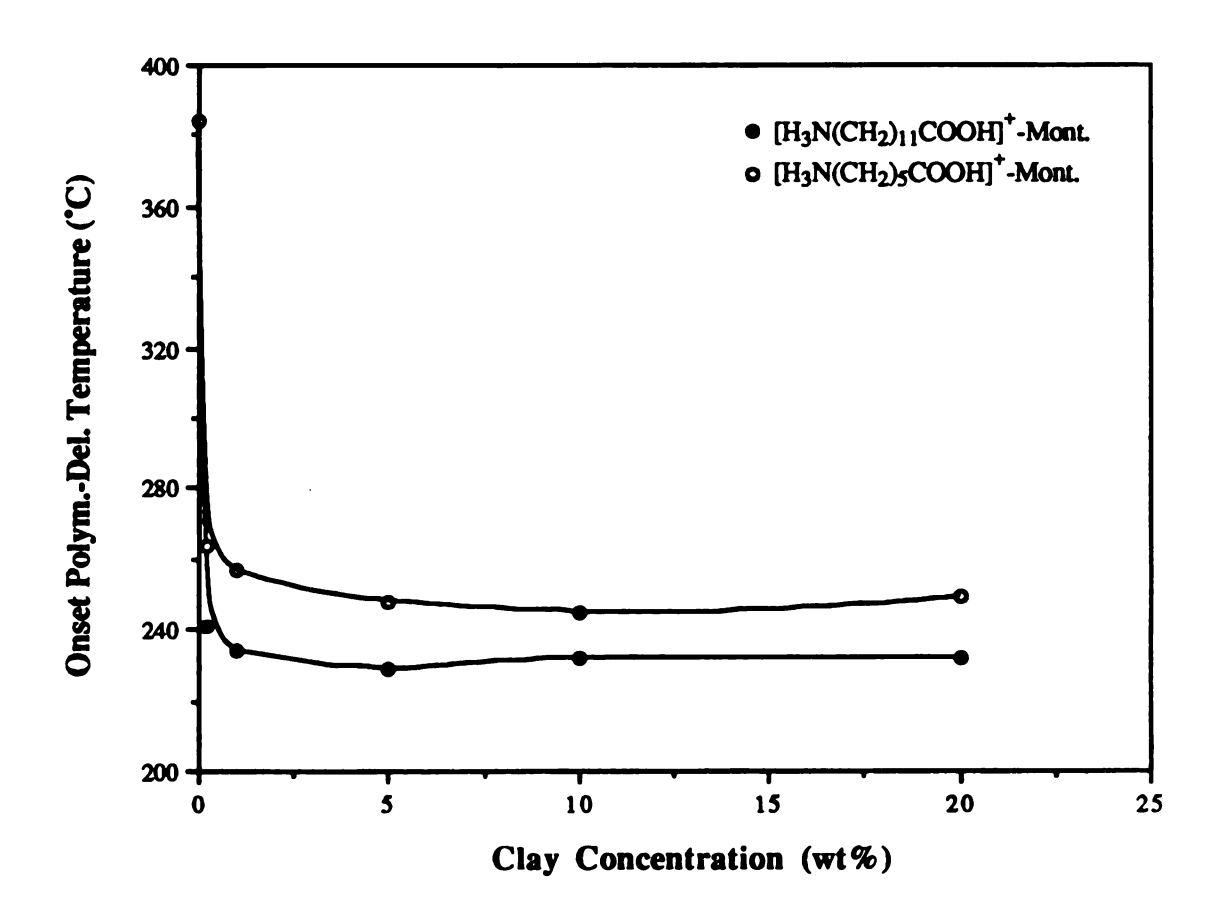


Figure II.8. Onset temperature of the epoxy polymerization-clay delamination as a function of the clay concentration for (\bullet) $[H_3N(CH_2)_1COOH]^+$ and (\circ) $[H_3N(CH_2)_5COOH]^+$ -montmorillonites.

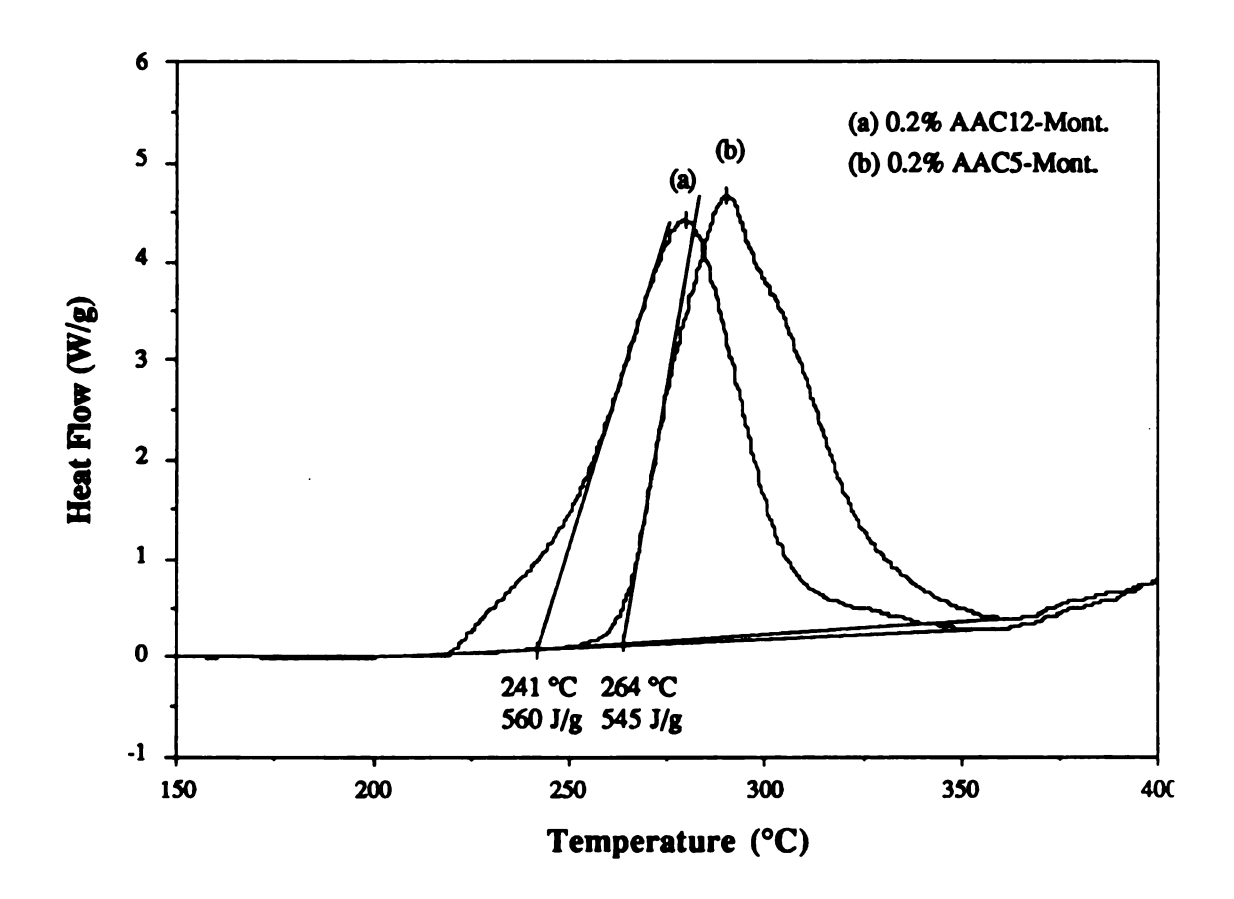


Figure II.9. DSC thermograms of epoxy polymerizations catalyzed by 0.2 wt% (a) $[H_3N(CH_2)_{11}COOH]^+$ and (b) $[H_3N(CH_2)_5COOH]^+$ -montmorillonites, a heating rate of 20 °C/min being used.

[H₃N(CH₂)₁₁COOH]⁺- and [H₃N(CH₂)₅COOH]⁺-montmorillonites, respectively.

In Figure II.10 the heat of reaction is plotted against the clay concentration for [H₃N(CH₂)₁₁COOH]⁺- and [H₃N(CH₂)₅COOH]⁺montmorillonite. In each case the heat of reaction is proportional to the epoxy concentration. The extrapolated values are 603 and 604 J/g or 54.5 kcal/mol for the neat epoxy resin. The linear relationship again shows that the heat of reaction is primarily due to the polymerization of the epoxy resin. The greater slope for $[H_3N(CH_2)_5COOH]^+$ -montmorillonite suggests that the polymerization of the epoxy resin is relatively incomplete, especially at high clay concentrations. The ratio of the heat of reaction for [H₃N(CH₂)₁₁COOH]⁺-montmorillonite to that for [H₃N(CH₂)₅COOH]⁺montmorillonite decreases from 1.00 to 0.94, as the clay concentration increases form 1 to 20 wt%. At higher clay concentrations, the entrapment of the epoxy resin between clay particles may limit the formation of longchain polyether. Thus, 5 wt% is an optimal clay concentration to obtain both high curing degree and low reaction temperature of the epoxy polymerization catalyzed by the onium ion-montmorillonite.

Kinetics Parameters

Non-isothermal or dynamic DSC have been used to obtain kinetics parameters such as the activation energy and the pre-exponential factor. Borchardt and Daniels (11) developed one of two basic methods for dynamic DSC, using a single DSC curve generated at a constant heating rate. However, compared with isothermal DSC, this method often overestimated activation energies and pre-exponential factors for most

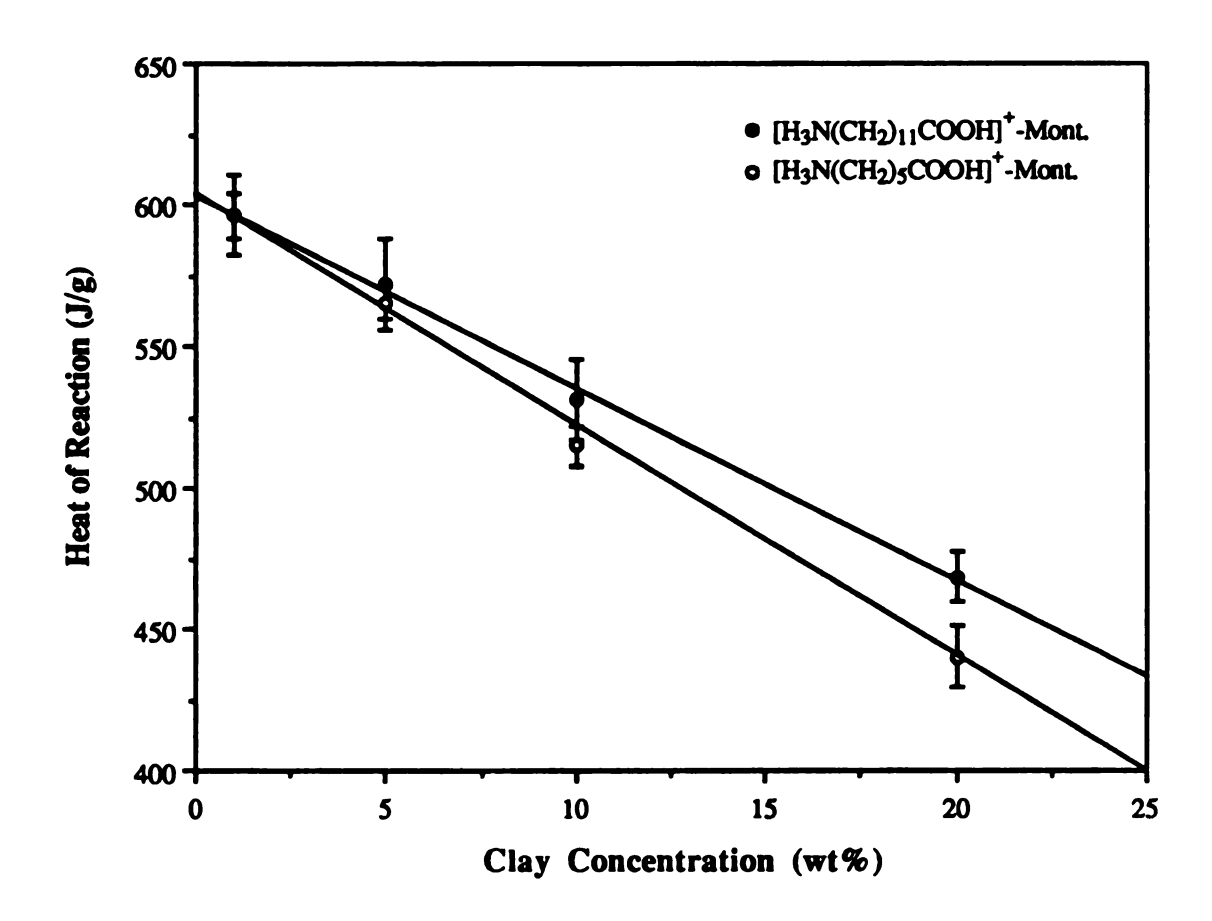


Figure II.10. Heat of reaction as a function of the clay concentration for (*) $[H_3N(CH_2)_{11}COOH]^+- \text{ and (o) } [H_3N(CH_2)_5COOH]^+-montmorillonites.$

reactions (12-14). Kissinger (15) derived the following equation to evaluate the activation energy (E_a) regardless of the reaction order (n), which was assumed to remain constant throughout the reaction:

$$\frac{d\ln \varphi}{d\left(\frac{1}{T_p}\right)} = -\frac{E_a}{R} - 2T_p \tag{II.8}$$

where T_p is the peak maximum temperature (K) and φ is the heating rate (°C/min or K/min). In case E_a/R is much greater than $2T_p$, the slope of the plot of $\ln \varphi$ vs. $1/T_p$ is equal to - E_a/R , where R is the gas constant (1.987 cal/Kmol).

A typical plot of multiple DSC curves generated at various heating rates (e.g., 15-25 °C/min) for the epoxy polymerization catalyzed by the cation-exchanged montmorillonite (e.g., 5 wt% $[H_3N(CH_2)_{11}COOH]^+$ -montmorillonite) is shown in Figure II.11. The peak maximum temperature increases with increasing the heating rate. Despite the increased peak area (A_p) and the heating rate, the heat of reaction (q) remains constant, as predicted by the following equations:

$$A_{p} = \int_{T_{i}}^{T_{f}} W dT = \int_{T_{i}}^{T_{f}} \left(\frac{dq}{dt}\right) dT = \int_{0}^{q} \left(\frac{dT}{dt}\right) dq = \int_{0}^{q} \varphi dq$$

where W is the heat flow and T is the temperature. Figure II.12 clearly shows excellent linear relationships between $\ln \varphi$ and $1/T_p$ for epoxy polymerizations catalyzed by 5 wt% $[H_3N(CH_2)_{11}COOH]^+$ - and $[H_3N(CH_2)_5COOH]^+$ -montmorillonites, respectively. However, the ratios

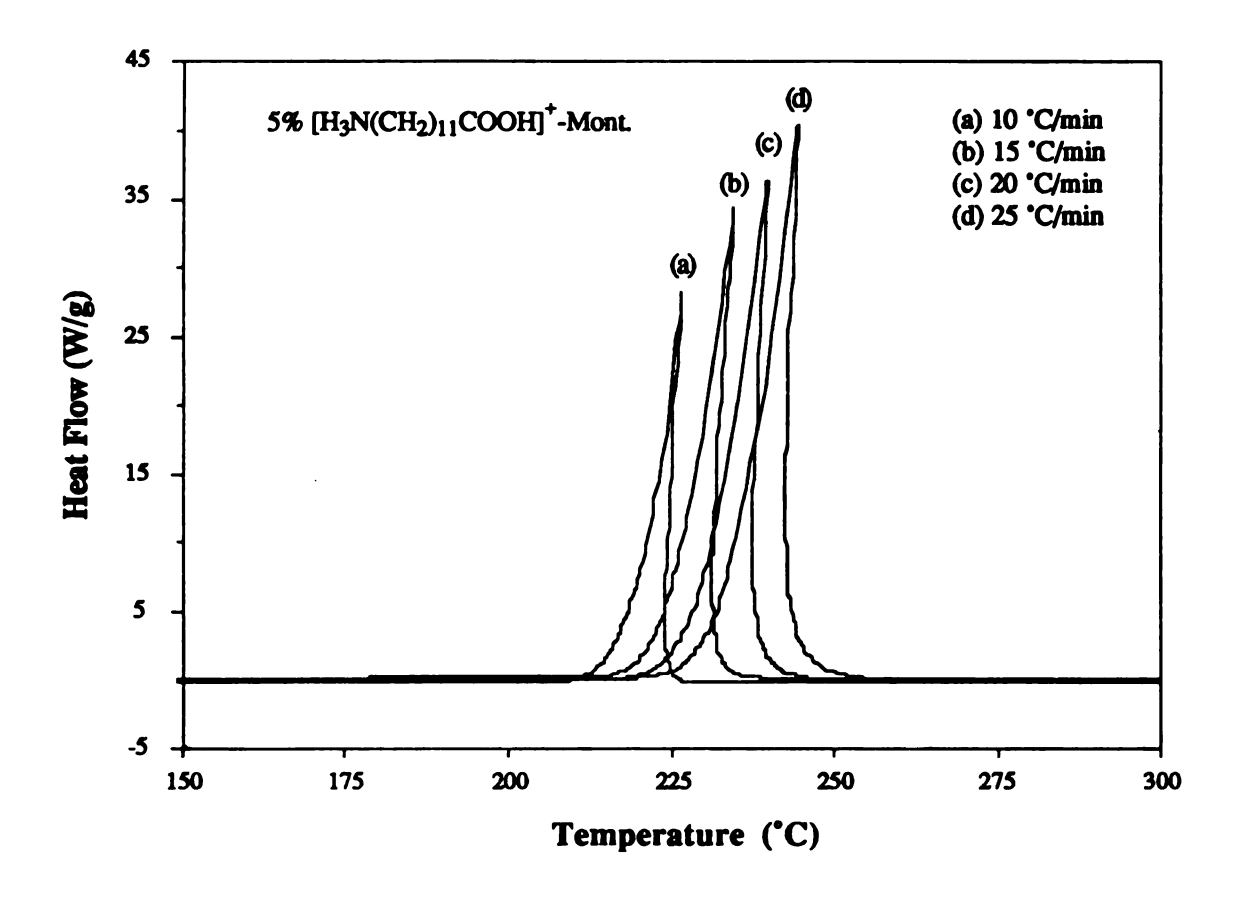


Figure II.11. DSC thermograms of the epoxy polymerization catalyzed by 5 wt% $[H_3N(CH_2)_{11}COOH]^+$ -montmorillonite at various heating rates: 10, 15, 20, and 25 °C/min.

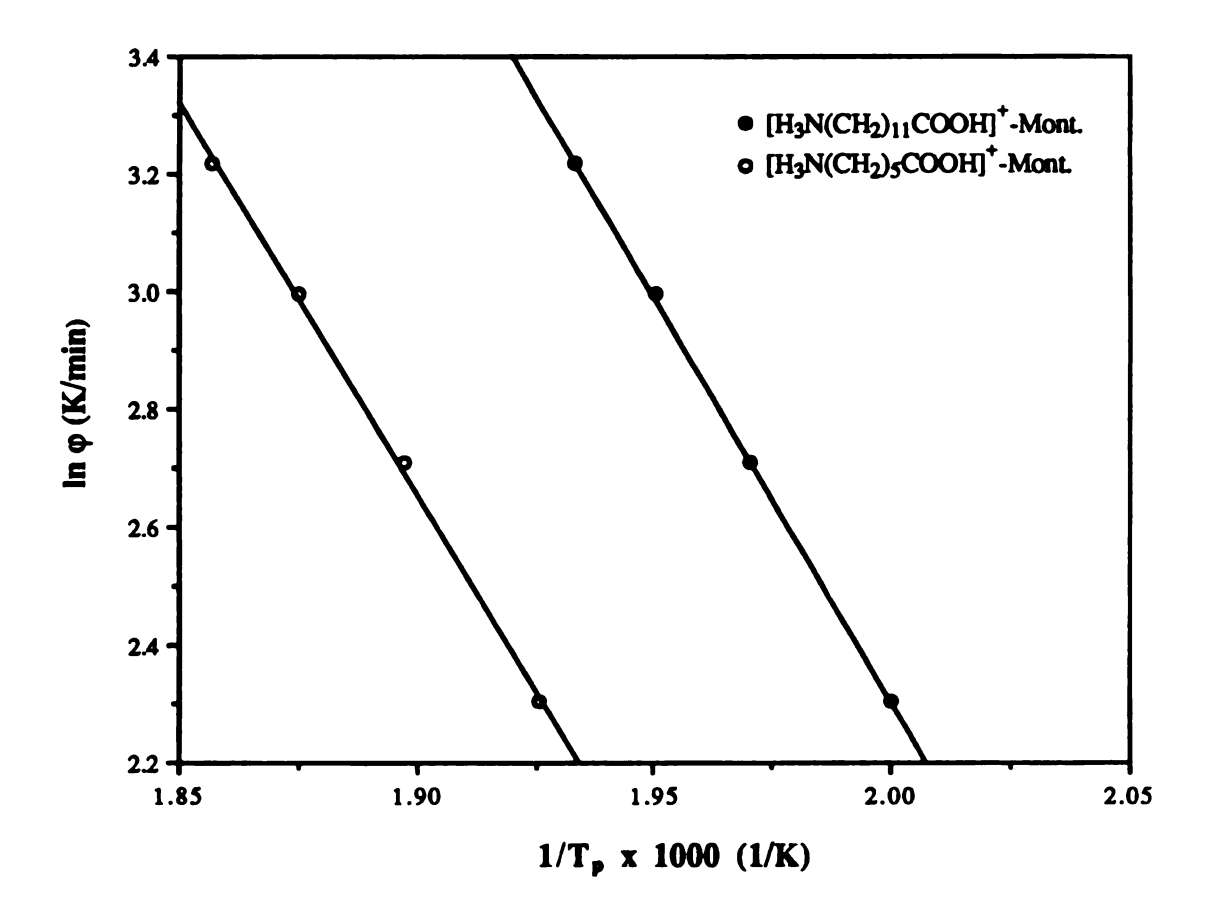


Figure II.12. Linear relationship between the natural logarithm of the heating rate φ and the reciprocal of the peak maximum temperature T_p for epoxy polymerizations catalyzed by 5 wt% (•) $[H_3N(CH_2)_{11}COOH]^+$ and (o) $[H_3N(CH_2)_5COOH]^+$ montmorillonites.

of $2T_p$ to E_a/R range 7.7-7.9% and 8.2-8.5%, respectively, so that $2T_p$ is too large to be omitted. Prime (16) reviewed several papers and concluded that the Ozawa equation (17) together with Doyle's data (18) should be used to obtain more accurate activation energies.

$$\frac{d\ln\varphi}{d\left(\frac{1}{T_p}\right)} \approx -\frac{1.052E_a}{R} \tag{II.9}$$

The difference in E_a obtained between the Ozawa and Kissinger methods is 5.2%. According to Equation II.9, the activation energies of epoxy polymerizations catalyzed by 5 wt% $[H_3N(CH_2)_{11}COOH]^+$ - and $[H_3N(CH_2)_5COOH]^+$ -montmorillonites are 25.9 \pm 0.1 and 25.2 \pm 0.3 kcal/mol, respectively. Compared to typical activation energies (18-21 kcal/mol) for other epoxy systems reported in the literature (19-21), the higher values might be attributed to steric hindrance caused by the intercalation of the onium ions (confined between clay layers).

Kissinger also derived an equation to evaluate the pre-exponential or frequency factor (A) for nth-order reactions:

$$A = \frac{\varphi E_a \exp\left(\frac{E_a}{RT_p}\right)}{RT_p^2 n(1-\alpha_p)^{n-1}} \approx \frac{\varphi E_a \exp\left(\frac{E_a}{RT_p}\right)}{RT_p^2}$$
(II.10)

where α_p is the extent of reaction at the peak exotherm and is independent of the heating rate. The value of $n(1-\alpha_p)^{n-1}$ is equal to unity by definition for first-order reactions. Prime (13) showed that $n(1-\alpha_p)^{n-1}$ was only 2-4%

greater than unity for nth-order epoxy cure reactions, and Kissinger reported that the value was independent of the heating rate as well. By using Equation II.10 and the activation energies obtained above, the pre-exponential factors of epoxy polymerizations catalyzed by 5 wt% $[H_3N(CH_2)_{11}COOH]^+$ - and $[H_3N(CH_2)_5COOH]^+$ -montmorillonites are calculated as $1.80 \pm 0.02 \times 10^9$ and $3.06 \pm 0.06 \times 10^8$ s⁻¹, respectively (Table II.3).

The relationship between the pre-exponential factor and the activation entropy in the standard state $(\Delta S^{o^{\ddagger}})$ is given by the following equation:

$$\Delta S^{o\ddagger} = R \ln \frac{Ah(c^o)^{m-1}}{kTe^m} \tag{II.11}$$

where m is the molecularity of an elementary reaction or the number of molecules that come together to form the activated complex; $(c^{\circ})^{m-1}$ is the factor required to keep the equilibrium constant (K^{\ddagger}) dimensionless; and h and k are the Plank and Boltzman constants, respectively. The acid-catalyzed epoxy ring opening has been proved to be a substitution nucleophilic bimolecular (S_{N}^{2}) reaction, although it has considerable substitution nucleophilic unimolecular (S_{N}^{1}) character. Based on Equation II.11 and m=2, the activation entropies of epoxy polymerizations catalyzed by 5 wt% $[H_{3}N(CH_{2})_{11}COOH]^{+}$ - and $[H_{3}N(CH_{2})_{5}COOH]^{+}$ -montmorillonites are -21.2 \pm 0.1 cal/Kmol (at 229 °C or 502 K) and -24.8 \pm 0.1 cal/Kmol (at 248 °C or 521 K), respectively. In each case, the negative activation entropy implies that the activated complex has a more ordered structure with less rotational and vibrational freedom than the reactants.

Table II.3. Pre-exponential Factors for Epoxy Polymerizations Catalyzed by 5 wt%

Protonated Aminocarboxylic Acid-Montmorillonites

Interlayer Cation	Heating Rate (°C/min)	Peak Max. Temperature (°C)	Pre-exponential Factor (s ⁻¹)
[H ₃ N(CH ₂) ₁₁ COOH] ⁺	10	226.8	1.82 x 10 ⁹
	15	234.6	1.78×10^9
	20	239.6	1.81 x 10 ⁹
	25	244.3	1.77 x 10 ⁹
[H ₃ N(CH ₂) ₅ COOH] ⁺	10	246.2	3.07 x 10 ⁸
	15	253.9	3.13×10^8
	20	260.2	3.07 x 10 ⁸
	25	265.4	2.98 x 10 ⁸

Note: The activation energies of epoxy polymerizations catalyzed by 5 wt% $[H_3N(CH_2)_{11}COOH]^+$ - and $[H_3N(CH_2)_5COOH]^+$ -montmorillonites are 25.9 \pm 0.1 and 25.2 \pm 0.3 kcal/mol, respectively.

Furthermore, by using the kinetics data obtained above and the following equations:

$$\Delta H^{ot} = E_a - mRT \tag{II.12}$$

$$\Delta G^{ot} = \Delta H^{ot} - T\Delta S^{ot} \tag{II.13}$$

the activation enthalpies ($\Delta H^{\circ \dagger}$) and free energies ($\Delta G^{\circ \dagger}$) of epoxy polymerizations catalyzed by 5 wt% $[H_3N(CH_2)_{11}COOH]^+$ - and $[H_3N(CH_2)_5COOH]^+$ -montmorillonites are calculated as 23.9 \pm 0.1 and 34.6 \pm 0.1 kcal/mol (at 502 K) and 23.1 \pm 0.3 and 35.6 \pm 0.4 kcal/Kmol (at 521 K), respectively. Clearly, the activation entropies, as reflected in the pre-exponential factors, account for the difference in the polymerization reactivity between the two organoclay-epoxy resin systems, although the activation enthalpies are the major parts (69.3 and 64.9%) of the activation free energies.

Extended Work

Since the clay delamination-epoxy polymerization is proton-catalyzed, other cations such as $[H_3N(CH_2)_{n-1}CH_3]^+$ (n = 6 and 12), NH_4^+ , and H^+ may also be used as delaminating agents or catalysts for the formation of clay-polyether nanocomposites. As shown in Table II.4, these alkylammonium ions and inorganic cations cause clay delamination-epoxy polymerization over a wide range of onset temperatures (198-287 °C). It appears that basal spacing and cation acidity are two of the factors affecting the delamination-polymerization temperature. The lowest and the second lowest temperatures correspond to $[H_3N(CH_2)_{11}CH_3]^+$

Table II.4. DSC and XRD Data for Epoxy Polymerizations Catalyzed by 5 wt%

Proton-, Ammonium ion, and Protonated Primary Amine-Montmorillonites^a

Interlayer Cation	PolymDel. Temp. ^b (°C)	Heat of Reaction (J/g)	Heat of Polym.c (kcal/mol)	Basal Spacing (Å)
$[H_3N(CH_2)_{11}CH_3]^{\dagger}$	198 ± 1	550 ± 3	52.3 ± 0.3	15.89 ± 0.19
$[H_3N(CH_2)_5CH_3]^+$	287 ± 1	554 ± 6	52.7 ± 0.6	14.90 ± 0.13
NH ₄ ⁺	247 ± 1	554 ± 5	52.7 ± 0.5	12.52 ± 0.12
H ⁺	231 ± 1	555 ± 12	52.8 ± 1.1	13.95 ± 0.08

^aDSC data were obtained by using a heating rate of 20 °C/min.

bThe onset epoxy polymerization-clay delamination temperature.

^cThe heat of polymerization for the epoxy equivalent is halved.

montmorillonite with the largest basal-spacing and H⁺-montmorillonite with the most acidic cation.

However, in Figure II.13 the DSC curves show the contrast between $[H_3N(CH_2)_{11}CH_3]^+$ -and $[H_3N(CH_2)_5CH_3]^+$ -montmorillonites in terms of the delamination-polymerization temperature and the peak shape (or reaction rate). The great difference in reactivity makes the alkylammonium-montmorillonites a unique class among all the cation-exchanged montmorillonites studied. The reason is that chemical and physical properties of the primary amines (e.g., basicity), alkylammonium ions (e.g., acidity), and alkylammonium-montmorillonites (e.g., basal spacing), respectively, are similar to each other. Moreover, among all the cation-exchanged montmorillonites (5 wt%) studied, only $[H_3N(CH_2)_5CH_3]^+$ -montmorillonites gives a very broad DSC peak (or sluggish reaction).

Table II.4 also shows that the heat of reaction (550-555 J/g) remains constant within experimental errors regardless of the exchange cations used. The average heat of reaction is 553 J/g for 5/95 (w/w) organoclay/epoxy resin or 582 J/g for the neat epoxy resin. This value is equivalent to 52.6 kcal/mole, which is essentially the same as that (53.7 kcal/mole) derived from the values listed in Table II.1.

D. CONCLUSIONS

In this work we have achieved the direct nanoscopic delamination of smectite clay layers in a polyether matrix derived from an epoxy resin. The exfoliation of the acidic montmorillonites in the epoxy resin takes place instantaneously at the delamination-polymerization temperature. In addition to simple acidic cations such as H^+ and NH_4^+ , various onium ions

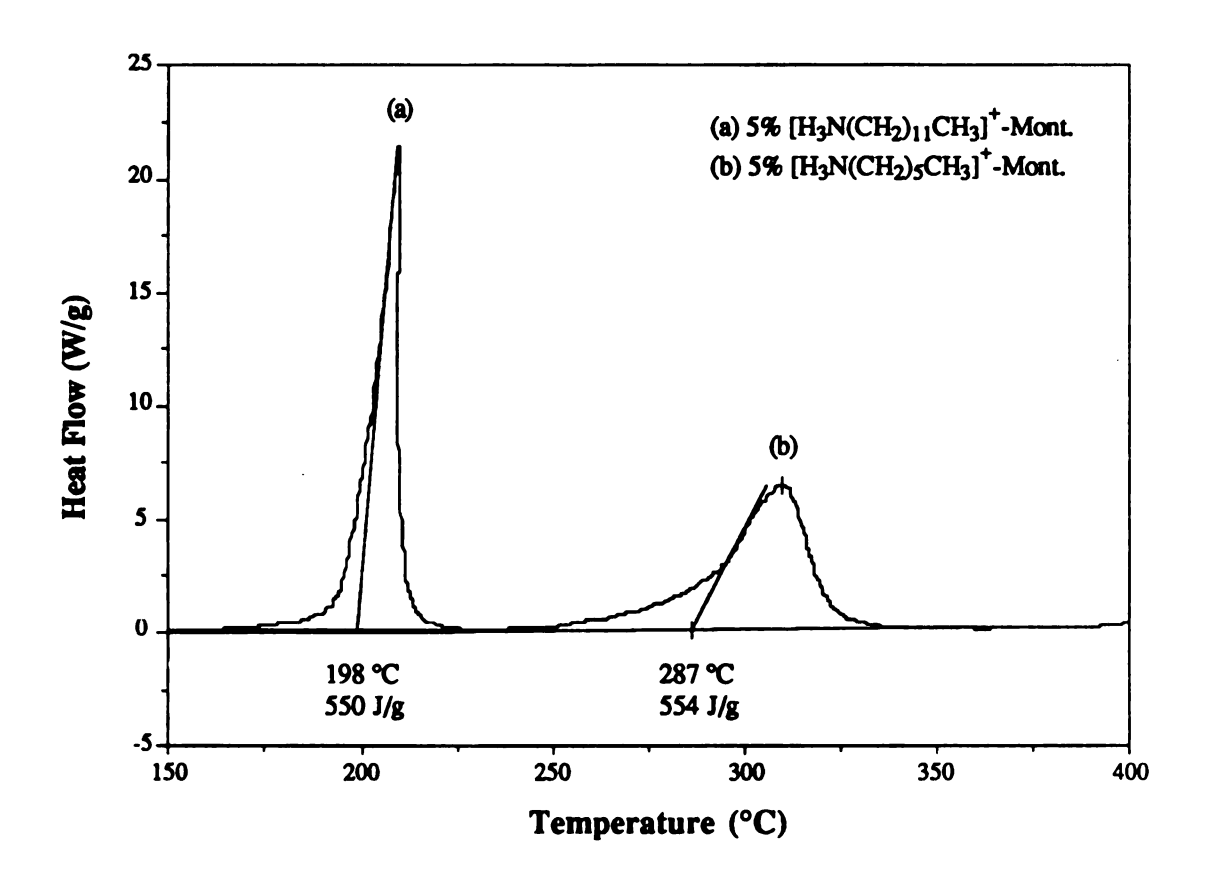


Figure II.13. DSC thermograms of epoxy polymerizations catalyzed by 5 wt% (a) [H₃N(CH₂)₁₁CH₃]⁺- and (b) [H₃N(CH₂)₅CH₃]⁺-montmorillonites, a heating rate of 20 °C/min being used.

(protonated primary amines, diamines, and aminocarboxylic acids) are suitable delaminating agents.

The delamination-polymerization temperature depends on the heating rate and cation-exchanged montmorillonite. The heating rate being equal, cation acidity (or proton availability) and interlayer gallery height (or steric hindrance) are two important factors affecting the delamination-polymerization temperature. Within experimental errors, the heat of epoxy polymerization is independent of the cation exchanged form of montmorillonite, suggesting that differences in the clay exfoliation energy are small relative to the epoxy polymerization energy. The activation entropy, as reflected in the pre-exponential factor, is important in determining the reactivity of the organoclay-epoxy system, although the activation enthalpy is the major component of the activation free energy.

Owing to their powdery texture, the clay-polymer nanocomposites of the present work are not conducive to mechanical measurements. Power formation is caused by phase segregation of the clay-bound polyether and the epoxy resin. It should be possible, however, to circumvent this limitation using more compatible cyclic ethers as polymer precursors. Also, powder processing studies currently in progress may offer a convenient route to the formation of monolithic structures.

LIST OF REFERENCES

- 1. A. Okada, M. Kawasumi, A. Usuki, Y. Kojima, T. Kurauchi, and O. Kamigaito, Mater. Res. Soc. Symp. Proc., 171, 45 (1990).
- 2. A. Okada, M. Kawasumi, T. Kurauchi, and O. Kamigaito, *Polym. Prepr.*, 28 (2), 447 (1987).
- 3. Y. Kojima, A. Usuki, M. Kawasumi, A. Okada, T. Kurauchi, and O. Kamigaito, J. Polym. Sci.: Part A: Polym. Chem., 31, 983 (1993).
- 4. S. Fujiwara and T. Sakamota, Japan Patent 51,109,998 (1976).
- 5. Y. Fukushima, A. Okada, M. Kawasumi, T. Kurauchi, and O. Kamigaito, Clay Miner., 23, 27 (1988).
- 6. Y. Fukushima and S. Inagaki, J. Incl. Phenom., 473 (1987).
- 7. A. Usuki, T. Mizutani, Y. Fukushima, M. Fujimoto, K. Fukumori, Y. Kojima, N. Sato, T. Kurauchi, and O. Kamigaito, U. S. Patent 4,889,885 (1989)
- 8. R. E. Grim, "Clay Mineralogy," 2nd ed., McGraw-Hill, New York (1968).
- 9. C. A. May, Ed., "Epoxy Resins," 2nd ed., Marcel Dekker, New York (1988).
- 10. H. Lee and K. Neville, "Handbook of Epoxy Resins," McGraw-Hill, New York (1967).
- 11. H. J. Borchardt and F. Daniels, J. Am. Chem. Soc, 79, 41 (1957).
- 12. L. J. Taylor and S. W. Watson, Anal. Chem., 42, 297 (1970)

- 13. R. B. Prime, Polym. Eng. Sci., 13, 365 (1973)
- 14. A. A. Duswalt, Thermochim. Acta., 8, 57 (1974)
- 15. H. E. Kissinger, Anal. Chem., 29, 1702 (1957).
- R. B. Prime, "Thermal Characterization of Polymeric Materials," E.
 Turi, Ed., Academic Press, New York (1981).
- 17. T. Ozawa, J. Therm. Anal., 2, 301 (1970).
- 18. C. D. Doyle, Anal. Chem., 33, 79 (1951).
- P. Peyser and W. D. Bascom, J. Polym. Sci., Polym. Phys. Ed., 18, 129 (1975).
- 20. S. J. Swarim and A. M. Wims, Anal. Calorim., 4, 155 (1976).
- 21. M. Cizemciogly and A. Gupta, SAMPLE Q., 16 (April, 1982)

CHAPTER III

CLAY-POLYMER NANOCOMPOSITES FORMED FROM BASIC HYDROTALCITES AND EPOXY RESIN

A. INTRODUCTION

As mentioned earlier, delaminated montmorillonite has been shown very useful in the design of polymer-based composite materials with improved mechanical and physical properties. Recently, Yano and coworkers (1) reported that delaminated montmorillonite (e.g., 5 wt%) reduced the gas permeability (25 vs. 110 g.mm/m², 24 h) and thermal expansion (50 vs. 67 x 10⁻⁶/°C, 250 °C) of polyimide. In addition, Usuki and co-workers (2) used protonated 12-aminolauric acid as the exchange cation and showed that delaminated montmorillonite was a better reinforcement for nylon-6 than delaminated saponite (another smectite clay). However, no delaminated clay-polymer nanocomposites formed from non-smectite clays have been reported in the literature.

In general, clay minerals are divided into cationic and anion clays by their layer charges and interlayer ions. Mica, talc, kaolinite, and montmorillonite are typical cationic clays. Figure III.1 shows the general structure of anionic clays or layered double hydroxides (LDHs). A LDH results from the partial isomorphous substitution of M^{2+} ions for M^{3+} ions in octahedral $M(OH)_2$ layers. The resulting positive layer charge is

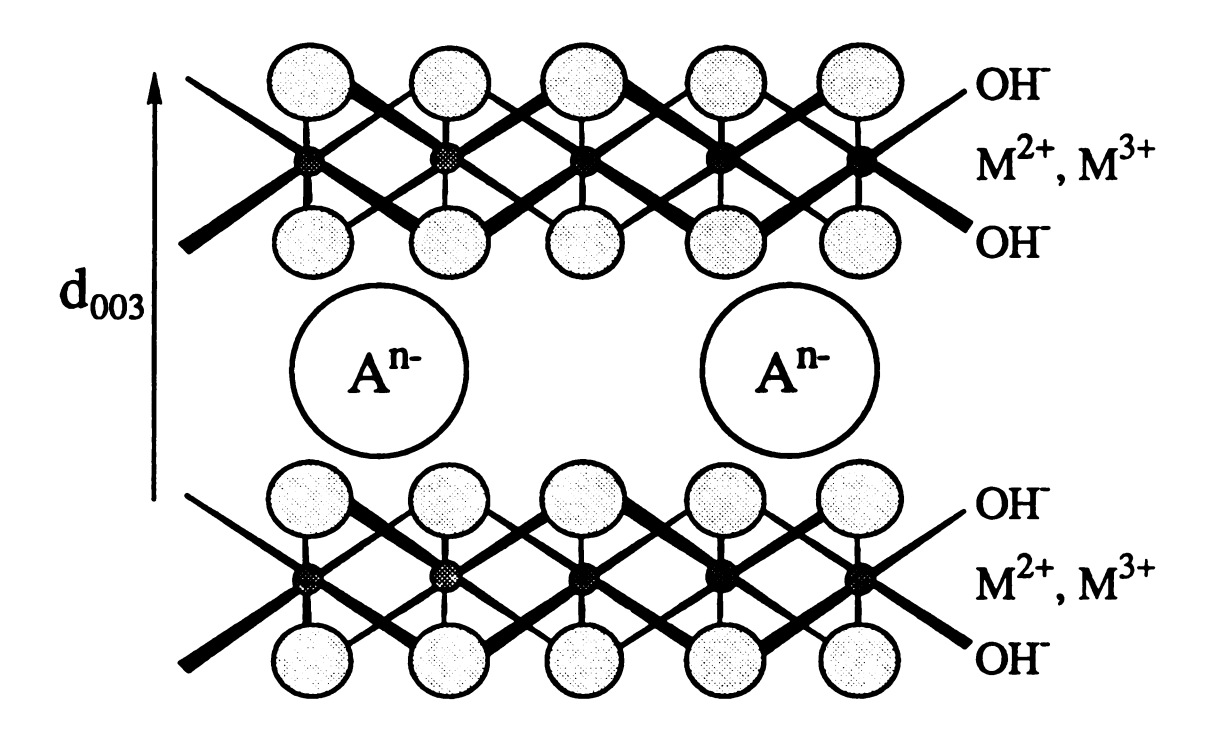


Figure III.1. General structure of anionic clays or layered double hydroxides (LDHs); e.g., hydrotalcite $Mg_6Al_2(OH)_{16}(CO_3)\cdot 4H_2O$, where $M^{2+} = Mg^{2+}$; $M^{3+} = Al^{3+}$; and $A^{n-} = CO_3^{-2-}$.

balanced by interlayer anions A^{n-} solvated by water molecules. The general formula of LDHs can be written as $[M_{1-x}^{2+}M_x^{3+}(OH)_2]A_{x/n}^{n-}\cdot yH_2O$ (0.15 < x < 0.44), where $M^{2+}=Mg^{2+}$, Zn^{2+} , Co^{2+} , Ni^{2+} , Cu^{2+} , etc.; $M^{3+}=Al^{3+}$, Cr^{3+} , Fe^{3+} , etc.; and $A^{n-}=CO_3^{-2}$, SO_4^{-2} , OH^- , NO_3^- , Cl^- , etc. (3-7). For instance, hydrotalcite $Mg_6Al_2(OH)_{16}(CO_3)\cdot 4H_2O$ is the most well-known natural and synthetic LDH.

Miyata and Kimura (8) first reported a series of dicarboxylate ions intercalated in LDHs. However, Drezdon (9) used the coprecipitation method but failed to duplicate the sample preparation. Several groups used the anion-exchange method (10) and especially, the calcination method (11-13) instead and succeeded in preparing the same organic anion-LDHs. Among them, Dimotakis and Pinnavaia (13) reported a new route to well-ordered organic anion-LDHs, although this method required glycerol and meixnerite as a swelling agent and a precursor, respectively.

Calcined synthetic hydrotalcite $Mg_6Al_2O_8(OH)_2$ or mixed metal oxide $(MgO)_6\cdot Al_2O_3$ has been used as a catalyst for polymerizations of B-propiolactone (14) and propylene oxide (15-16). The catalytic property of calcined hydrotalcite arises from its extremely high basicity $(pK_a \approx 35)$ and surface area ($\sim 200 \text{ m}^2/\text{g}$). Tanaka et al. (17) used NO_3^- -hydrotalcite as a precursor to prepare polyacrylate-hydrotalcite $(d_{003} = 13.4 \text{ Å})$. However, the preparation of acrylate-hydrotalcite $(d_{003} = 13.8 \text{ Å})$ required very high acrylate concentrations (e.g., 1.69 M for 5 g of NO_3^- -hydrotalcite) and long reaction time (1 week, 25 °C).

Our interest in the design of new clay-polymer nanocomposites led us to examine aminocarboxylate- and dicarboxylate-hydrotalcites as catalysts for the epoxy polymerization. In this study we emphasized the synthesis and delamination of aminocarboxylate-hydrotalcite, neither which has been reported in the literature. The epoxy resin selected for this study was the same epoxy resin EPON-828 as used before.

B. EXPERIMENTAL

Materials

Epoxy resin EPON-828 (Shell), aminocarboxylic acids $H_2N(CH_2)_{n-1}COOH$, dicarboxylic acids $HOOC(CH_2)_{n-2}COOH$ (n = 6 and 12) (Aldrich), and hydrated metal nitrates $Mg(NO_3)_2 \cdot 6H_2O$ (EM Science) and $Al(NO_3)_3 \cdot 9H_2O$ (J. T. Baker) were used as received.

Sample Preparation

Hydrotalcite was prepared by using a slightly modified Reichele et at. method (18). Mg(NO₃)₂·6H₂O (0.50 mol) and Al(NO₃)₃·9H₂O (0.25 mol) were dissolved in 350 mL of deionized water. The solution was dropwise added to a solution of NaOH (1.75 mol) and Na₂CO₃ (0.472 mol) in 570 mL of deionized water. With vigorous agitation, the addition was carried out at 35 °C for 4 h and the reaction continued at 65 °C for another 18 h. The heavy white slurry was centrifuged and the hydrotalcite precipitate was washed with deionized water. Washing and centrifugation were repeated until no or little brown Ag₂O precipitate was observed when a drop of 0.1 N AgNO₃ was added to the centrifugate. The washed hydrotalcite was dried in an oven at 125 °C for 18 h. The oven-dried hydrotalcite was ground and then calcined at 500 °C for 3 h. During calcination, hydrotalcite lost CO₃²⁻ ions as CO₂ and became the mixed metal oxide.

 $H_2N(CH_2)_{n-1}COOH$, $H_2N(CH_2)_{n-1}COOH$ or $HOOC(CH_2)_{n-2}COOH$ (30 mmol) was dissolved in 1.5 L of a 0.02 N (0.04 N for $Na_2[OOC(CH_2)_{n-2}COO]$) NaOH solution at 80 °C. The deionized water used for sample preparation was boiled for an hour to remove dissolved CO_2 . Fresh calcined hydrotalcite (3.00 g) was thoroughly dispersed in the 0.02 N solution of interest at 80 °C for 12 h. The organic anion-exchanged hydrotalcite was centrifuged and washed with deionized water. Washing and centrifugation were repeated until no or little brown Ag_2O precipitate was observed when a drop of 0.1 N $AgNO_3$ was added to the centrifugate. The washed organic anion-hydrotalcite was dispersed in 250 mL of deionized water and freeze-dried in a Labconco Freeze Dryer Model 18. The freeze-dried organic anion-hydrotalcite was then sieved to < 325-mesh.

 $H_2N(CH_2)_{11}COO^-$ -hydrotalcite (0.79 g) was added to 15 g of epoxy resin EPON-828 and the 5/95 (w/w) clay/epoxy mixture was magnetically stirred in a 250-mL beaker at 75 °C for 30 min. The beaker was sealed with aluminum foil and the temperature was then raised at a rate of ~ 20 °C/min to 280 °C. The partial liquid-to-powder transformation of the clay-epoxy mixture took place within 13 min. The clay-epoxy nanocomposite powder was separated from the solidified polyether and sieved to < 325-mesh, with grounding if necessary.

No other clay-epoxy nanocomposite was prepared from the other anion-exchanged hydrotalcites because their polymerization-delamination temperatures are well above the flash point of the epoxy resin, ~ 325 °C.

Characterization

The hydrotalcite-epoxy nanocomposite sample for powder XRD studies was firmly pressed onto a Rigaku sample holder. The diffraction

pattern was then recorded by monitoring the diffraction angle 20 from 2° to 45° on a Rigaku Rotaflex Ru-200BH X-ray diffractometer. The diffractometer was equipped with a Ni-filtered Cu- K_{α} radiation source operated at 45 kV and 100 mA. The scanning speed and the step size used were 2°/min and 0.02°, respectively. Quartz was used as a calibration standard.

A small amount of hydrotalcite-epoxy nanocomposite powder for TEM studies was added to a Spurr's mixture in a silicon rubber mold, which was then placed in an oven at 70 °C overnight. The cured epoxy block was trimmed and thin-sectioned with a diamond knife in a microtome. The resulting ultra-thin sections (~ 90 nm in thickness) were mounted on a plastic-film support on a copper grid and examined by a JEOL 100CX transmission electron microscope operated at an accelerating voltage of 100 kV.

The mixture of organic hydrotalcite-epoxy resin for DSC analysis (4 mg) was placed in an aluminum sample pan, which was then sealed hermetically. The sample and reference pans were placed in the cell of a Du Pont 910 differential scanning calorimeter. The DSC cell was then heated under nitrogen (50 mL/min) to 450 °C at a rate of 20 °C/min. Indium (mp, 156.6 °C and ΔH_m , 28.42 J/g) was used for DSC calibrations.

 $H_2N(CH_2)_{11}COO$ -hydrotalcite (20 mg) for TGA analysis was placed in a platinum sample container, which was then placed in the thermobalance of a Du Pont 990 thermogravimetric analyzer. The sample weight was tared and the sample was then heated under nitrogen (100 mL/min) to 650 °C at a rate of 20 °C/min.

C. RESULTS AND DISCUSSION

Calcined hydrotalcite or amorphous mixed metal oxide $(MgO)_6\cdot Al_2O_3$. (Figure III.2c) was prepared just before use to prevent it from absorbing water and CO_2 in the air. The extremely basic mixed metal oxide easily converts absorbed CO_2 and water into CO_3^{2-} ions to form hydrotalcite (Figure III.2a). For instance, Figure III.2b shows the XRD pattern of the partially reconstituted hydrotalcite formed from calcined hydrotalcite stored in a plastic bottle for a month.

Deprotonated aminocarboxylic acids $H_2N(CH_2)_{n-1}COOH$, and dicarboxylic acids $HOOC(CH_2)_{n-2}COOH$ (n = 6 and 12) were used as delaminating agents or catalysts rather than curing agents in this work. It is essential to treat these organic acids with dilute aqueous NaOH (or NH_4OH) solution. Alkaline treatment converts aminocarboxylic acids and dicarboxylic acids into the corresponding water-soluble anions, which can be intercalated in reconstituted hydrotalcite. In the case of an aminocarboxylic acid, deprotonation converts the dipolar ion I into the anion II.

$$H_3N(CH_2)_{n-1}C-O$$
 $+OH$ $+OH$

Evidence of Clay Delamination

As shown in Figure III.3d, no clay diffraction peaks are observed for a clay-epoxy nanocomposite containing 5 wt% $H_2N(CH_2)_{11}COO^2$ -hydrotalcite. Only a very diffuse scattering peak characteristic of the amorphous cured epoxy resin (or polyether) appears in the XRD powder

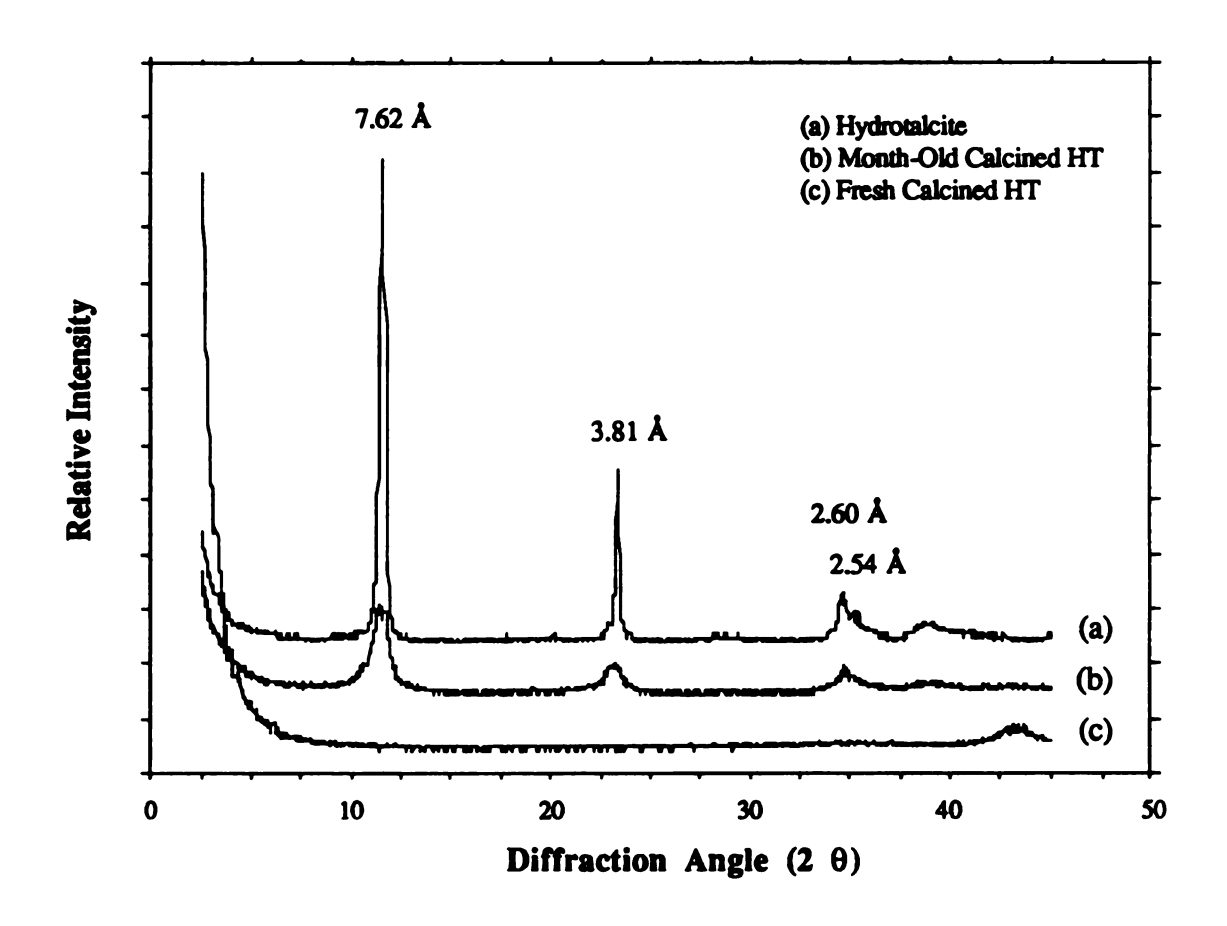


Figure III.2. XRD patterns of (a) hydrotalcite (HT), (b) month-old calcined HT, and (c) fresh calcined HT (500 °C, 3 h) (i.e., Mg₆Al₂O₈(OH)₂ or mixed metal oxide (MgO)₆·Al₂O₃).

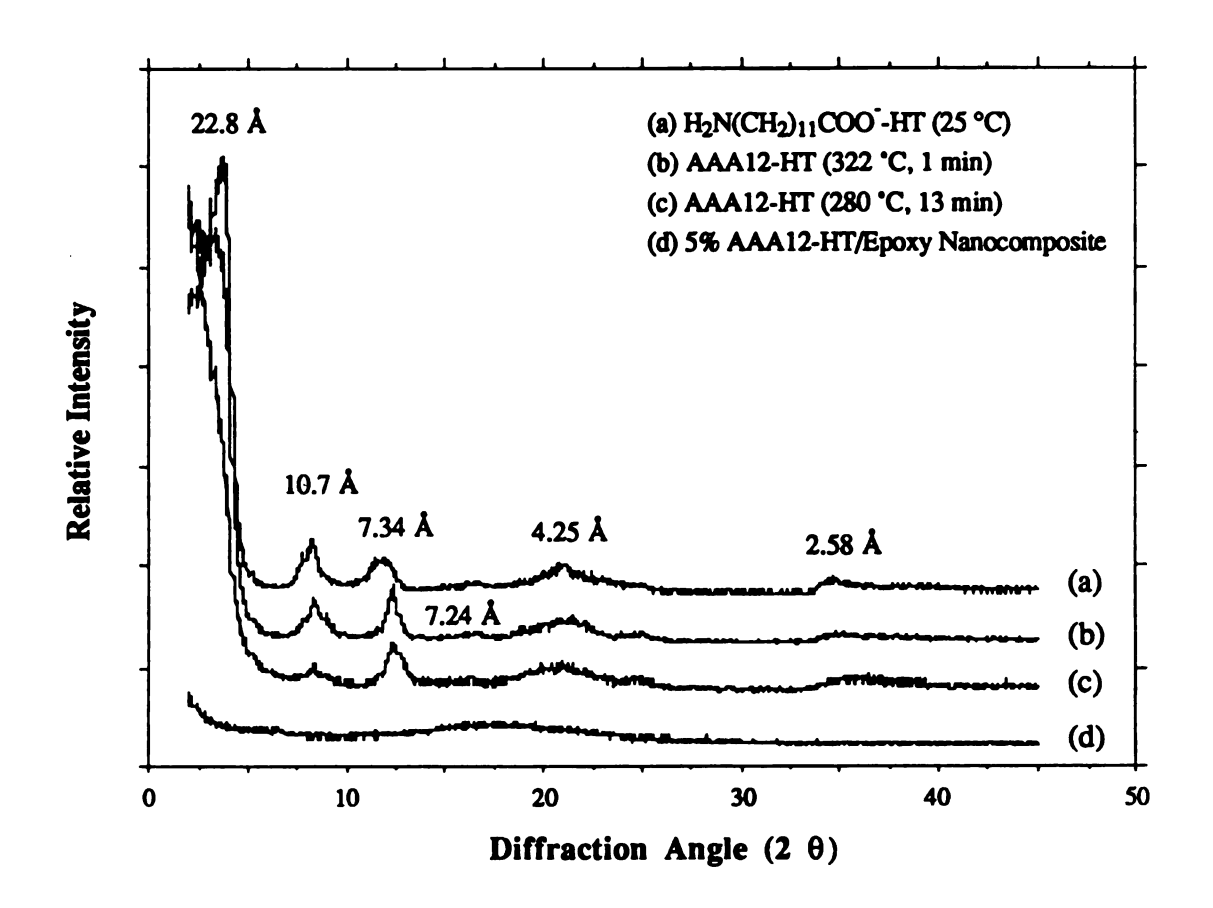


Figure III.3. XRD patterns of (a) H₂N(CH₂)₁₁COO⁻-hydrotalcite (AAA12-HT) (25 °C), (b) AAA12-HT (322 °C, 1 min), (c) AAA12-HT (280 °C for 13 min), (d) a clay-epoxy nanocomposite containing 5 wt% AAA12-HT.

pattern. The absence of a 22.8-Å peak for $H_2N(CH_2)_{11}COO$ -hydrotalcite (Figure III.3a) suggests that the clay tactoids have been exfoliated and the 4.8-Å-thin clay layers dispersed at the molecular level. However, the clay peaks with reduced intensities (Figures III.3b and III.3c) show that the partial thermal decomposition of pristine $H_2N(CH_2)_{11}COO$ -hydrotalcite occurs when it is heated at 322 °C for 1 min and to the greater extent, at 280 °C for 13 min under nitrogen.

As shown in Figure III.4, the TEM micrograph of a clay-epoxy nanocomposite containing 5 wt% $H_2N(CH_2)_{11}COO^-$ -hydrotalcite reveals that the cured epoxy resin infiltrates submicron-sized clay tactoids and expands interlayer spacing up to ~ 200 Å. Apparently the epoxy resin is responsible for the retention of the clay layered structure. That is, the epoxy resin reacts with the organoclay and affects its degree of thermal decomposition. Figure III.5 shows the DSC thermogram for a 5/95 (w/w) mixture of $H_2N(CH_2)_{11}COO^-$ -hydrotalcite and epoxy resin EPON-828. The thermogram indicates that the clay delamination-epoxy polymerization takes place at an onset temperature of 321 °C and the heat of reaction is 572 J/g.

For comparison, the DSC thermograms of the neat epoxy resin and $H_2N(CH_2)_{11}COO^2$ -hydrotalcite are shown in Figures II.4 and III.6, respectively. It should be noted that the scale of the heat flow in Figure III.6 is much smaller than that in either Figure II.4 or III.5.

The DSC and TGA (Figure III.7) curves indicate that $H_2N(CH_2)_{11}COO^-$ -hydrotalcite loses surface and interparticle pore water between 40 and 200 °C. Interlayer water is liberated in the region of 200-300 °C. The losses of hydroxyl groups in the clay framework (or dehydroxylation) and CO_3^{2-} ions as CO_2 (or decarbonation) occur between

Figure III.4. TEM micrograph of a clay-epoxy nanocomposite containing 5 wt% $H_2N(CH_2)_{11}COO^-$ -hydrotalcite: x72,000.



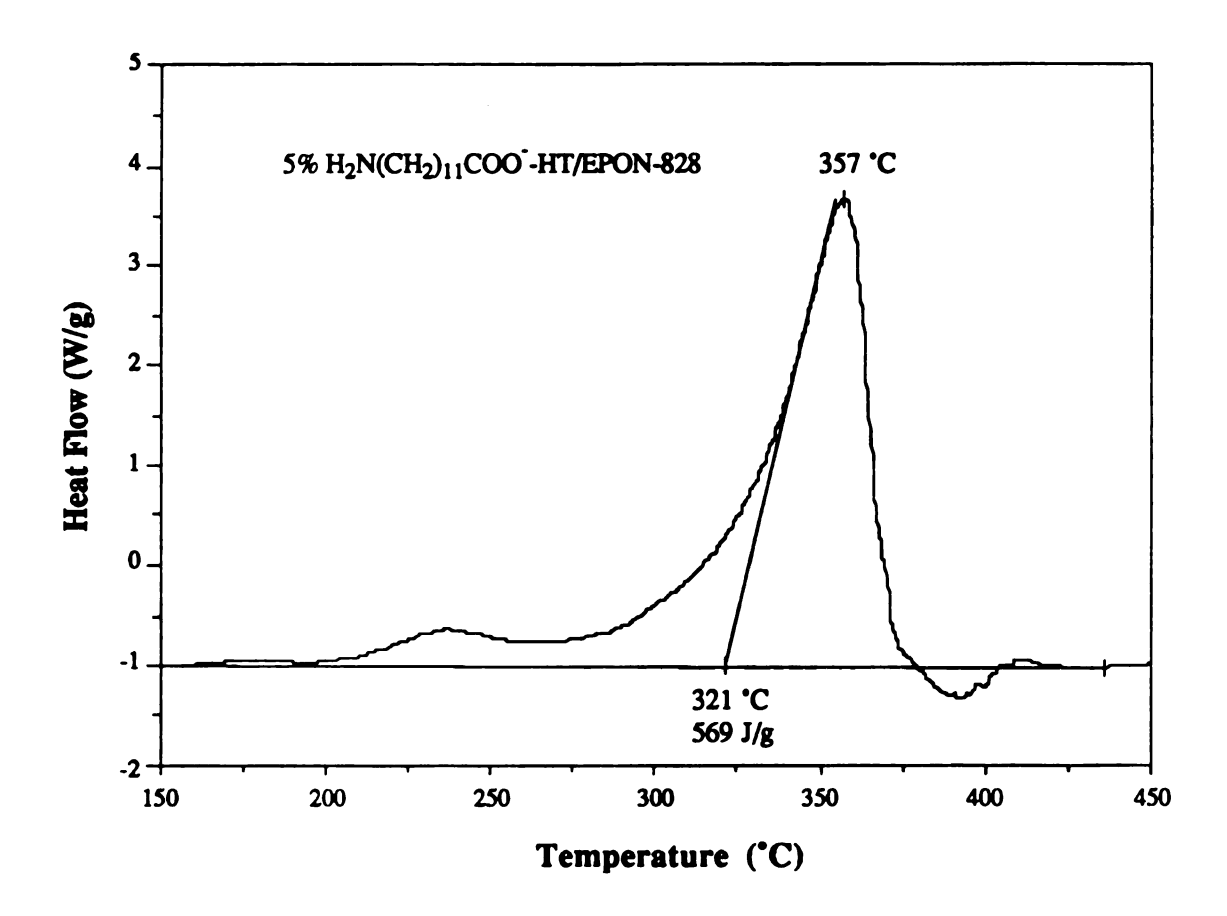


Figure III.5. DSC thermogram of the epoxy polymerization catalyzed by 5 wt% $H_2N(CH_2)_{11}COO^-$ -hydrotalcite, a heating rate of 20 °C/min being used.

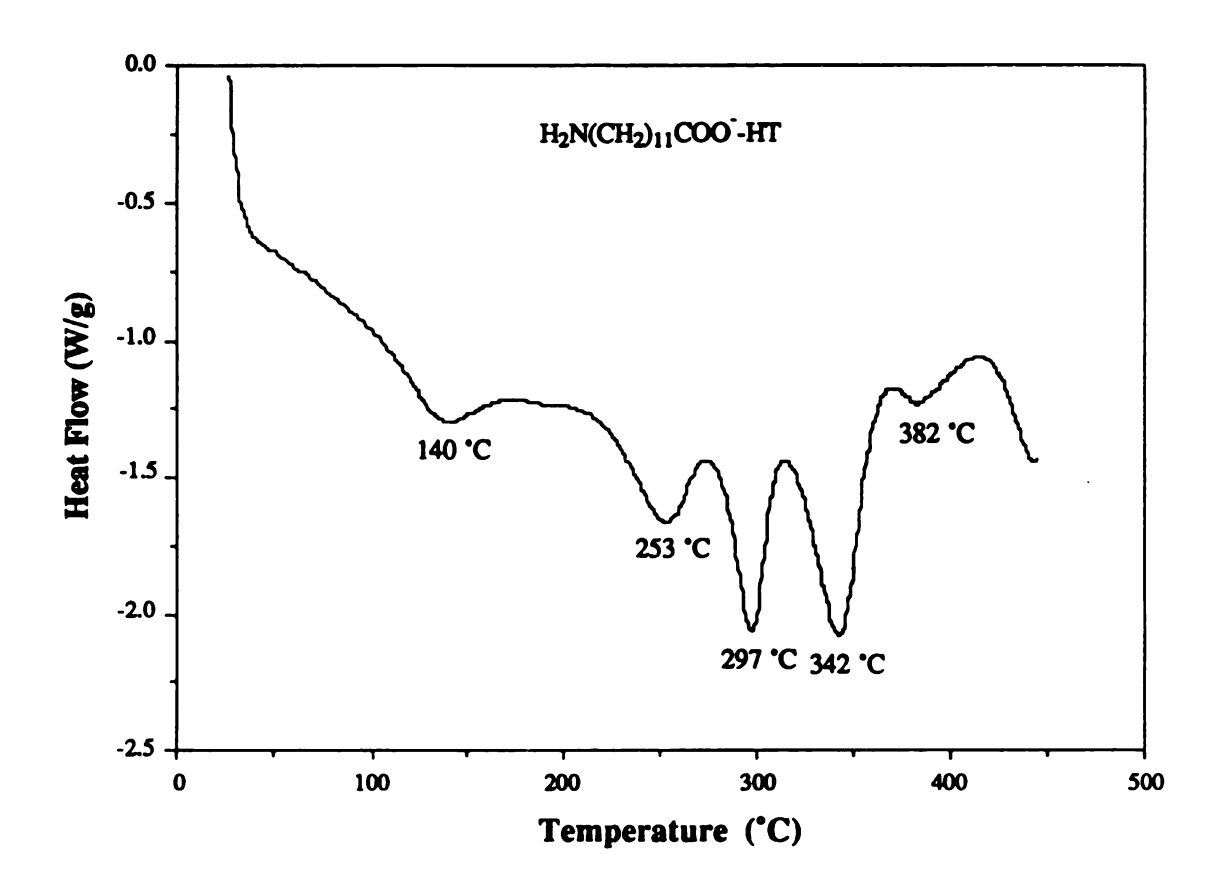


Figure III.6. DSC thermogram of H₂N(CH₂)₁₁COO -hydrotalcite, a heating rate of 20 °C/min being used.

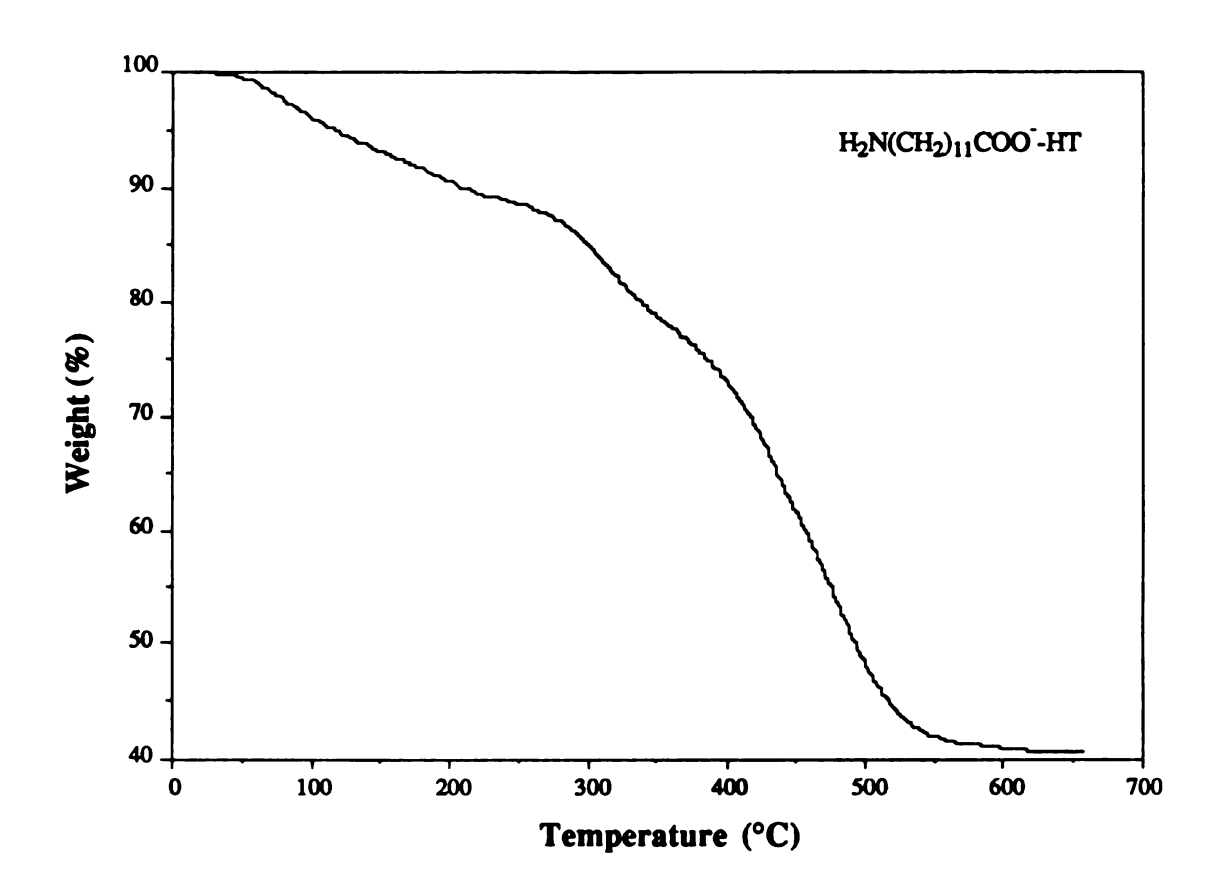


Figure III.7. TGA curve of H₂N(CH₂)₁₁COO⁻-hydrotalcite, a heating rate of 20 °C/min used.

300 and 650 °C (18, 19). The heat absorption and the weight loss shown by the DSC and TGA curves, respectively, substantiate the XRD pattern (Figure III.3b) that the partial loss of interlayer water results in the reduced peak intensity for $H_2N(CH_2)_{11}COO^-$ -hydrotalcite heated at 322 °C for 1 min. More importantly, the heat of reaction for $H_2N(CH_2)_{11}COO^-$ -hydrotalcite (especially 5 wt%) is much smaller than that for either the uncatalyzed epoxy polymerization or the epoxy polymerization catalyzed by 5 wt% $H_2N(CH_2)_{11}COO^-$ -hydrotalcite.

Reaction Mechanism

According to the evidence presented above, the delamination of the organic anion-hydrotalcites in the epoxy resin or epoxy polymerizations catalyzed by the organic anion-hydrotalcites at elevated temperatures can be rationalized by the following general equations:

Initiation:

Propagation:

$$R^{2}OH + n CH_{2}-CHR \xrightarrow{+ OH^{-}} R^{2}O(CH_{2}-CHRO)_{n-1}CH_{2}-CHR$$
 (III.4)

where R¹COO is any molecule containing one or two carboxyl groups and R²OH is monomer or oligomer possessing one or more hydroxyl groups. At the delamination-polymerization temperature, epoxy monomers first react with aminocarboxylate and dicarboxylate ions intercalated on the edges of hydrotalcite particles. Through an S_N2 mechanism, the cleavage of epoxy rings (Equation III.1) takes place first. In the case of H₂N(CH₂)₁₁COO ion, the other two epoxy ring openings or amine-epoxy reactions (Equations III.2-3) also occur. The reactions propagate toward clay interlayer space and the propagation causes the expansion of the clay gallery region. In the meantime, various base-catalyzed etherifications (Equation III.4) occur to form polyether in the expended region and this results in the complete delamination of clay layers. The cured epoxy resin or polyether in the clay galleries becomes phase-segregated from the uncured resin. This gives rise to the liquid-to-powder transformation characteristic and an increase in the bulk volume upon the formation of hydrotalcite-epoxy nanocomposites. A large heat of reaction also accompanies the clay delamination-epoxy polymerization.

Reaction Temperature

Listed in Table III.1, the onset temperatures of the epoxy polymerization-hydrotalcite delamination reactions increase in the order $H_2N(CH_2)_{11}COO^- < HOOC(CH_2)_{n-2}COO^- \approx [OOC(CH_2)_{n-2}COO]^{2^-}$ (n = 6 and 12) < $H_2N(CH_2)_5COO^-$. That is, the polymerization-delamination temperature increases with decreasing the basal (d₀₀₃) spacing of the

Table III. 1. DSC and XRD Data for Epoxy Polymerizations Catalyzed by 5 wt%

Aminocarboxylate- and Dicarboxylate-Hydrotalcites^a

Interlayer Anion	PolymDel. Temp.b (°C)	Heat of Reaction (J/g)	Heat of Polym. ^c (kcal/mol)	Basal Spacing (Å)
H ₂ N(CH ₂) ₁₁ COO	322 ± 2	571 ± 13	54.3 ± 1.2	22.79 ± 0.43
H ₂ N(CH ₂) ₅ COO	383 ± 2	569 ± 11	54.1 ± 1.0	7.69 ± 0.02
HOOC(CH ₂) ₁₀ COO	372 ± 2	572 ± 11	54.4 ± 1.0	17.60 ± 0.29
HOOC(CH ₂) ₄ COO	371 ± 1	571 ± 17	54.3 ± 1.6	14.02 ± 0.25
[OOC(CH ₂) ₁₀ COO] ²⁻	372 ± 2	568 ± 16	54.0 ± 1.5	17.50 ± 0.16
[OOC(CH ₂) ₄ COO] ²⁻	373 ± 2	569 ± 16	54.1 ± 1.5	13.29 ± 0.26

^aDSC data were obtained by using a heating rate of 20 °C/min.

^bThe onset epoxy polymerization-clay delamination temperature.

^cThe heat of polymerization for the epoxy equivalent is halved.

organic anion-hydrotalcite. A larger basal spacing gives the epoxy monomers easier access to the interlayer anions and this leads to a lower polymerization-delamination temperature. In general, the basal spacing of an organic hydrotalcite depends primarily on the alkyl chain length (or carbon number) and the spatial arrangement of the organic anion intercalated on the gallery surfaces.

As shown in Figure III.8, the XRD pattern of " $H_2N(CH_2)_5COO^-$ "-hydrotalcite indicates that $H_2N(CH_2)_5COO^-$ is not intercalated in hydrotalcite and that the anionic clay is OH^- -hydrotalcite or meixnerite $Mg_6Al_2(OH)_{16}(OH)_2\cdot 4H_2O$. Besides, in Table III.1 the relatively high onset temperature of the meixnerite-epoxy reaction shows that meixnerite is not a catalyst for the epoxy polymerization.

Heat of Reaction

Table III.1 shows that the heat of the polymerization-delamination reaction remains constant within experimental errors regardless of the organic anion-hydrotalcites studied. Since the heat of reaction arises primarily from the polymerization of the epoxy resin, it should remain unchanged, provided the epoxy concentration (wt%) is constant. The average heat of reaction is 570 J/g for 95 wt% epoxy resin, or 600 J/g for the neat epoxy resin. This value is equivalent to a value of 54.2 kcal/mole or 27.1 kcal/mole for the epoxy equivalent, which is a typical value for the epoxy resin cured by primary amines. However, Table III.2 shows that the amount of the organic anions used (6.34-12.2 mmol) to form the nanocomposites is sufficient to cure only 2.5-7.3 % of the epoxy resin. Therefore, the major reaction is the base-catalyzed epoxy etherification.

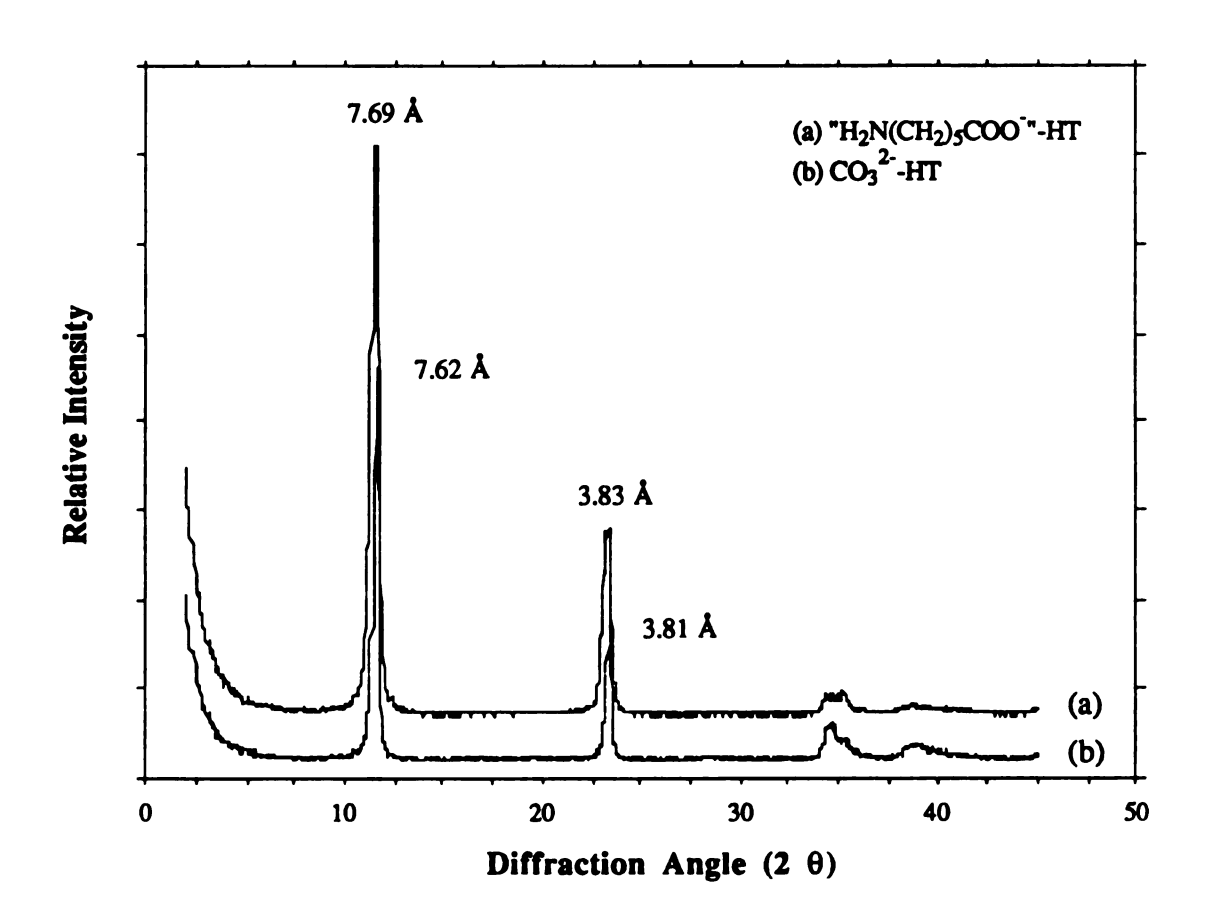


Figure III.8. XRD patterns of (a) " $H_2N(CH_2)_5COO$ "-hydrotalcite or more accurately, meixnerite $Mg_6Al_2(OH)_{16}(OH)_2\cdot 4H_2O$ and (b) hydrotalcite.

Table III.2. Estimated Epoxy Cure Percents Due to Aminocarboxylate and
Dicarboxylate Anions

Interlayer Anion	Formula Weight	Equiv. Weight ^a	# mmol ^b	Cure Equiv.	%Epoxy Cure ^b
H ₂ N(CH ₂) ₁₁ COO	214	988	10.12	3	6.04
H ₂ N(CH ₂) ₅ COO ⁻	130	820	12.20	3	7.28
HOOC(CH ₂) ₁₀ COO	229	1018	9.28	2	3.91
HOOC(CH ₂) ₄ COO	145	850	11.76	2	4.68
[OOC(CH2)10COO]2-	228	778	6.34	2	2.52
[OOC(CH ₂) ₄ COO] ²⁻	144_	704	7.10	2	2.83

^aThe resulting weight of 1 mol of hydrotalcite Mg₆Al₂(OH)₁₆(CO₃)·4H₂0 (F.W., 604) after the anion-exchange reaction.

^bBased on 100g of 5/95 (w/w) organoclay/epoxy resin (251 mmol or 503 meq).

Effects of Clay Concentration

H₂N(CH₂)₁₁COO⁻-hydrotalcite has been chosen for further investigation because it has a relatively low polymerization-delamination temperature. Figure III.9 shows a plot of multiple DSC curves for epoxy polymerizations catalyzed by H₂N(CH₂)₁₁COO⁻-hydrotalcite at various clay concentrations (1-20 wt%). As the organoclay (or organic anion) concentration increases, the initiation reactions (Equations III.1-3) become more comparable to the propagation reaction (Equation III.4) with respect to the amount of heat released. At a high clay concentration (e.g., 20 wt%), high-temperature side reactions complicate the DSC curve, which is composed of several peaks with relatively small heat flows.

As shown in Figure III.10, the polymerization-delamination temperature is inversely proportional to the clay concentration up to 20 wt%. The base-catalyzed epoxy ring opening is an S_N^2 reaction of which the reaction rate depends on the concentrations of the reactants. The linear relationship suggests that the pre-exponential factor increases with increasing the organoclay or the organic anion concentration.

In Figure III.11 the heat of reaction is plotted against the clay concentration for $H_2N(CH_2)_{11}COO$ -hydrotalcite. That is, the heat of reaction is proportional to the epoxy concentration. The extrapolated values are 607 J/g or 54.9 kcal/mol for the neat epoxy resin. The linear relationship again shows that the heat of reaction is mainly due to the polymerization of the epoxy resin.

Kinetics Parameters

Figure III.12 shows a plot of multiple DSC curves generated at various heating rates (15-25 °C/min) for the epoxy polymerization

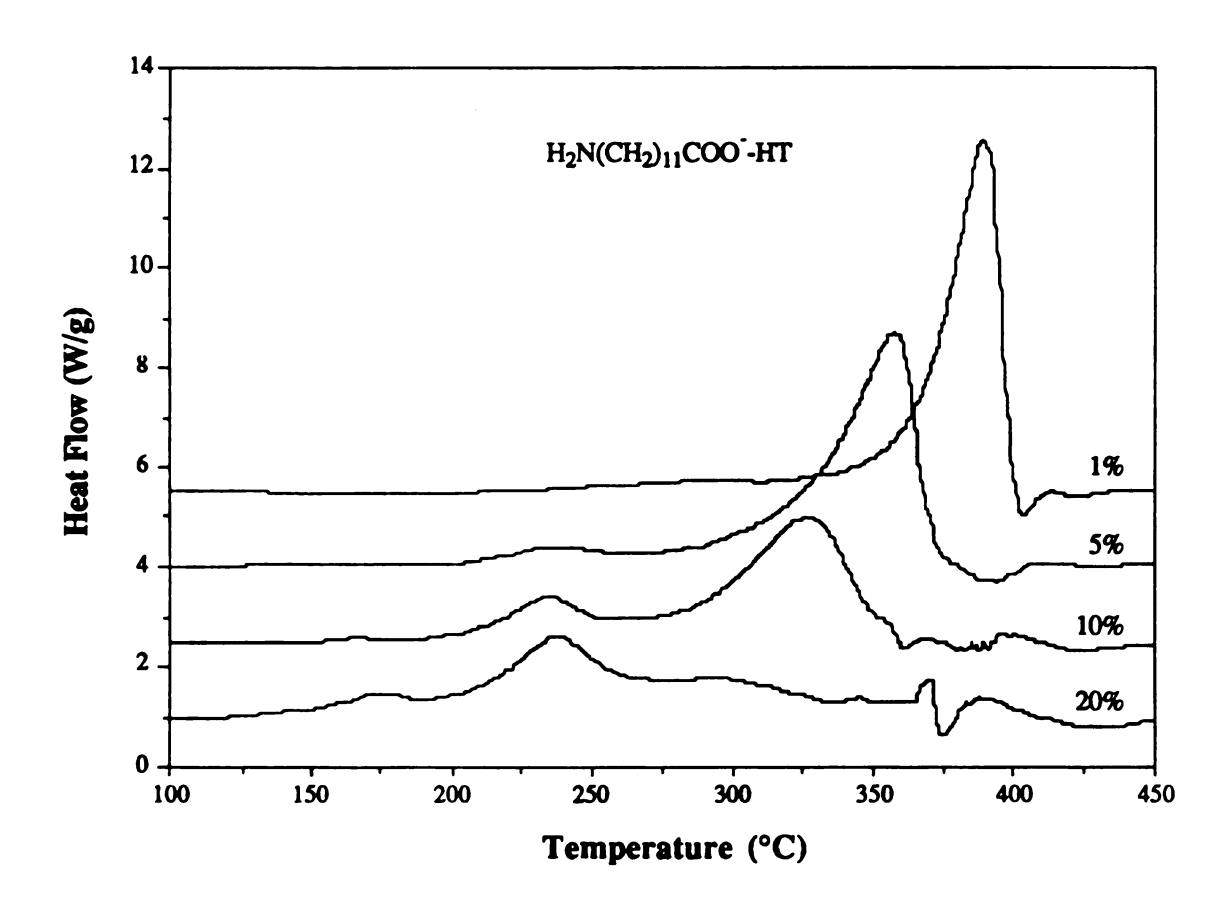


Figure III.9. DSC thermograms of epoxy polymerizations catalyzed by $H_2N(CH_2)_{11}COO$ -hydrotalcite at various clay concentrations: 1, 5, 10, and 20 wt%.

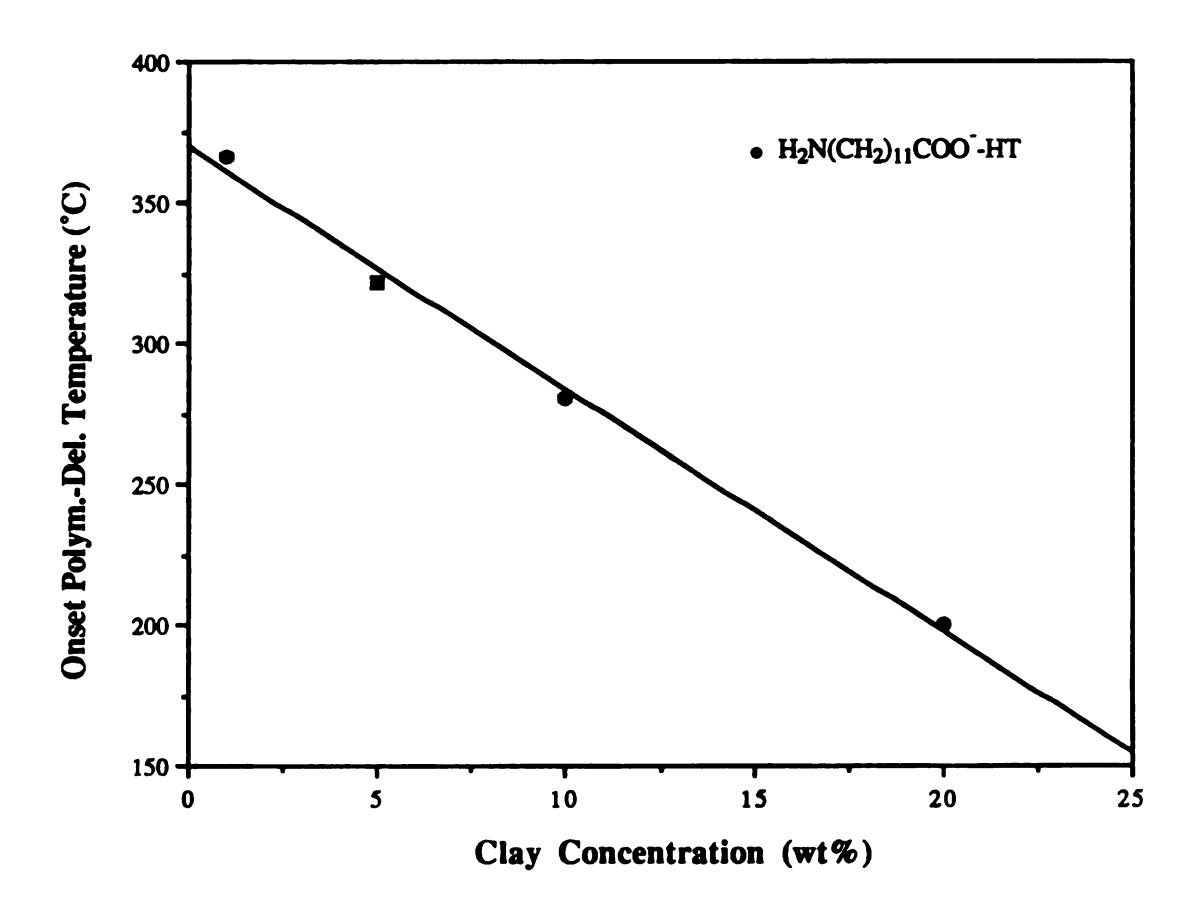


Figure III.10. Onset temperature of the epoxy polymerization-clay delamination as a function of the clay concentration for $H_2N(CH_2)_{11}COO^-$ -hydrotalcite.

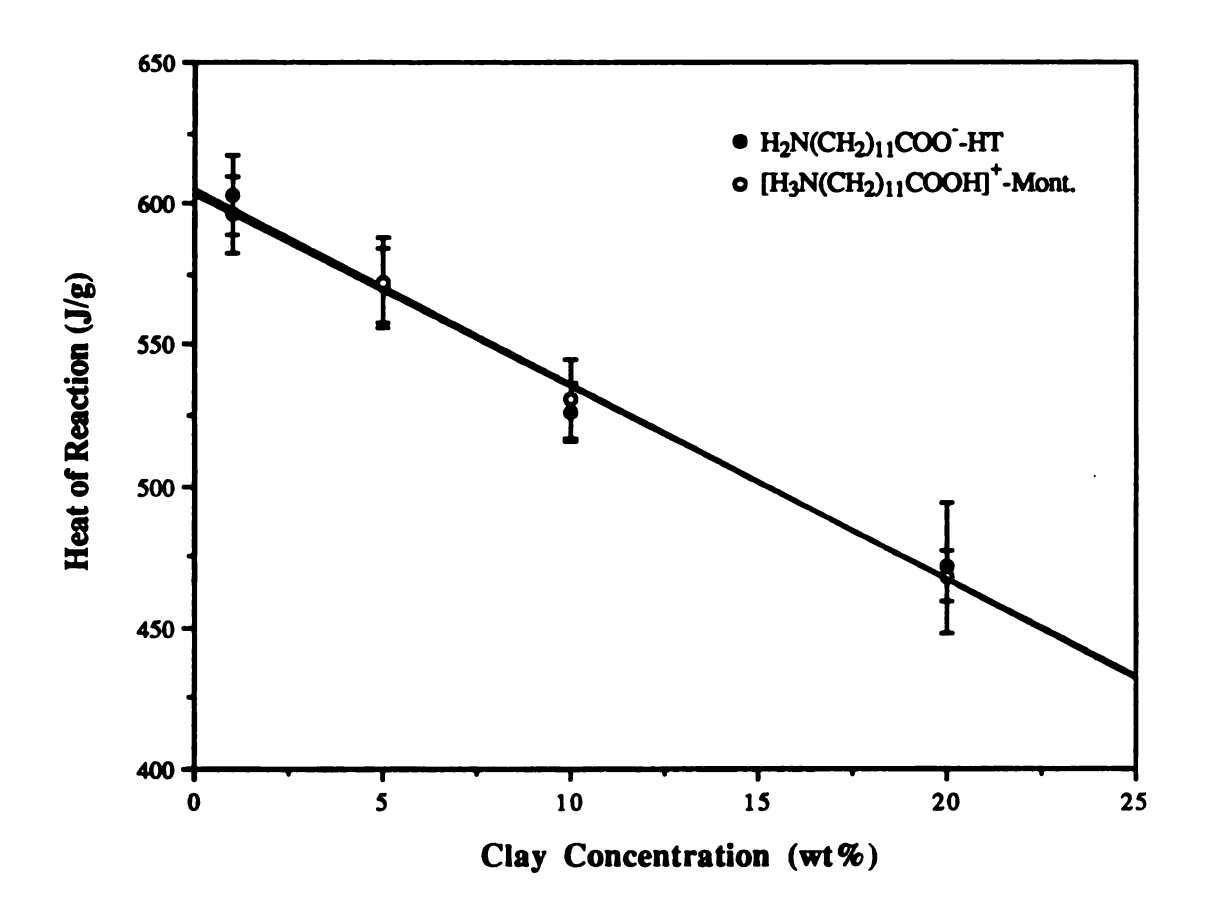


Figure III.11. Heat of reaction as a function of the clay concentration for (\cdot) $H_2N(CH_2)_{11}COO^-$ -hydrotalcite (\circ) $[H_3N(CH_2)_{11}COOH]^+$ -montmorillonite.

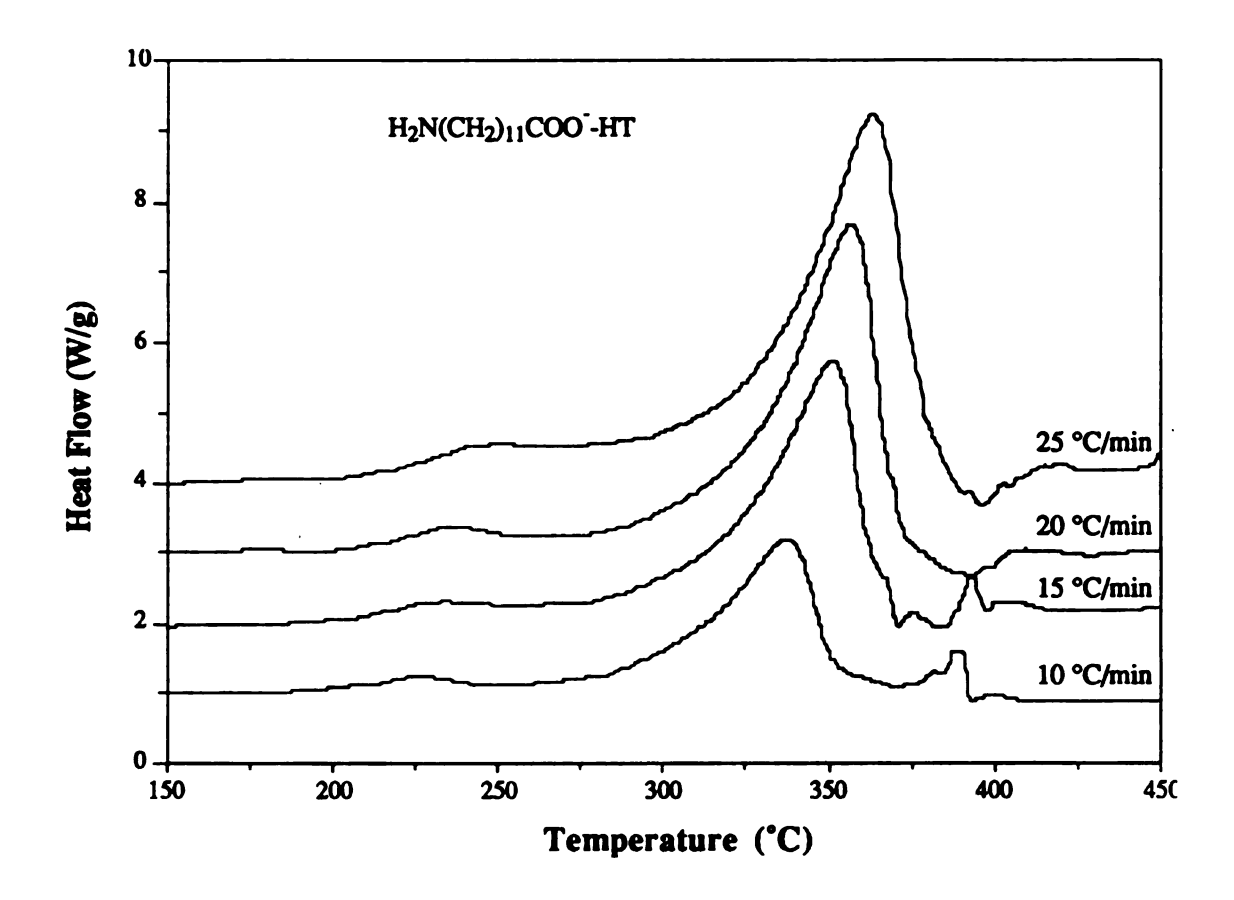


Figure III.12. DSC thermograms of the epoxy polymerization catalyzed by 5 wt% $H_2N(CH_2)_{11}COO^-$ -hydrotalcite at various heating rates: 10, 15, 20, and 25 °C/min.

catalyzed by 5 wt% $H_2N(CH_2)_{11}COO^-$ -hydrotalcite. The peak maximum temperature increases with increasing the heating rate. Despite the increased peak area and the heating rate, the heat of reaction remains constant.

Figure III.13 shows a linear relationship between $\ln \varphi$ and $1/T_p$ for the epoxy polymerization catalyzed by 5 wt% $H_2N(CH_2)_{11}COO^2$ -hydrotalcite. However, the ratio of $2T_p$ to E_a/R ranges from 9.45 to 9.84%, so that $2T_p$ is too large to be omitted. According to Equation II.9, the activation energy of the basic organoclay-catalyzed epoxy polymerization is 25.7 ± 0.5 kcal/mol. By using Equation II.10 and the activation energy obtained above, the pre-exponential factor is calculated as $8.66 \pm 0.38 \times 10^6 \text{ s}^{-1}$ (Table III.3). Moreover, based on Equations II.11-13 and m=2, the activation entropy, enthalpy, and free energy of the catalyzed epoxy polymerization are -32.1 \pm 0.2 cal/Kmol and 23.3 \pm 0.5 and 42.5 \pm 0.7 kcal/Kmol (at 595 K or 322 °C), respectively.

Comparison of Organoclays

Table III.4 summarizes DSC, XRD, and TEM data for epoxy polymerizations catalyzed by 5 wt% $H_2N(CH_2)_{11}COO^-$ -hydrotalcite and $[H_3N(CH_2)_{11}COOH]^+$ -montmorillonite, respectively. The polymerization-delamination temperature is 93 °C higher for $H_2N(CH_2)_{11}COO^-$ -hydrotalcite, although its basal spacing is 5.8 Å greater than that of $[H_3N(CH_2)_{11}COOH]^+$ -montmorillonite. The reason is that the steric effect is much more important in the base-catalyzed epoxy ring opening, considering the fairly bulky epoxy monomer and the organic anion confined between hydrotalcite layers. Both organophilic anionic and cationic clays

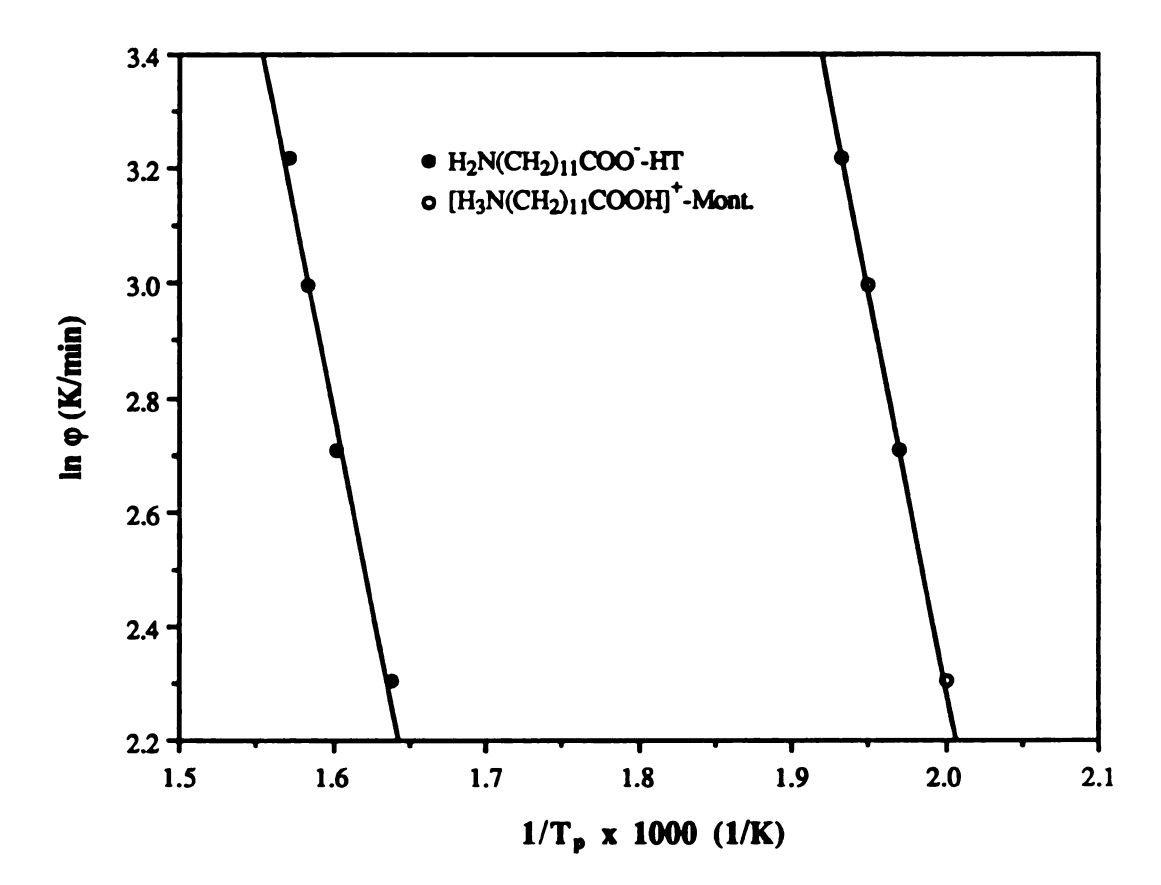


Figure III.13. Linear relationship between the natural logarithm of the heating rate φ and the reciprocal of the peak maximum temperature T_p for epoxy polymerizations catalyzed by 5 wt% (•) $H_2N(CH_2)_{11}COO^-$ -hydrotalcite (o) $[H_3N(CH_2)_{11}COOH]^+$ -montmorillonite.

Table III.3. Pre-exponential Factors for Epoxy Polymerizations Catalyzed by 5 wt%

12-Aminolaurate-Hydrotalcite

Interlayer Anion	Heating Rate (°C/min)	Peak Max. Temperature (°C)	Pre-exponential Factor (s ⁻¹)
H ₂ N(CH ₂) ₁₁ COO	10	337.4	9.08×10^6
	15	350.8	8.29 x 10 ⁶
	20	358.5	8.39 x 10 ⁶
	25	363.1	8.89 x 10 ⁶

Note: The activation energies of the epoxy polymerization catalyzed by 5 wt% $H_2N(CH_2)_{11}COO^-$ -hydrotalcite is 25.7 \pm 0.4 kcal/mol.

Table III. 4. DSC, XRD, and TEM Data for Epoxy Polymerizations Catalyzed by 5 wt% Protonated 12-Aminolauric Acid-Montmorillonite and 12-Aminolaurate-Hydrotalcite^a

Organoclay	Polym Del. Temp. (°C)	Heat of Polym. (kcal/mol)	Activation Energy (kcal/mol)	Polym Heat of Activation Preexponential Del. Temp. Polym. Energy Factor (°C) (kcal/mol) (kcal/mol) (s-1) (Activation Entropy (cal/Kmol)	Activation Enthalpy (kcal/mol)	Act. Free Energy (kcal/mol)	Basal Spacing (A)	Interlayer Spaçing ^b (Å)
AAA12-HT	322 ± 2	54.3±1.2	25.7 ± 0.4	54.3±1.2 25.7±0.4 8.66±0.38×10 ⁶ -32.1±0.2	-32.1 ± 0.2	23.3 ± 0.4 42.5 ± 0.6 22.8 ± 0.4	42.5 ± 0.6	22.8 ± 0.4	~ 200
AAC12-Mont.	229±1	54.4±1.5 25.	25.9 ± 0.1	$.9 \pm 0.1 1.80 \pm 0.02 \times 10^9$	-21.2±0.1 23.9±0.1 34.6±0.1 17.0±0.1	23.9 ± 0.1	34.6±0.1	17.0 ± 0.1	~ 2000

⁴DSC data were obtained by using a heating rate of 20 °C/min.

^bThe maximum interlayer spacing of delaminated organoclay.

give rise to virtually the same heat of reaction, Arrhenius activation energy, and activation enthalpy. These nearly identical reaction energies strongly suggest that the heat of epoxy polymerization is much larger than that of either clay delamination, and that the activation entropy accounts for the difference in the reaction reactivity between the two organoclay-epoxy systems. The more negative activation entropy reflects the smaller pre-exponential factor and imparts the higher activation free energy to the anionic clay-epoxy system. The activation free energies indicate that basic $H_2N(CH_2)_{11}COO^2$ -hydrotalcite is a less effective catalyst for the epoxy polymerization than acidic $[H_3N(CH_2)_{11}COOH]^+$ -montmorillonite.

D. CONCLUSIONS

In this work we have achieved the direct nanoscopic delamination of hydrotalcite layers in a polyether matrix derived from an epoxy resin, although deprotonated 12-aminolauric acid is the only delaminating agent or catalyst that substantially reduces the delamination-polymerization temperature, we also first used a relatively simple method to prepare a well-ordered aminocarboxylate-LDH (12-aminolaurate-hydrotalcite) with a super gallery $(d_{003} = 22.8 \text{ Å})$.

The delamination-polymerization temperature depends on the heating rate, clay concentration, and anion-exchanged hydrotalcite. The heating rate and the clay concentration being equal, interlayer gallery height or steric hindrance is an important factor affecting the delamination-polymerization temperature. Within experimental errors, the heat of epoxy polymerization is independent of the anion exchanged form of hydrotalcite, suggesting that

differences in the clay delamination energy are small relative to the epoxy polymerization energy.

Compared with acidic $[H_3N(CH_2)_{11}COOH]^+$ -montmorillonite, basic $H_2N(CH_2)_{11}COO^-$ -hydrotalcite is a less effective catalyst for the epoxy polymerization. The activation entropy, as reflected in the pre-exponential factor, accounts for the difference in reactivity between the two organoclay-epoxy systems.

LIST OF REFERENCES

- 1. K. Yano, A. Usuki, A. Okada, T. Kurauchi, and O. Kamigaito, Polym. Prepr., 32, 65 (1991).
- 2. A. Usuki, Y. Kojima, M. Kawasumi, A. Okada, T. Kurauchi, and O. Kamigaito, *Polym. Prepr.*, 31, 651 (1990).
- 3. H. C. B. Hansen and R. M. Taylor, Clay Miner., 26, 311 (1991).
- 4. K. A. Carrado, A. Kostapapas, and S. L. Suib, Solid State Ionics, 26, 77 (1988).
- 5. W. T. Reichel, Solid State Ionics, 22, 135 (1986)
- 6. W. T. Reichle, CHEMTECH, 16, 58 (1986).
- 7. S. Miyata, Clays Clay Miner., 31, 305 (1983).
- 8. S. Miyata and T. Kumura, Chem. Lett., 843 (1973).
- 9. M. A. Drezdzon, Inorg. Chem., 27, 4628 (1988).
- 10. M. Meyn, K. Beneke, and G. Lagaly, Inorg. Chem., 29, 5201 (1990).
- 11. K. Chibwe and W. Jones, J. Chem. Soc., Chem. Commun., 926 (1989).
- 12. E. Narita and T. Yamagishi, Proc. 9th Inter. Clay Conf., 145 (1990).
- 13. E. D. Dimotakis and T. J. Pinnavaia, Inorg. Chem., 29, 2393 (1990).
- 14. T. Nakatsuka, H. Kawasaki, S. Yamashita, and S. Kohjiya, Bull. Chem. Soc. Jpn., 52, 2449 (1979).
- 15. S. Kohjia, T. Sato, T. Nakayama, and S. Yamashita, Makromol. Chem., Rapid Commun., 2, 231 (1981).

- D. E. Laycock, R. J. Collacott, D. A. Skelton, and M. F. Tchir, J. Catal., 130, 354 (1991).
- M. Tanaka, I. Y. Park, K. Kuroda, and C. Kato, Bull. Chem. Soc.
 Jpn., 62, 3442 (1989).
- 18. W. T. Reichle, S. Y. Kang, and D. S. Everhardt, J. Catal., 101, 352 (1986).
- F. Rey, V. Fornes, and J. M. J. Rojo, Chem. Soc., Faraday Trans.,
 88, 2233 (1992).

HICHIGAN STATE UNIV. LIBRARIES
31293010517948